

NORTHWESTERN UNIVERSITY

Iron Regulates Cellular Metabolism and Mitophagy Through Epigenetic Control of mTORC1

A DISSERTATION

SUBMITTED TO THE GRADUATE SCHOOL  
IN PARTIAL FULFILLMENT OF THE REQUIREMENTS

DOCTOR OF PHILOSOPHY  
Field of Life Sciences

By  
Jason Solomon Shapiro

EVANSTON, ILLINOIS  
September 2020

**Abstract**

Iron is an essential nutrient and is critical for cellular growth and metabolism. Here, we delineate a novel mechanism by which iron alters amino acid homeostasis and mTOR activity by remodeling the cellular epigenetic landscape. We find that iron deficiency inactivates Jumonji-C domain containing histone-demethylases, resulting in histone hyper-methylation and silencing of the leucine transporter LAT3 and obligatory mTORC1 cofactor RAPTOR. Additionally, we identify that mTOR-mediated regulation of RNA stability through tristetraprolin (TTP) is a novel and requisite step in selective-autophagy. TTP is required for cell survival during prolonged iron deprivation and is transcriptionally induced downstream of mTORC1 inactivation. In the absence of TTP, mitochondria damaged by the loss of iron cannot undergo fission, rendering the mitochondria too large for engulfment and subsequent recycling. Accumulation of damaged mitochondria leads to defective oxidative metabolism and impairs hepatic gluconeogenesis in response to fasting. These studies uncover a novel pathway that integrates iron sensing with cellular metabolism, mitochondrial dynamics and autophagy.

I dedicate this dissertation with heartfelt gratitude to:

My New York Family

For raising, nurturing and loving me unconditionally.

My Chicago Family

For their warm friendship and laughter during the brightest and darkest times.

My Lab Family

For constantly supporting, challenging and inspiring me to achieve more than I thought possible.

Pre-doctoral Advisor: Hossein Ardehali, M.D., Ph.D.

Thesis Committee: Paul Shumacker, Ph.D.

Richard Scarpulla, Ph.D.

Lewis D. Landsberg, M.D., Ph.D

Thank You!

## TABLE OF CONTENTS

**COVER PAGE ..... 1**

**DEDICATION ..... 2**

**ABSTRACT ..... 3**

**TABLE OF CONTENTS ..... 4-5**

**LIST OF TABLES and FIGURES ..... 6**

**FOREWORD ..... 7**

### **CHAPTER 1: INTRODUCTION**

**1.1.0 Systemic Iron Handling ..... 7-11**

1.1.1 Systemic Iron Uptake .....7-8

1.1.2 Regulation of Iron Uptake by Hepcidin ..... 8-9

1.1.3 Iron Recycling ..... 9

1.1.4 Hypoxia and Systemic Iron Regulation ..... 9

1.1.5 Inflammation and Systemic Iron Regulation ..... 9-10

1.1.6 Diseases of Systemic Iron Deficiency ..... 10

1.1.7 Diseases of Systemic Iron Overload ..... 10-11

**1.2.0 Cellular Iron Handling ..... 11-16**

1.2.1 Iron Toxicity ..... 11-12

1.2.2 Cellular Iron Homeostasis ..... 12

1.2.3 Mitochondrial Iron Homeostasis ..... 12-13

1.2.4 Fe-S Cluster Biosynthesis ..... 13-14

1.2.5 Heme Synthesis .....	14
1.2.6 Epigenetic Regulation .....	14-15
1.2.7 The IRP System .....	15
1.2.8 Alternative Pathways Involved in Iron Homeostasis .....	15-16
1.2.9 Iron Conservation .....	16
<b>1.3.0 General Regulation and Function of TTP .....</b>	<b>16-17</b>
<b>1.4.0 Cellular Control of mTOR Function .....</b>	<b>17-21</b>
1.4.1 mTOR Regulates Cellular Anabolic Pathways .....	17
1.4.2 Nutrient Sensing by mTOR – The RAG Pathway .....	17-18
1.4.3 Nutrient Sensing by mTOR – The TSC2 Pathway .....	18-19
1.4.4 General Mechanisms of Autophagy .....	19
1.4.5 Regulation of Mitochondria Dynamics and Mitophagy .....	19-20
1.4.6 The Link Between mTOR, Mitochondria, and Cellular Nutrients.....	20-21
<b>1.5 Highlight of Current Studies.....</b>	<b>21</b>

## **CHAPTER 2: RESULTS**

2.1 Iron deprivation inactivates mTOR through changes in leucine homeostasis. ....	<b>22-23</b>
2.2 Iron sensing by Jumonji-C histone demethylases controls amino acid signaling and represses mTORC1. ....	<b>23-24</b>
2.3 Iron deficiency alleviates repression of TTP by the transcription factor SP1. ....	<b>24</b>
2.4 mTOR regulates both mitochondrial dynamics and mitophagy through the TTP-OPA1 axis. ....	<b>24-26</b>
2.5 TTP is required to sustain mitochondrial	

metabolism during iron deficiency. .... **26**

2.6 TTP-mediated mitophagy is important for

hepatic gluconeogenesis during iron deprivation. .... **26-27**

### **CHAPTER 3: DISCUSSION**

3.1 The Requirement for Redundancy ..... **27-28**

3.2 Histone Methylation and Cancer ..... **28**

3.3 Connections Linking Mitophagy and Autophagy ..... **28-29**

3.4 Physiologic Limitations of Hepatic Mitophagy ..... **29**

3.5 Human Genetics and TTP ..... **29**

### **CHAPTER 4: SUMMARY AND FUTURE DIRECTIONS**

4.1 Summary ..... **29**

4.2 Future Directions ..... **30**

### **CHAPTER 5: MATERIALS and METHODS ..... 30-34**

5.1 Cell culture, gene downregulation, and overexpression

5.2 Drug treatments

5.3 *In silico* analysis of AU-rich elements

5.4 RNA isolation, reverse transcription and quantitative RT-PCR

5.5 mRNA stability assay and RNA co-IP

5.6 Western blots

5.7 Iron quantification

5.8 Amino acid profiling

5.9 <sup>3</sup>H-leucine and <sup>14</sup>C-glucose uptake

5.10 <sup>35</sup>S-methionine based measurement of protein synthesis

5.11 Luciferase assay

5.12 Confocal imaging

5.13 Mitochondrial DNA content determination

5.14 Cell growth and apoptosis analysis

5.15 Metabolomics

5.16 Mouse strain and iron deficiency diet

5.17 *In vivo* metabolic studies

5.18 Blood count and red blood cell measurements

5.19 Organ harvest, and histological analysis

5.20 Transmission Electron Microscopy

5.21 Statistical analysis

**TABLES and FIGURES ..... 35-49**

**FIGURE LEGENDS ..... 50-54**

**REFERENCES ..... 55-66**

**CURRICULUM VITAE ..... 67-69**

**Table 1.** Hepatic Expression of Major Leucine Transporters.

**Figure 1.** Iron chelation inhibits mTOR activity by altering amino acid homeostasis.

**Figure 2.** Iron chelation inhibits mTOR activity by altering amino acid homeostasis (Cont.).

**Figure 3.** Iron chelation causes H3 hypermethylation and represses RAPTOR expression.

**Figure 4.** Iron chelation causes H3 hypermethylation and represses *RAPTOR* expression (Cont.).

**Figure 5.** Transcription factors SP1 and AP2 regulate *TTP* expression during Iron deficiency.

**Figure 6.** TTP mediated degradation of *Opa1* mRNA is required for mitochondrial fission in response to iron chelation.

**Figure 7.** TTP mediated degradation of *Opa1* mRNA is required for mitochondrial fission in response to iron chelation (Cont.).

**Figure 8.** Iron deficiency induces conventional mitophagy that is dependent on TTP-mediated mitochondrial fission.

**Figure 9.** Iron deficiency induces conventional mitophagy that is dependent on TTP-mediated mitochondrial fission (Cont.).

**Figure 10.** Failure of mitochondrial fission in iron deficient *Ttp* KO MEFs causes mitochondrial dysfunction and altered metabolism.

**Figure 11.** Failure of mitochondrial fission in iron deficient *Ttp* KO MEFs causes mitochondrial dysfunction and altered metabolism (Cont.).

**Figure 12.** Liver-specific deletion of *Ttp* causes failure of mitochondrial fission and mitophagy and defective gluconeogenesis during iron deficiency *in vivo*.

**Figure 13.** Liver-specific deletion of *Ttp* causes failure of mitochondrial fission and mitophagy and defective gluconeogenesis during iron deficiency *in vivo* (Cont.).

**Figure 14.** Graphical Summary.

## **Foreword**

Life is orchestrated by a symphony of processes designed to allow an organism, whether it be a bacterial, plant, or animal, the ability to consume, grow, adapt, replicate, and eventually die.

Although the details differ, this fundamental pattern is repeated time and time again amongst all living things on earth. As scientists, our calling is to carefully observe these processes and attempt to understand how they work and how they came to be. Experiments are the language scientists use to comprehend phenomenon that are locked away from all other forms of inquiry.

The Ph.D. is a brand that marks a new scientist as having sufficient training and experience to speak the language of science fluently and allows him or her permission to engage in scientific inquiry professionally. With the Ph.D. in hand, I believe it is a scientist's professional and moral obligation to apply their expert knowledge and training to the benefit of society by ameliorating disease, creating new technologies, and upholding the values of truth, honesty, and community.

## **Chapter 1**

### **Introduction**

Iron is an elemental metal that is found abundantly in the earth's molten core. Because of its relative abundance and unique physical chemistry, evolution has advantageously incorporated it into many of the chemical reactions and enzymatic functions that have become necessary to sustain life. Iron is easily oxidized and generally exists in either a  $\text{Fe}^{2+}$  or  $\text{Fe}^{3+}$  state. Perhaps the best known role for iron is its ability to pass and donate electrons to oxygen in cells undergoing aerobic oxidative metabolism. In addition to electron transport, organisms with systemic circulatory systems, such as mammals, can incorporate iron into heme and subsequently load the heme prosthetic group into the protein hemoglobin to transport oxygen to

tissues otherwise too deep or distal to receive oxygen by passive diffusion. Iron can also be used to coordinate reactions independent of oxygen, such as demethylation, dehydrogenation and reduction of sulfur [1-3]. Many iron-containing enzymes that catalyze reactions with and without oxygen are critical for cell survival and have been shown to mediate DNA replication and repair, translation, carbon metabolism, and reactive oxygen species detoxification.

### **1.1.0 Systemic Iron Handling**

#### **1.1.1 Systemic Iron Uptake**

Ensuring an adequate supply of iron is an evolutionary imperative and multiple systems have arisen to handle iron acquisition and maintenance. These systems can be roughly partitioned into cellular iron handling and systemic iron handling for multicellular organisms. Although the focus of this dissertation is on eukaryotic cellular iron homeostasis, it is first necessary to understand how iron supply is regulated in the mammalian system. Iron, as an elemental nutrient, must be acquired through the diet. Iron can be absorbed either as molecular iron, or as a component of larger molecules such as heme. When iron-rich food is consumed, the acidic environment of the stomach is necessary to release iron from various chemical bonds and allow for its reduction to  $\text{Fe}^{2+}$ . Once past the stomach, additional acidifying enzymes in the brush border of the duodenum further promotes the formation of  $\text{Fe}^{2+}$  where it can then be imported into the duodenal epithelia by Divalent Metal Transporter 1 (DMT1) [4, 5]. Transport of molecular iron is the primary means by which iron is acquired in mammals. Iron that remains conjugated to porphyrin heme can be transported across the apical membrane by Heme Carrier Protein 1 (HCP1), however, the contribution of this transport to overall iron homeostasis is minimal and HCP1 mainly functions as a folate transporter [6, 7]. Clinically, the use of proton pump inhibitors for gastric reflux and gastric ulcers is associated with a risk of iron deficiency

due to the difficulty of iron to transition to the  $\text{Fe}^{2+}$  state at a neutral pH. Additionally, gastrointestinal malignancies that disrupt the structure or function of the duodenum can cause significant iron deficiency due to lack of absorption and bleeding. In the absence of pathology, after import into the duodenum, iron can be exported across the basal membrane and into circulation by the iron exporter Ferroportin (FPN1, SLC40A1) or held intracellularly coupled to the iron storage protein Ferritin (FTN) [8-10]. This bifurcation in the destination of iron is the most critically regulated step in systemic iron handling. When body iron stores are low, iron is oxidized to  $\text{Fe}^{3+}$  by the enterocyte ferroxidase Hephaestin (HEPH) after being exported by FPN1 [11].  $\text{Fe}^{3+}$  iron has a high affinity for the soluble serum protein Transferrin (TF) which carries the iron for distribution throughout the body [10]. When body iron stores are high, the liver secretes the small (25 amino acid) hormone peptide Heparin (HAMP1) which binds to FPN1 and promotes its internalization and degradation [12, 13]. Unpublished data indicate that hepcidin can also directly inhibit FPN function independent of degradation by altering the confirmation of the pore and restricting the passage of iron. With these two mechanism acting in concert, iron becomes trapped in the duodenal epithelia and is excreted when the duodenal cell is eventually sloughed, a process that occurs approximately every 4-7 days. It is important to note that, with the exception of acute blood loss, mammals have no robust system to excrete excess iron. This is somewhat paradoxical, because excess iron is extremely detrimental to cells due to its participation in damaging ROS generation. For example, inactivating mutations in HAMP1 causes hereditary hemochromatosis (HHC), a disease of iron overload that manifests as cirrhosis, cardiomyopathy, skin darkening, diabetes and eventually death if left untreated [14]. This speaks to the evolutionary pressure under which mammals have evolved to obtain and conserve iron, despite the risks posed by iron excess.

### **1.1.2 Regulation of Iron Uptake by Heparin**

The regulation of hepcidin production is the primary method the mammalian system uses to integrate the demand for iron uptake and its subsequent distribution and utilization throughout the body [15]. hepcidin is upregulated in the liver by multiple signals, including high TF iron saturation, inflammation, and deficient hematopoiesis [16]. Each pathway can function independently of the others, however, multiple levels of cross-talk exist. The BMP-SMAD signaling pathway is the most well characterized pathway involved in the upregulation of hepcidin transcription. This pathway was characterized somewhat circuitously when Hemojuvelin (HJV) was discovered to act as a BMP co-receptor [17]. Mutations in HJV, most commonly G320V, cause HHC similar to mutations found in Hemochromatosis protein (HFE) and HAMP1 [18]. Just a few years earlier, it was shown that ablation of SMAD4 signaling downstream of BMP and TGF- $\beta$  resulted in hemochromatosis and blocked hepcidin induction by iron-dextran [19]. Subsequent studies have identified multiple modulators of this pathway including the negative regulator of hepcidin production, Membrane serine protease matriptase-2 (TMPRSS6), which when mutated causes a hereditary form of iron-refractory iron deficiency anemia (IRIDA) secondary to hepcidin overproduction [20, 21]. Although systemic iron levels can regulate the expression of some of the components of the HJV-BMP pathway, the complete mechanism by which systemic iron levels are sensed by the liver and how it couples to the BMP pathway in normal physiologic circumstances remains elusive.

The most direct sensing of iron status by the liver is accomplished by the binding of holo-TF (iron bound) to Transferrin Receptor 1 and 2 (TFR1, TFR2) on the surface of hepatocytes. Binding of holo-TF to TFR1 causes dissociation of HFE from TFR1 and subsequent movement to TFR2, which is also bound by holo-TF [22, 23]. Although physical interaction of HFE with TFR2 is capable of promoting hepcidin production, the exact mechanism by which the signal is transduced to the nucleus is under current investigation. Some data suggests that the HFE-TFR2 complex is able to bind HJV and promote BMP signaling when iron levels are high [24].

However, this interaction has yet to be demonstrated *in vivo* and it is likely that other signaling molecules downstream of HFE-TFR2 are critical to holo-TF mediated hepcidin induction.

### 1.1.3 Iron Recycling

Erythrocyte recycling is another major mechanism by which vertebrates maintain sufficient levels of iron. While dietary uptake can supply new iron into the body, less than 1% of total iron stores is absorbed from the diet each day [10]. The vast majority of iron is recycled from heme containing erythrocytes by specialized macrophages in the spleen and liver which can recognize and phagocytose damaged or senescent red blood cells. Erythrocytes targeted for recycling are coated with IgG antibody and opsonized by binding to CD47 on the macrophage surface [25, 26]. The acidic and proteolytic environment of the phagolysosome frees the heme prosthetic group from the globin protein and the heme is then exported into the cytoplasm via the heme transporter HRG1 [27]. Once in the cytoplasm, heme-oxygenase 1 (HO-1) liberates iron from heme and metabolizes the empty heme into biliverdin and carbon monoxide [28]. The liberated iron can then be exported via FPN1 to neighboring hepatocytes for storage or stored within the macrophage bound to FTN.

### 1.1.4 Hypoxia and Systemic Iron Regulation

A third, and indirect form of systemic iron regulation is established by oxygen sensing via hypoxia inducible factors 1 and 2 (HIF1/2). Restricted erythropoiesis due to iron deficiency and conditions associated with chronic bleeding can cause distributed hypoxia within tissues. Reduction in O<sub>2</sub> tension inactivates cytoplasmic proline hydroxylases (PHD) which require molecular oxygen to add an –OH moiety to proline residues on the HIF1/2 proteins [29, 30]. Under oxygen sufficient conditions, proline hydroxylation facilitates recognition of HIF1/2 by Von

Hippel-Lindau tumor suppressor (VHL) which subsequently promotes ubiquitination and proteolytic degradation of HIF1/2 in the cytoplasm [31]. When O<sub>2</sub> tension drops, PHD enzymes are inactivated and HIF1/2 levels accumulate, leading to nuclear translocation and activation of target gene transcription. HIF1/2 transcriptional targets include mediators of iron uptake TF, TFRC, and DMT1 in enterocytes, as well as the erythropoietic stimulatory hormone EPO in the kidney [32-34]. Although there are published reports suggesting that HIF1 $\alpha$  can repress hepcidin production in the hepatocytes *in vitro*, the physiologic impact of this is still unknown [35].

#### 1.1.5 Inflammation and Systemic Iron Regulation

Analysis of the HAMP1 promoter also revealed conserved binding sites for STAT3, a major transducer of inflammatory signaling in mammalian cells [36]. The regulation of systemic iron handling by inflammation is extremely pertinent for multicellular organisms. Invading bacterial species require sufficient quantities of iron to proliferate and establish sustained infection. In a form of evolutionary iron “arms race”, some bacterial species evolved specialized iron sequestering proteins called siderophores which bind iron in serum for use by the bacteria [37]. In response to infection, inflammatory signals in the host strongly induce hepcidin production which degrades FPN on the surfaces of cells, particularly in the duodenum and on macrophages, preventing iron release into the serum. By blocking iron release and serum TF saturation, invading bacteria are starved of the necessary iron they require to proliferate facilitating clearance by macrophages and neutrophils. Although the production of hepcidin and resulting iron sequestration in tissue is highly beneficial in the setting of bacterial infection, it can become problematic in the setting of long-term pro-inflammatory states. The resulting hepcidin over-production and drop in TF saturation can restrict red blood cell production in the bone marrow and cause anemia of chronic disease (ACD). Although other etiologies of ACD exist,

such as lack of erythropoietin (EPO) production in the setting of chronic kidney disease, inflammatory based ACD is commonly seen in patients with heart failure, cancer, HIV, and autoimmune disease such as rheumatoid arthritis, who otherwise have no deficit in kidney function [38]. Thus, not only is the total quantity of iron within the body tightly regulated but the relative distribution and localization of iron in different tissues is a critical part of mammalian physiology.

### **1.1.6 Diseases of Systemic Iron Deficiency**

Diseases associated with iron deficiency are the result of either insufficient iron uptake, abnormal loss, or improper partitioning of iron stores between tissue and the circulation. While iron deficiency associated with insufficient iron uptake or excessive loss tend to respond well to iron supplementation, systemic iron deficiency due to improper handling of iron stores are referred to as iron-refractory iron deficiency anemia (IRIDA). Classically, IRIDA is the clinical term for an autosomal recessive disease arising from mutations in *TMPRSS6* which cause excessive hepcidin production and iron sequestration in enterocytes and macrophages [21]. However, conceptually there is little reason why ACD, for example, should not be considered an acquired form of IRIDA as the fundamental pathology underlying ACD is an inflammatory mediated production of hepcidin against which iron supplementation is of little utility. In contrast to IRIDA, whether genetic or acquired, by far the most common iron associated disease is iron deficiency anemia (IDA). This disease occurs when the total iron stores within the body are insufficient to meet the demand for erythropoiesis. The WHO estimates that nearly 30% of the world population has IDA and that the greatest burden is concentrated in developing nations where malnutrition, malaria, and parasitic infections are significant concerns [39, 40]. At a national level, IDA contributes to significant loss in earnings and quality of life among individuals due to fatigue, productivity loss, and premature mortality [41]. Additionally, menstruating and pregnant women are at the greatest risk for IDA due chronic blood loss and increased

erythropoietic demand. Perinatal iron deficiency has a profoundly negative impact on maternal-fetal outcomes, most pertinently maternal and fetal survival [42, 43]. The effects of iron deficiency are magnified in infants and children in both post-industrialized and developing nations due to increased demand for iron as the body grows. Rapid neural development occurs during the last trimester of pregnancy and continues roughly until the age of two by which children will have developed almost 90% of their brain mass. Subsequent neurogenesis continues in the hippocampus throughout life in addition to cortical myelination, global synapse remodeling and glial turnover. Due to the high demand for iron during development, iron deficiency in children is associated with delayed neurodevelopment resulting in inferior motor skills, sensory perception, and memory function when compared to iron sufficient children [44, 45]. Despite the negative sequelae of IDA in vulnerable populations such as pregnant women and children, particularly when compounded with comorbidities such as infection and other micronutrient deficiencies, most mammalian organs, besides the brain and bone marrow, are well adapted to withstand prolonged periods of iron deficiency. The mechanisms underlying the robust physiologic adaptations to iron deficiency, particularly secondary mechanisms when primary attempts by cells to absorb more iron fail, will be discussed later in this dissertation.

### **1.1.7 Diseases of Systemic Iron Overload**

Although systemic iron deficiency and IDA are common disorders with a massive global footprint that stem from a combination of insufficient dietary iron consumption and increased iron loss, disorders of iron overload are contrastingly quite rare and are usually genetic in origin. Systemic iron overload, academically referred to as hemochromatosis, is subdivided into hereditary hemochromatosis (HHC) and acquired hemochromatosis. Acquired hemochromatosis is a term used to describe iron overload that affects multiple organs, as in cases due to repeated blood transfusions to treat thalassemia [46, 47]. Alternatively, organ

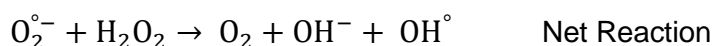
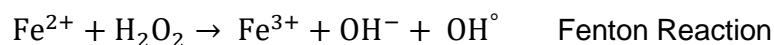
specific iron overload can occur secondary to other disease processes, such as heart failure, and this is not considered a true form of hemochromatosis [48-50]. Hemochromatosis is occasionally referred to clinically as “bronze diabetes” which is an acknowledgement of the primary clinical features patients present with. Hemochromatosis classically causes skin pigmentation (due to hemosiderin deposition and increased melanin production), cirrhosis (hepatocyte death and inflammation), diabetes (damage to  $\beta$ -cells in the pancreas and systemic insulin resistance secondary to liver dysfunction), cardiomyopathy (damage to the myocardium) and hypogonadism (damage to gonadotropin producing cells in the pituitary) [51-55]. HHC can result from mutations in multiple genes ranging from relatively common to exceedingly rare. These genes include HFE (Type 1), HAMP or HJV (Type 2), FPN1 (Type 3), TFR2 (Type 4), and FTH (Type 5) [56, 57]. One can immediately notice that all of these genes function either in the hepcidin production pathway or cellular iron binding and export.

## **1.2.0 Cellular Iron Handling**

### **1.2.1 Iron Toxicity**

While severe iron deficiency causes largely selective dysfunction in the bone marrow and developing brain, why is iron overload toxic to so many different cell-types and organ systems? The answer to this question is rooted in iron chemistry more than biology. Iron is a transition metal with an electron configuration of  $[\text{Ar}]3d^64s^2$ . The 8 electrons in its outer shell have similarly low electronegativities and therefore iron is able to donate electrons easily, becoming oxidized in the process. The most common oxidation states for iron are  $\text{Fe}^{2+}$  and  $\text{Fe}^{3+}$ , with  $\text{Fe}^{2+}$  predominating in acidic environments. The danger of iron overload arises from iron's ability to donate electrons to oxygen to generate hydroxyl free radicals. Hydroxyl radicals are an extremely potent form of reactive oxygen species (ROS) which damage lipids, proteins, and

DNA [58]. The Fenton and Haber-Weiss reactions describe the generation of hydroxyl radicals using iron as a catalyst [59].



Due to oxygen's role as an electron receptor for ATP generation during oxidative phosphorylation within the mitochondria, cells maintain a constant pool of  $\text{O}_2^{\circ-}$  that must remain physically sequestered away from iron [60, 61]. When iron levels increase beyond the capacity for FTN to bind and sequester it away, free iron sparks a cyclic reaction of ROS production that damages critical cellular components and can ultimately lead to a form of regulated cell death known as ferroptosis [62]. Increased ROS generated by excess free iron can damage lipids by peroxidation. Phospho-lipids containing poly unsaturated fatty acids, such as phosphoethanolamine-arachidonic acid, are easily oxidized and are potent signals for ferroptotic cell death [63]. Although the downstream effectors of ferroptosis are still largely unknown, ferroptosis has been shown to proceed in the absence of key mediators of apoptosis such as BAX and caspases, and necroptotic mediators MLKL and RIPK1 [64]. Interestingly, ferroptosis is promoted by p53, which inhibits cysteine uptake in the setting of advanced lipid damage by transcriptionally repressing the cysteine/glutamate antiporter SLC7A11 to abrogate detoxification by the glutathione antioxidant system [65]. Indeed, ROS mediated cell death is a hallmark of iron overload diseases, many of which cause specific iron accumulation in the mitochondria, where ROS production is greatest.

### 1.2.2 Cellular Iron Homeostasis

To wholly understand the mechanisms underlying disorders of iron homeostasis, it is critical to understand how iron is transported, stored, and utilized at the cellular level. While, systemic iron handling is largely governed by environmental factors and the peptide hormone hepcidin, cellular iron handling has evolved multiple layers of regulation that interact with one another. As mentioned previously, cells take up iron through expression of TFR1 on the cell surface [66, 67]. Each molecule of TF can bind two molecules of iron and has high affinity for Fe(III) at neutral and slightly basic pH. TFR1 itself is homo-dimer linked by disulfide bonds with each monomer able to bind one TF molecule. Binding of TF to TFR1 causes clathrin-dependent endocytosis of the complete holo-complex [68]. Subsequent acidification of the late endosome by vacuolar ATPase and reduction of Fe(III) to Fe(II) by the STEAP family of metallo-reductases prepares the iron to be pumped out from the lysosome via DMT1 [69-72]. The now apo-TF-TFR1 complex is shuttled back to the cell surface for reuse [73, 74]. In the cytoplasmic FTN binds the iron as a carrier and iron is oxidized back to more inert Fe(III). Since labile iron is extremely toxic to cells, FTN levels are tightly correlated with total cellular iron content. From this point, FTN bound iron can be stored for later use or degraded so the iron can be mobilized once again for use in enzymatic reactions [75]. The cytosolic iron chaperone PCBP1 play a significant role in shuttling cytosolic iron between storage in FTN and loading into enzymes that utilize molecular iron [76]. The mechanism mediating the release of iron from FTN for remobilization is termed ferritinophagy [77]. This is a process in which iron saturated FTN is targeted for autophagic degradation within the lysosome with the aid of the cargo receptor NCOA4 [78]. The acidic environment of the lysosome releases the iron from FTN and the FTN protein itself is proteolytically degraded to recycle its amino acids [79]. Studies have shown that NCOA4 mediated ferritinophagy is required for erythropoiesis in zebrafish and mice such that deletion of NCOA4 results in microcytic anemia with corresponding iron overload in tissues such

as the liver and spleen [80, 81]. While autophagy is a mechanism for liberating protein-bound iron when iron levels drop, the sole mechanism for expelling excess cellular iron is through the iron exporter FPN1 [9]. As mentioned previously, FPN1 transports iron in the  $\text{Fe}^{2+}$  state, which is the predominant form of cellular iron having passed through the lysosome [8]. However, serum TF binds only  $\text{Fe}^{3+}$  with high affinity. The major copper-containing protein in the body is ceruloplasmin (CP) which has potent ferroxidase activity [82]. CP oxidizes iron immediately after export via FPN1, allowing for prompt binding to TF, and genetic deficiency in CP causes aceruloplasminemia, which produces clinical symptoms very similar to hemochromatosis [83].

### 1.2.3 Mitochondrial Iron Homeostasis

A substantial proportion of cellular iron is shuttled into the mitochondria where it is used for Fe-S cluster biosynthesis and heme production [84]. Iron uptake into the mitochondria is mediated by Mitoferrin 1 and Mitoferrin 2 (MTFN1/2) [85]. MTFN1 expression is restricted to cells of the erythroid lineage while MTFN2 is expressed ubiquitously. Global knockout of MTFN1 results in embryonic lethality, while knockout in hematopoietic stem cells causes severe anemia [86]. Interestingly, although MFRN1 can compensate for MFRN2 deletion in fibroblasts, ectopic expression of MFRN2 in MFRN1-deficient hematopoietic cells failed to rescue defective heme synthesis and anemia [87]. The exact mechanism by which iron is brought in proximity to MFRN proteins expressed on the mitochondrial surface is still unclear. One potential mechanism is that MFRN imports labile iron available in the cytoplasm without the need for a specific protein carrier. However, due to the high reactivity of labile iron, cells actively restrict the size of the free iron pool [88]. Alternatively, microscopy experiments have demonstrated that endosomal-mitochondrial contact might facilitate transfer of labile iron [89]. In support of this mechanism, mutations in Sec15L1, an endosomal docking molecule, have been shown to cause defective hemoglobin production and anemia in mice as a result of the inability to utilize endosomal iron

[90, 91]. As was the case in the cytoplasm, the labile iron pool within in the mitochondria is kept at a minimum to prevent aberrant ROS production. This task is accomplished by the mitochondrial specific Ferritin (FTMT) which sequesters iron and aids in its proper delivery to different mitochondrial proteins [92]. Indeed, mutations in FTMT which prevent it from binding iron cause mitochondrial iron overload and reciprocal cytoplasmic iron deficiency, suggesting that FTMT not only stores iron but plays an active role in shuttling it to appropriate locations [93]. While export of iron across the cell membrane is facilitated by FPN, which transports labile iron, the mechanisms underlying mitochondrial iron efflux is more complicated. Thus far, no mechanisms for exporting labile iron have been identified. Instead mitochondria must export iron either in the form of Fe-S clusters, heme, or conjugated to glutathione. Iron export is mediated a family of ATP binding cassette proteins ABCB7, ABCB8 and ABCB10, which are localized to the mitochondrial membrane. ABCB7 and ABCB8 have been shown to be required for cytosolic Fe-S cluster maturation [94-96]. Depletion of either ABCB7 or ABCB8 causes mitochondrial iron-overload, ROS production, anemia (ABCB7), and cardiomyopathy (both ABCB7 and ABCB8) [95, 97]. Although the specific substrates for these proteins are unknown, the yeast homologue of ABCB7, Atm1p, has been shown to export Fe-S clusters conjugated to glutathione [98, 99]. It is still unclear if ABCB8 has any reliance on glutathione. ABCB10 is required for export of mitochondrial heme, although it does not transport heme itself, and ABCB10 knockout mice present with anemia and susceptibility to oxidative stress [100].

#### **1.2.4 Fe-S Cluster Biosynthesis**

Iron flux into the mitochondria is required to maintain cellular energy metabolism and anabolism due, in part, its incorporation into enzymes in the TCA cycle and ETC [101]. Mitochondrial aconitase, isocitrate dehydrogenase and succinate dehydrogenase accomplish their enzymatic reactions by coordinating electron transfer with an Fe-S cluster [101, 102].

Similarly, complex I, II and III contain Fe-S clusters, while complex II, III and IV and cytochrome C require heme [101, 103, 104]. Iron is present in both of these cofactors. Most iron containing enzymes utilize iron in the form of 2Fe-2S or 4Fe-4S clusters [105]. Fe-S cluster synthesis begins in the mitochondria as iron and sulfur are loaded onto the iron-sulfur cluster scaffolding protein (ISCU) [106]. Iron is delivered to ISCU by the carrier protein Frataxin (FXN) [107]. Mutations in ISCU cause a characteristic myopathy whose symptoms include exercise intolerance, fatigue and pain in working muscle [108, 109]. Expansion of a GAA tri-nucleotide sequence in the FXN gene causes an early onset neurodegenerative disease called Friedrich's Ataxia in which iron accumulation in dorsal root ganglia leads to neuronal cell death and disruption of motor function [110]. The vast majority of patients also develop cardiomyopathy due to direct damage to the myocardium [111]. After maturation on the scaffolding protein ISCU, Fe-S clusters are either inserted into mitochondrial proteins for use within the mitochondria or exported into the cytoplasm where they are inserted into cytoplasmic and nuclear targeted proteins via the cytoplasmic iron-sulfur assembly (CIA) system [96, 112]. Interestingly, mitochondria can only export mature Fe-S clusters bound to appropriate chaperones. Defects in mitochondrial Fe-S cluster protein assembly at any step causes accumulation of iron within the mitochondria and prevents downstream maturation of Fe-S containing extra-mitochondrial proteins. In addition to disruption of cellular processes mediated by cytoplasmic and nuclear Fe-S proteins, excess mitochondrial iron generates large quantities of ROS, which damages mitochondrial proteins and lipids leading to metabolic dysfunction and cell death. Most iron chelators such as deferoxamine (DFO) are only capable of chelating the labile iron pool and therefore cannot strip proteins of their Fe-S clusters. Instead iron chelation represses the levels Fe-S cluster-containing proteins by blocking the formation of assembly of Fe-S clusters. How cells match the levels of proteins destined to be fitted with Fe-S clusters when Fe-S cluster biosynthesis is impeded is still under investigation.

### 1.2.5 Heme Synthesis

Like Fe-S cluster biogenesis, the synthesis of the heme prosthetic group is a multi-step process with certain steps occurring exclusively within the mitochondria. In the first step of this process,  $\delta$ -aminolevulinic acid (ALA) synthase (ALAS) catalyzes the condensation of succinyl-CoA and glycine to generate the precursor to heme, ALA [113]. Mammals possess two copies of this gene which differ in their expression pattern. ALAS1 is expressed ubiquitously while ALAS2 is restricted to erythrocytes under basal conditions [114, 115]. Certain pathophysiological states such as ischemic injury and cardiomyopathy can aberrantly induce the expression of ALAS2 [50, 116]. Increased ALAS2 expression is associated with increased ROS mediated cell damage due to the excess iron housed within heme [116]. After synthesis, ALA is directly exported out of the mitochondria to the cytoplasm, where subsequent enzymatic reactions form coproporphyrinogen III (CPIII). Yet again, CPIII is imported back into the mitochondria to form protoporphyrin IX (PPIX). The final step of heme biosynthesis involves the insertion of iron into PPIX by the enzyme Ferrochelatase (FECH), which itself is a 2Fe-2S containing protein. Mature heme can then be incorporated into mitochondrial proteins such as Cytochrome-C in the respiratory chain or exported to the cytoplasm [117]. The primary mitochondrial heme transporter is thought to be FLVCR1b on the outer mitochondrial membrane, although direct transport of heme by FLVCR1b has never been demonstrated [118]. Like Fe-S clusters and labile iron, the iron stored within heme is essential to life sustaining enzymatic reactions. However unlike the iron coordinated within Fe-S clusters, heme containing iron readily produces ROS [119]. Therefore, the cell must find ways of quickly destroying excess heme to avoid oxidative damage. The enzymes Heme oxygenase 1 and 2 (HO-1/2) use oxygen to catalyze the cleavage of the heme ring to liberate iron and produce biliverdin and carbon monoxide [28, 120]. Biliverdin is then converted to bilirubin and excreted by body after

conjugation to glucuronic acid in the liver [121]. All cells express moderate levels of HO-2 which is responsible for baseline heme homeostasis. HO-1, on the other hand, is expressed at high levels only in splenic macrophages where senescent or damaged erythrocytes are recycled to recover iron. HO-2 expression can be induced by iron levels, oxidative stress, hypoxia, and a build-up of heme itself [116, 122-124]. Deletions or mutations in the enzymes involved in heme synthesis can collectively cause a family of diseases called porphyrias which can cause hemolytic anemia, and either nervous system involvement or cutaneous lesions depending on the etiology. Defects associated with ALAS2 or the mitochondrial glycine importer SLC25A38 specifically underlie a form of anemia called sideroblastic anemia in which nucleated, immature erythroblasts with perinuclear iron deposition are found by peripheral blood smear [125]. Anemias resulting from defects in heme synthesis do not respond to iron supplementation and treatment of cutaneous porphyrias, in fact, often involves phlebotomy to rid the body of excess iron.

### 1.2.6 Epigenetic Regulation

The regulation of gene transcription in response to fluctuations in iron levels is a critical aspect of cellular physiology. Methods mammalian cells employ to restore iron and redox homeostasis in response to iron insufficiency or overload will be explained in subsequent sections. Here, I would like to take the opportunity to briefly discuss the current knowledge pertaining to a large family of Jumonji-C (Jmj-C) domain-containing histone demethylases. This family of histone demethylases removes tri-di- and mono-methyl marks from a variety of lysine residues on histones 3 and 4 [126-129]. The impact of demethylase activity on gene transcription is mark dependent. H3K27me<sup>2/3</sup> and H3K9me<sup>2</sup> are classically associated with gene repression whereas H3K36me<sup>3</sup> is associated with active transcription [130]. Perhaps the most fascinating aspect about Jmj-C domain biology is that the demethylation reaction it catalyzes

requires molecular iron and  $\alpha$ -ketoglutarate [131]. The initial work done to characterize these proteins in purified systems even utilized iron chelators, such as DFO, to demonstrate their reliance on iron [132-134]. Despite their reliance on iron, there are currently no reports of Jmj-C domain-containing histone demethylases playing critical roles in regulating iron homeostasis or mediating adaptive processes in response to changes in iron levels. My work is the first to demonstrate a physiologic role for Jmj-C domain containing histone demethylases as cellular iron sensors linking iron levels to mTOR activity.

### **1.2.7 The IRP System**

The process of iron uptake, storage/mobilization and export must be tightly coordinated with cellular activity. Too little iron renders several anabolic processes and proliferation impossible while too much iron can lead to ROS production and death. Therefore eukaryotic cells have evolved a system of direct iron sensing that can in turn rapidly adjust intracellular iron handling to balance supply and demand. Yeast accomplish this task via transcriptional regulation. Sufficient iron levels sequester the transcription factor Aft1 in the cytoplasm [135]. When iron levels drop below threshold, Aft1 translocates to the nucleus and promotes the expression of genes involved in iron uptake and mobilization. Mammalian cells, however, do not possess a homolog of Aft1. Instead Mammalian cells express the Iron regulatory proteins 1 and 2 (IRP1/2) which control cellular iron handling post-transcriptionally. The IRPs bind to iron response elements (IREs) in either the 5'-untranslated region (UTR) or 3'-UTR of target mRNAs [136]. The specific sequences within the IREs allow the mRNA to adopt a unique secondary structure which can be recognized by the IRPs [137]. IRP1 is a bifunctional protein whose specific activity is dependent on whether it is bound to its Fe-S cluster. Holo-IRP1 functions as cytosolic aconitase and does not bind to mRNA. When iron levels drop, apo-IRP1 is formed and apo-IRP1 binds to IREs [138]. IRP2, however, is constitutively active, but its expression is

regulated by iron. In the presence of iron and oxygen, IRP2 is ubiquitinated and proteolytically degraded in a process dependent on FBXL5 [139, 140]. Binding of IRP1/2 to the 3'-UTR of a target transcript slows its degradation and allows for more protein to be translated, as is the case with TFR1. Increased levels of TFR1 bring more iron in from the extracellular space helping to restore normal iron levels. Contrastingly, binding of IRP1/2 to the 5'-UTR sterically blocks ribosomal entry and thus prevents translation. In this way, IRP1/2 repress the levels of FPN and FTN to retard iron export and mobilize iron stores, respectively [135]. When extracellular iron levels are sufficient, the combination of increased iron import, increased mobilization, and reduced iron export should temporarily normalize states of intracellular iron deficiency. As iron levels return to normal, IRP1 regains its Fe-S cluster and IRP2 is degraded, thus shutting off the system.

### **1.2.8 Alternative Pathways Involved in Iron Homeostasis**

For several decades, the canonical message of the field was that the IRP system was the sole mechanism by which mammalian cells relied on to achieve iron homeostasis. However, recent evidence has shown this is not the case. As discussed earlier, autophagy mediated degradation of FTN is just one example of IRP-independent methods of iron mobilization. Additionally, FPN1 expression can be transcriptionally induced in a heme-dependent manner [141]. Elevated heme levels induce oxidative stress to which cells respond by stabilizing a key factor in the antioxidant response pathways, Nuclear factor erythroid-like 2 (NRF2). Stabilized NRF2 subsequently translocates to the nucleus and promotes transcription of FPN1, FTN and HO-1, which contain antioxidant response elements in their promoters [142]. Additionally, heme has been shown to regulate translation through heme regulated eIF2 $\alpha$  kinase (HRI) [143, 144]. Induction of HRI by loss of heme prevents translation of globin proteins so as to match the levels of the two counterparts. Conversely, this same mechanism explains how increased heme

levels in erythroid progenitors promotes hemoglobin production and erythrocyte differentiation. Therefore, it is clear that auxiliary pathways have evolved to supplement the IRP system and expand the cells adaptive repertoire.

### **1.2.9 Iron Conservation**

Conditions of iron overload aside, the capability for the IRP and other auxiliary systems to maintain cellular iron levels during periods of deficiency is predicated on the assumption that there is sufficient extracellular iron available to be imported into the cell after all intracellular iron stores are mobilized. What if this were not the case, such as during prolonged periods of severe iron deficiency or when adjacent tissues are given priority over limited iron resources? Over the past decade, work by our lab and others has led to the identification of another major pathway that is engaged when the IRP system fails to maintain sufficient levels of iron [145, 146]. Our lab has termed this system the iron conservation pathway and it is orchestrated by the tandem zinc finger protein Tristetraprolin (TTP) [145]. Induction of TTP by low iron promotes an adaptive response that paradoxically represses TFR1 expression and instead alters how the cell consumes iron. Expression of TTP during iron deficiency is required for cell survival as TTP deletion in mouse embryonic fibroblasts (MEFs) and knockdown of TTP in cardiomyoblasts result in increased sensitivity to iron deficiency-induced cell death. This pathway is conserved all the way to yeast, in which two tandem zinc finger proteins, Cth1 and Cth2, carry out similar functions to TTP [147]. Unlike the IRP system, which regulates iron homeostasis by modulating the expression of genes that control the flux of iron directly, TTP and its yeast counterparts Cth1/2 bind to and promote the degradation of mRNA transcripts encoding proteins involved in a myriad of processes. Of these processes, TTP targets are enriched for Fe-S cluster-containing proteins. This ensures that when iron levels are limiting, excess apo-proteins are not produced and limited iron can be utilized by only the most essential proteins. However, the full

scope to which the iron conservation pathway mediated by TTP promotes cellular adaptation to iron deficiency remains largely unknown. The studies included in this dissertation constitute a major step in elucidating these processes.

### **1.3.0 General Regulation and Function of TTP**

To fully understand the role of TTP during iron deficiency, it is prudent to first familiarize oneself with the biology of TTP in general. TTP, also known as ZFP36, is a Cys-Cys-Cys-His (CCCH) tandem zinc finger (TZF) protein that binds to AU-rich elements (AREs) in the 3'-UTR of target mRNAs and promotes their degradation [148]. The minimal ARE sequence is five bases arranged as AUUUA, whereas optimal sequences are longer and flanked by additional uracils, UUAUUUAUU [149-151]. While hundreds of genes contain at least one ARE, the binding of TTP to any specific target appears to be cell-type and context specific. When TTP does bind to the ARE of a target transcript, it promotes recruitment of the deadenylation machinery and subsequent transcript decay [152]. TTP was first studied for its role in inflammation where high TTP expression in macrophages directly represses tumor necrosis factor (TNF)- $\alpha$  [153]. Global knockout of TTP in mice causes a severe systemic autoimmune inflammatory syndrome consisting of arthritis, hair loss, and cachexia [154]. TTP has also been implicated as a tumor suppressor gene through its role in regulating Cyclin-D1 and c-Myc [155]. Work from our lab has shown that TTP is a critical regulator of cellular iron conservation and metabolism [145]. In corroboration, studies involving the yeast orthologs of TTP, CTH1/2, have shown that CTH1/2 degrade several mRNAs involved in mitochondrial metabolic processes [147]. Interestingly, TTP also possesses AREs within its own 3'-UTR and is capable of a certain degree of autoregulation.

The upstream signaling pathways regulating TTP expression and function are less well understood. Although TTP has been shown to be heavily phosphorylated, the functional significance of these phosphorylation events are still debated [156, 157]. Transcriptionally, TTP responds to multiple environmental signals including inflammation, insulin, hypoxia, and mTOR inhibition [145, 158, 159]. Sequence analysis of the promoter and single intron of TTP has identified the presence of transcription factor binding sites for STAT3, EGR1, SP1, and TFAP2A (AP2) [160, 161]. While it has been shown that STAT3 mediates TTP's responsiveness to inflammatory signaling, all seem to play a partial role in the response by insulin [160, 162]. However, it is still unclear how iron deprivation, hypoxia and mTOR inhibition directly regulate TTP transcription. In terms of signaling iron deficiency, previous work has determined that inhibition of mTOR is a key upstream event, while the IRP1/2 and HIF1/2 pathways are not required [145]. Precise delineation of the process by which mTOR and TTP respond to iron deprivation is a major subject of my graduate work.

#### **1.4.0 Cellular Control of mTOR Function**

##### **1.4.1 mTOR Regulates Cellular Anabolic Pathways**

mTOR largely exists as one of two complexes that govern cellular growth and metabolism. Members of both complexes and the key proteins that control their activity are highly enriched as tumor suppressors and oncogenes, underscoring their critical importance. The rapamycin sensitive mTORC1 complex, defined by the presence of the protein cofactors RAPTOR, DEPTOR, mLST8, and PRAS40, is a serine threonine kinase that is a master regulator of the switch between anabolism and catabolism [163, 164]. mTORC2 is a rapamycin insensitive complex containing RICTOR, PROTOR, mSIN1, DEPTOR and mLST8 that regulates AKT signaling, actin polymerization and cell survival pathways [165, 166]. When

activated at the lysosome by GTP-bound RHEB, mTORC1 autophosphorylates at Ser2481 and engages the cell in protein synthesis, lipogenesis and ribosome biogenesis [167, 168]. Active mTORC1 binds to and phosphorylates p70 S6 Kinase (S6K) at Thr389 which, in turn, phosphorylates mTOR at Ser2448, establishing a reinforced loop necessary for mTOR's activation by growth factors [169, 170]. Phosphorylated S6K subsequently engages ribosomal protein S6 (S6) at five sites, including Ser235, promoting its activity and ribosomal biogenesis [171]. The second of mTORC1's effectors is Eukaryotic translation initiation factor 4E- (eIF4E) binding protein 1 (4E-BP1). Unlike S6K, mTORC1 phosphorylation on 4E-BP1 at Thr70 inhibits its function [172]. By binding eIF4E, 4E-BP1 sequesters it away from the ribosome and blocks cap-dependent translation [173]. A critical subset of 4E-BP1 dependent genes encode mitochondrial proteins involved in ATP production [174]. Thereby, mTOR is able to coordinate cellular energy production with translation. In addition to protein anabolism, growing cells require the synthesis of new lipids to facilitate expansion of membranes. mTOR positively regulate the sterol regulatory element binding protein 1 and 2 (SREBP1/2) and peroxisome proliferation-activated receptor gamma (PPAR $\gamma$ ), the two key regulators of lipogenesis [175, 176]. Due to its role in regulating pathways that consume massive amounts of energy and resources, the eukaryotic cells have evolved multiple, intersecting layers of regulation that match mTOR activity with active substrate and energy sensing.

#### **1.4.2 Nutrient Sensing by mTOR – The RAG Pathway**

The mechanistic target of rapamycin (mTOR) is a master regulator of protein synthesis, glucose metabolism and autophagy and its activity is fine-tuned by the levels of amino acids, ATP, purines, oxygen and growth factors. The amino acids leucine and arginine govern mTOR activity by controlling its translocation to the lysosome and subsequent activation by RHEB [164, 177]. Because mammalian cells cannot synthesize leucine, it must be imported into the cell.

Multiple amino acid transporters can import leucine and other neutral amino acids across the plasma membrane. The major family of leucine transporters include the four L-type neutral amino acid transporters (SLC7A5, SLC7A8, SLC43A1-2; better known as LAT1-4). LAT1 is highly expressed in fibroblasts while LAT3 is the dominant leucine transporter in the liver [178, 179]. Both LAT1 and 3 are commonly overexpressed in cancers to facilitate mTOR-mediated anabolic metabolism. In the presence of leucine, inhibition of the GATOR2 complex by SESTRIN is prevented, allowing the GATOR1 complex to act as a GTP-ase activating protein (GAP) on the heterodimer RAG A/B proteins [180, 181]. Similarly, the FLCN-FNIP complex is a GAP for RAG C/D, the other half of the RAG GTP-ase complex, which shuttles to the lysosome in the absence of amino acids [182]. Active RAG A/B or C/D are then able to recruit mTOR to the lysosome where RHEB resides [183]. The GATOR2 complex consists of Mios, WDR24, WDR59, Seh1L, and Sec13. The GATOR1 complex includes DEPDC5, Npr12 and Npr13 and functions as a tumor suppressor [184]. Genetic loss of GATOR1 or DEPDC5 have been shown to constitutively activate mTOR and confer resistance to amino acid deprivation [180, 185]. Arginine sensing involves both the CASTOR complex and SLC38A9, which function through distinct mechanisms to control mTOR activity at the lysosome. CASTOR, like the SESTRINs, inhibits GATOR2 to activate the RAG complex [186]. SLC38A9 is embedded within the lysosomal membrane and senses lysosomal arginine directly. Regulation of the RAG proteins by SLC38A9 is dependent on its ability to bind arginine and on the activity of the vacuolar H<sup>+</sup> ATPase [187, 188]. Additionally, SLC38A9 can efflux leucine from the lysosomal lumen in an arginine dependent manner, thereby controlling RAG activity indirectly through the GATOR complex [189]. Depletion of SLC38A9 or expression of mutant SCL38A9<sup>T133W</sup> causes intralysosomal accumulation of multiple essential amino acids and sensitizes cells to amino acid deprivation by preventing arginine transport and recycling of leucine generated from lysosomal proteolysis. A second pathway for amino acid sensing involves surveillance of tRNAs by GCN2.

Accumulation of uncharged tRNAs during amino acid deprivation activates GCN2 which subsequently phosphorylates eIF2 $\alpha$  at Ser51 to prevent translation initiation [190, 191]. While phosphorylated eIF2 $\alpha$  blocks general translation, thereby slowing the rate of amino acid utilization, it still allows for the select translation of ATF4 [192]. Sestrin2 was identified as a transcriptional target of ATF4, extending regulation of GCN2 to mTOR to further repress translation and engage autophagy [193]. Interestingly, another transcriptional target of ATF4 is LAT1, whose expression would help rectify the loss of leucine [194]. In light of this information, it is feasible that both iron and amino acids can potentially regulate mTOR through a common mechanism involving ATF4.

#### **1.4.3 Nutrient Sensing by mTOR – The TSC2 Pathway**

In a separate pathway, growth factors, ATP levels, hypoxia, and purine levels are signaled to mTOR through Tuberous Sclerosis Complex (TSC1/2), which acts as GAP to negatively regulate RHEB at the lysosome [195-197]. Insulin, via PI3K, stimulates activity of AKT which subsequently phosphorylates TSC2 at residue Ser939 [198]. Phosphorylated TSC2 is unable to complex with RHEB, prolonging the RHEB-GTP bound state. Insulin mediated sustainment of RHEB-GTP is associated with phosphorylation of mTORC1 at Ser2448 and its activation. Interestingly, although amino acids can activate mTORC1 even in the absence of growth factors, growth factors require amino acids to activate mTOR. Activation of AMPK by glucose deprivation or loss in ATP/AMP ratio can inhibit TSC2 by phosphorylating it at Ser1345, similar in mechanism to AKT [199]. Additionally, AMPK can inactivate mTOR directly by phosphorylating RAPTOR at Ser792 [200]. The mechanism by which hypoxia regulates mTOR is still under debate. There is evidence to support that hypoxia induces the transcription of REDD1 which, in turn, binds 14-3-3 proteins and dislodges TSC2 [201]. Free TSC2 is then capable of negatively regulating RHEB and preventing mTORC1 activation. However, a major

caveat to these findings was that differential localization of TSC2 and mTOR at the lysosome was never shown. Finally, recent work shown the mTORC1 is also sensitive to purine levels, specifically adenine and guanine [202, 203]. Both acute and chronic deprivation of adenine and guanine disrupt the TSC2-RHEB axis. Inhibition by prolonged deprivation resulted in a significant down regulation of RHEB protein levels, which were partially rescued by readdition of guanine. Interestingly, acute readdition of adenine was sufficient to restore mTORC1 activity, although the mechanism isn't fully understood. Together these pathways collaborate to ensure the balance between anabolic and catabolic pathways are tethered to environmental conditions and substrate availability.

#### **1.4.4 General Mechanisms of Autophagy**

Through a process called autophagy, nutrient poor conditions push cells towards catabolism of excess macromolecules thereby liberating amino acids, lipids and other substrates [204]. Autophagy requires the formation of specialized double-membraned organelles called autophagosomes and the formation of which is mediated by a family of Autophagy-regulated proteins (ATGs). Autophagosome formation is a step-wise process beginning with initiation, nucleation and expansion [77]. After ingestion of desired cargo, autophagosomes fuse with lysosomes to allow for proteolytic and chemical cleavage of a wide variety of substrates [205]. The kinase mechanistic target of rapamycin (mTOR) is the master switch controlling autophagy initiation and therefore conditions that contribute to mTOR inhibition generally promote autophagy. Classic examples of this would be amino acid deprivation, hypoxia, and a decrease in cellular ATP/AMP ratio. Loss of mTOR activity alleviates repressive phosphorylation of Unc-51 like kinase (ULK1; Atg1 in yeast) at Ser757 which subsequently allows for recruitment and assembly of the initiation complex containing ATG12, FIP200, and ATG101 [77, 206]. Alternatively, AMPK can phosphorylate ULK1 directly at

Ser317, Ser555, and Ser777 when activated by low-glucose or low ATP, bypassing mTOR [206]. Next, during the nucleation stage, the activated ULK complex engages a class III PI3K complex consisting of Beclin1 (Atg6 in yeast), VPS15, VPS34 and ATG14 [207]. This class III PI3K complex generates local production of PiP3 that is specific to autophagosomes. Beclin1 contains a Bcl-2-homology (BH3) domain and a coiled-coiled domain (CCD) which facilitate its interactions with various partners and determines its function. Inactive Beclin1 associates with Bcl-2/X<sub>L</sub> through its BH3 domain and forms homodimers through interaction of their CCDs. Phosphorylation of Beclin1 at Thr108 by Mst1 promotes association with Bcl-2/X<sub>L</sub> and represses autophagy [208]. Conversely, phosphorylation at Ser14 by ULK1, or Ser93 and 96 by AMPK, directly activates Beclin1 to promote its interaction with the CCD on ATG14 [209]. During the final expansion stage, a complex comprising of ATG12, ATG5, and ATG16 is recruited to the autophagosome membrane where it facilitates the maturation of microtubule-associated protein 1 light chain 3 (MAP1LC3; also known as LC3) via lipidation with phosphatidylethanolamine [210]. Conversion of LC3I to LC3II (lipidated) is one of the essential methods for binding autophagic membrane around cargo targeted for degradation. Alternative methods for cargo recognition also exist. Misfolded proteins can be recognized and directly shuttled to the lysosome via the chaperone Heat-shock cognate 70KD protein (HSC70) [211]. Additionally, while LC3II mediated autophagy is dependent on ATG5 and ATG12, distinct autophagic vesicles derived from RAB9<sup>+</sup> membrane can engulf cargo via a MAPK14 dependent mechanism without engaging LC3 lipidation [212]. Recent work suggests that mitophagy occurs predominantly via the RAB9 alternative pathway [213], however my data clearly shows that the pathway by which mitophagy proceeds is context dependent.

#### **1.4.5 Regulation of Mitochondria Dynamics and Mitophagy**

Mitochondria are dynamic structures and have the ability to fuse and divide, resulting in a chronic remodeling of their tubular networks. These processes are called fusion and fission, respectively. Mitochondrial dynamics are crucial for the health of the eukaryotic cells, and their disruption is associated with a number of genetic disorders [214, 215]. It did not escape our attention that a major intersection between iron, TTP and mTOR are their abilities to each individually regulate mitochondrial metabolism and function. However, there has been minimal understanding of how these three molecules might work together in a single pathway and if this connection contributes to iron conservation. Although the functional significance is unknown, an interesting feature of iron deprivation is its ability to induce mitochondrial fission. Several GTPase proteins regulate the process of mitochondrial fission and fusion, and are grouped into three groups: 1) mitofusins (MFN1/2), 2) OPA1/MGM1, and 3) DRP1/DNML1. MFN1 and MFN2 are membrane-anchored dynamin proteins that mediate fusion between mitochondrial outer membranes [216]. MFN2 also has a role as a mitophagy receptor and permits docking of PARKIN [217]. The biology of OPA1 is more complicated with multiple isoforms generated by alternative splicing and two sites of proteolytic cleavage that combined generate at least 5 protein isoforms discernable by gel electrophoresis [218, 219]. Long form OPA1 (l-OPA1), together with the cleavage product from S1, mediate fusion between mitochondrial inner membranes. Of the two cleavage sites, S1 resides in exon 5 and S2 resides in an alternative exon 5b. Short form OPA1 (s-OPA1) alone has no fusion activity. The balance between l-OPA1 and cleavage at S1 or S2 is dependent on adjacent exons, the activity of different mitochondrial proteases, and mitochondrial health. Inclusion of exon 4b dramatically increases the rate of proteolytic cleavage when next to the S1 site in exon 5, thus promoting exclusive production of s-OPA1 and mitochondrial fission. The i-AAA mitochondrial protease YMEL1, is responsible for basal cleavage at the S2 site. Although the activity of YMEL1 increases with mitochondrial stress, another protease OMA1 is stabilized by mitochondrial depolarization and promotes

cleavage at the S1 site [220]. Active mitochondrial fission is accomplished by phosphorylation dependent oligomerization of DRP1 together with the mitochondrial fission factor MFF and FIS1, which leads to the "pinching-off" of the outer mitochondrial membrane and mitochondrial fission [221, 222]. As the result of normal metabolic wear and tear or toxic insults, mitochondrial components can become damaged and proper quality control is required for maintaining mitochondrial function. The damaged parts of mitochondria are compartmentalized into specific domains that are later pinched off from the network through fission, followed by recycling through mitophagy [223]. After fission, multiple adaptor proteins can bridge damaged mitochondria with the autophagosome, including PARKIN/PINK1, BNIP3, FUNDC1, and ATG32 [224]. Although it is still unclear which adaptor proteins mediate mitophagy during iron deficiency, disruption of effective fission and mitophagy can eventually lead to mitochondrial dysfunction and cell death. Antecedent mitochondrial fission is, in fact, required for effective mitophagy and is governed by a variety of signals including mitochondrial membrane depolarization and AMPK activity [225, 226]. Recent microscopic evidence revealed that the process of mitochondrial fission is dependent on mitochondrial-lysosomal contacts, which are the physical location of fission initiation. Recruitment of lysosomal TBC1D15, a RAB7 GTPase-activating protein, by FIS1 is needed to initiate mitochondrial fission [227]. Although the close physical association of mitochondria with lysosomes suggests the possibility of bidirectional signaling, it is still unknown if alteration in mitochondrial dynamics is required for lysosomal maturation.

#### **1.4.6 The Link Between mTOR, Mitochondria, and Cellular Nutrients**

Under optimal conditions, mitochondria require a substantial proportion of the cellular iron pool to sustain metabolic activity and deliver ATP and other metabolites to the cytoplasm. However, in the absence of iron, non-functional mitochondria represent a substantial depot of

molecular building blocks for the cell to recycle via mitophagy. As mentioned, the same inducers of mTOR inhibition and autophagy, such as nutrient deprivation and hypoxia, also cause mitochondrial fission [213, 228, 229]. However, no unified mechanism directly linking these two processes has been elucidated nor is it known if this coordination is required for all forms of starvation induced autophagy. We hypothesized that mTOR mediated regulation of TTP, which targets multiple mitochondrial proteins, could be the missing link.

### **1.5 Highlight of Current Studies**

Integration of diverse environmental cues is indispensable for both unicellular and multicellular organisms to appropriately modulate life processes. Of these processes, those involved in energy metabolism and macromolecule synthesis are paramount and require robust mechanisms of substrate sensing. Although all cells depend on iron for survival, it is still unclear how iron sensing is achieved and integrated with other nutrient signals to control critical cellular functions. Additionally, the mechanisms underlying how distinct organelles are regulated to elicit a unified response to nutrient starvation are poorly understood.

1. Determine the mechanism by which iron deprivation regulates mTOR activity.
  - mTOR has been shown to be regulated by growth factors, amino acids, hypoxia, ATP, and purines. However, it is still unknown whether iron deprivation inhibits mTOR via one of these conserved pathways or through an as yet undiscovered pathway. I used extensive genetic, pharmacologic and imaging techniques to definitively show that mTOR senses iron levels through an amino acid dependent mechanism. Additionally, I show that the regulation of amino acid homeostasis

downstream of iron is accomplished through a novel role for Jmj-C domain-containing histone demethylases as cellular iron sensors.

2. Identify a novel role for TTP in regulating mitochondrial dynamics.
  - Previous work from our lab and others has already identified TTP as key player in iron conservation. However, the full extent to which TTP regulates cellular physiology to achieve this goal remains unclear. I have identified a novel role for TTP in mediating mitochondrial fission in response to mTOR inhibition through posttranscriptional regulation of the mitochondrial fusion gene OPA1. Importantly, deletion of TTP blocks mitochondrial fission, thereby preventing recycling of damaged mitochondrial components by mTOR mediated mitophagy. Additionally, the studies contained within this thesis answer a critical debate within the field of autophagy, namely whether concurrent mitochondrial fission is necessary to facilitate autophagosomal maturation and general autophagy. At least within the context of iron deficiency and direct pharmacologic inhibition of mTOR, this is not the case.
  
3. Establish the mTOR-TTP axis as critical component of iron conservation by preserving mitochondrial metabolism in response to iron deficiency.
  - Without TTP to promote mitochondrial fission and mitophagy during iron deficiency, mammalian cells cannot mitigate mitochondrial damage resulting in TCA cycle dysfunction and altered glucose metabolism. Using an *in vivo* iron deficiency protocol on mice with liver-specific deletion of TTP, I demonstrate that deficient mitochondrial metabolism results in defective hepatic gluconeogenesis during fasting.

## Chapter 2

### Results

#### **2.1 Iron deprivation inactivates mTOR through changes in leucine homeostasis.**

To study the mechanism by which mTOR senses cellular iron levels, we used deferoxamine (DFO) and 2,2'-bipyridyl (BPD), two iron chelators with distinct structures, and measured multiple downstream effectors of mTOR function, including p70S6 Kinase (S6K) and TTP expression. Iron chelator treatment in MEF cells resulted in a reduction in cellular iron and increased *Ttp* mRNA expression within 24 hours in a dose dependent manner (Fig. 1A, Fig. 2A-B). Inhibition of mTOR by iron chelation constituted a late process beginning at 12 hours and extending through 24 hours (Fig. 1B). This late regulation was not due to ineffective iron chelation as DFO induced the expression ATF4 (a stress response gene whose translation is repressed by iron-containing heme) (Fig. 1B). Iron chelation resulted in a reduction in protein synthesis in HEK293T cells, functionally confirming mTOR inhibition (Fig. 1C). To avoid the potential influence of iron chelation on the uptake of radioactive methionine into the cell, we performed this experiment by preloading the cells with <sup>35</sup>S methionine and then chasing in cold media with or without DFO. An increase in <sup>35</sup>S methionine enrichment in the protein fraction indicates reduction in new protein synthesis which would incorporate non-radioactive <sup>32</sup>S methionine and dilute the radioactive signal. Additionally, the response of *Ttp* to iron deficiency was not specific to rapidly dividing, immortalized cells which have high rates of iron turnover, as freshly isolated non-dividing primary murine hepatocytes also increased *Ttp* expression in response to iron chelation (Fig. 2C).

Reduction in S6K phosphorylation and protein translation with DFO suggests that iron chelation selectively inhibits the mTORC1 complex. To confirm this, we knocked down the rapamycin-insensitive companion of mTOR (RICTOR), an obligatory component of mTORC2, and exposed the cells to iron chelation. RICTOR knockdown had no effect on *TTP* induction by iron chelation, suggesting an mTORC1-dominated pathway (Fig. 2D). We next studied which of the substrate sensing pathways is responsible for the inhibition of mTORC1 during iron deprivation by systematically removing key elements of each pathway. While *TTP* expression is regulated by mTOR, the existence of a potential feedback loop to modulate mTOR input has not been investigated. We first confirmed that mTOR inhibition by iron chelation was not dependent on *TTP* (Fig. 2E). MEFs with *Tsc2* deletion displayed loss of *Ttp* expression at baseline, consistent with mTOR hyper-activation (Fig 2F). However, these cells still demonstrated reduced pS6K levels and increased *TTP* levels under iron chelation (Fig. 2F,H). Deletion of the catalytic alpha subunits of AMP-activated protein kinase (AMPK) in MEFs (*Ampka1/a2* dKO; termed *Ampk* KO) also did not prevent mTOR inhibition by iron chelation and resulted in super-induction of *Ttp* (Fig. 2G,H). Additionally, our previously published data has shown that *TTP* induction is not dependent on hypoxia inducible factors (HIF) 1/2 signaling [145]. Therefore, our data indicate that none of the growth factor and energy signaling pathways upstream of mTORC1 are necessary or sufficient for the inhibition of mTOR by iron loss. We next turned our attention to the remaining branch of mTOR signaling and investigated the effect of cellular iron on amino acid homeostasis and its sensing upstream of mTOR.

We profiled the concentrations of 16 amino acids before and after iron chelation to determine which one(s) are regulated by iron. Iron chelation decreased the total cellular amino acid pool, with the greatest reductions occurring in the essential branched-chain amino acids leucine and isoleucine, and phenylalanine (Fig. 2I-J). Consistent with iron deprivation, total

amino acid deprivation increased *Ttp* expression (Fig. 1D). Since leucine is a potent activator of mTOR and must be taken up by cells, we tested whether iron chelation specifically disrupts leucine import. We first profiled the expression of the L-type neutral amino acid transporter (LAT) family members, which are the dominant leucine importers in non-neural tissues. Only *Lat3* was consistently repressed by iron deficiency in MEFs, HepG2 cells, and murine livers (Fig. 2K). Importantly, LAT3 is the dominant family member in the liver suggesting that repression by iron chelation might have functional significance (Table 1). Iron chelation significantly reduced intracellular levels and uptake of radioactive leucine across the cell membrane (Fig. 1E-F), which was both independent of TTP and not a direct result of mTOR inhibition (Fig. 2L-M). Consistent with loss of amino acid signaling, iron chelation caused dissociation of mTOR from the lysosome, as evidenced by loss of colocalization of mTOR with the lysosomal marker LAMP2 at 24 hours (Fig. 1G-H). Leucine can also be effluxed from the lysosome in an SLC38A9 dependent manner leading to mTOR recruitment and activation [189]. However, *Slc38A9* expression did not change with iron chelation in either WT or *Ttp* KO MEFs (Fig. 2N). Similarly, we did not observe lysosomal leak as inferred from equivalent acridine orange fluorescence before and after iron chelation (Fig. 2O-P). To independently confirm our findings, we constructed a luciferase reporter driven by a minimal mouse *Ttp* promoter and first intron as a read-out of mTOR activity (Fig. 2Q). HEK293T cells co-transfected with the luciferase reporter and constitutively active RAG B\*/C\* proteins, which preserve mTORC1 activity in the absence of amino acids, resulted in mTOR hyper-activation and blunting of luciferase induction by iron chelation (Fig. 1I, 2R). On the other hand, overexpression of RHEB, which maintains mTOR activity in the absence of growth factors, but not amino acids, did not block induction of luciferase by iron chelation, confirming our previous experiments using *Tsc2* KO MEFs (Fig. 2S-T). Thus, our data suggest iron chelation causes a primary deficit in amino acid signaling by restricting leucine uptake from the extracellular environment.

We then studied whether restoring leucine levels was sufficient to rescue the loss of mTOR activity downstream of iron deficiency. Co-administration of cell-permeable leucine (LLOME), but not standard leucine, with DFO for 24 hours partially rescued the loss of S6K phosphorylation and mitigated *Ttp* induction (Fig. 1J-L), underpinning a role for leucine import in the regulation of mTOR with iron chelation. A central feature of mTOR regulation by amino acids is the speed by which addition of amino acids is able to reconstitute mTORC1 activity after deprivation.

## **2.2 Iron sensing by Jumonji-C histone demethylases controls amino acid signaling and represses mTORc1.**

Since cell-permeable leucine supplementation only partially rescued mTORC1 inhibition, we turned our attention to the core mTORC1 machinery and investigated whether the expression of regulatory associated protein of mTOR complex 1 (gene: *RPTOR*), which encodes the protein RAPTOR, the defining structural component of the mTORC1 complex, was regulated by iron. *RAPTOR* expression was strongly downregulated by iron chelation in HEK293T cells (Fig. 3A). Re-expression of WT RAPTOR was insufficient to reverse *TTP* induction under iron deficiency, consistent with a concurrent decrease in leucine levels under these conditions (Fig 3B, 4A). On the other hand, the induction of *TTP* by iron deficiency was partially rescued in cells overexpressing RAPTOR-RHEB15, a modified form of RAPTOR that is permanently associated with the lysosome and therefore renders mTORC1 resistant to both amino acid deprivation and loss of endogenous RAPTOR (Fig. 3B, 4A).

Our data demonstrating that 1) the increase in expression of ATF4, a major driver of *LAT3* transcription, was discordant with the effect of iron chelation to repress *LAT3* (Fig. 1B)

and 2) *RAPTOR*, a gene located on a different chromosome from *LAT3*, was simultaneously repressed by iron chelation (Fig. 3A), led us to hypothesize that iron chelation may mediate epigenetic silencing of these genes through a single common mechanism. Jumonji-C domain containing (JmjC) histone demethylases require iron in the form of  $\text{Fe}^{2+}$  to remove methyl groups from a variety of histone substrates, including activating marks at H3K36 and repressive marks at H3K9 and H3K27. Because we observed loss of *LAT3* and *RAPTOR* expression with iron chelation, we focused our attention on the repressive histone marks H3K9me<sup>2/3</sup> and H3K27me<sup>3</sup>. We observed a global increase in H3K9me<sup>2</sup> and H3K27me<sup>3</sup> marks, but minimal change in global H3K9me<sup>3</sup> levels in cells exposed to iron chelation for 24 hours (Fig. 3C-D). Chromatin immunoprecipitation (ChIP)-PCR demonstrated that iron chelation significantly increased H3K9me<sup>2</sup> methylation at the promoters of *LAT3* and *RAPTOR*, but neither loci had detectable H3K27me<sup>3</sup> methylation at baseline nor did they become hypermethylated at H3K27 after iron chelation (Fig. 3E and Fig. 4B-F). We confirmed the activity of our H3K27me<sup>3</sup> antibody by examining a neighboring gene, *NPTX1*, which is predicted to be hypermethylated at baseline, and confirmed strong enrichment compared to IgG (Fig. 4G). To directly test whether H3K27me<sup>3</sup> and H3K9me<sup>2</sup> methylation contributed to iron deprivation mediated mTOR inhibition, we incubated HEK293T cells with GSK-J4 or JIB-04, pharmacologic inhibitors of JmjC-domain histone demethylases with biased activity at H3K27me<sup>2/3</sup> and H3K9me<sup>2</sup> marks, respectively [230, 231]. Incubation with either GSK-J4 or JIB-04 led to marked reduction in *RAPTOR* expression, loss of S6K phosphorylation, and induction of *TTP* (Fig. 3F-I). Conversely, co-administration of the EZH1/2 methyltransferase inhibitor 3-Deazaneplanocin A (DZNep) with DFO partially blocked *RAPTOR* repression and *TTP* induction by DFO (Fig. 3J-K). Administration of UNC-0642, a G9a and GLP specific methyltransferase inhibitor, had no effect on *RAPTOR* repression or *TTP* induction (Fig. 3J-K). Based on this data, we subsequently

focused on the role of H3K27me<sup>3</sup> demethylation in mediating the effect of iron chelation on mTORC1 activity.

### **2.3 Iron deficiency alleviates repression of TTP by the transcription factor SP1**

Mammalian cells do not possess a homolog to yeast Aft1 nor has a directly iron-sensing transcription factor been identified. Previous work has demonstrated that transcriptional upregulation of TTP in response to iron deficiency is independent of HIF signaling [145]. To identify the transcription factor responsible for TTP expression during iron deficiency, we took advantage of the 137bp *Ttp*-promoter luciferase construct we generated which possessed consensus sequences to EGR1, STAT3, SP1, and AP2 (Fig. 5A). We deleted or mutated each binding site individually and measured their response to iron chelation when expressed in HEK293T cells (Fig. 5B). Deletion of EGR1 and mutation of STAT3 had no effect on induction of the luciferase signal by DFO. However, induction was lost in the SP1 and AP2 deleted constructs, suggesting SP1 and AP2 might mediate the transcriptional response to iron chelation. Since promoter-bashing experiments can result in false positive results due to unforeseen effects on cis-acting elements within the promoter, we directly tested whether the function of SP1 and AP2 changed with iron deficiency. Cell fractionation revealed that iron deficiency induced translocation of SP1 and AP2 out of the nucleus (Fig. 5C-D). While iron chelation reduced total SP1 expression, expression of AP2 remained unchanged (Fig. 5E). SP1 and AP2 have been shown to act as a heterodimer to negatively regulate gene expression. We therefore reasoned that modulation of SP1 expression was the dominant factor mediating TTP induction by iron chelation. Knockdown of SP1 resulted in enhancement in *TTP* expression over non-targeting control (Fig. 5F-G). Conversely, overexpression of SP1 strongly suppressed *Ttp*-promoter driven luciferase expression and blocked induction by iron chelation (Fig. 5H-I).

Together, these data suggest that de-repression of the *TTP* promoter by SP1 and AP2 mediate the TTP transcriptional response to iron deficiency.

#### **2.4 mTOR regulates both mitochondrial dynamics and mitophagy through the TTP-OPA1 axis.**

We next investigated the physiological consequences of this novel mTOR pathway. Although mTOR has pleiotropic effects on protein synthesis, purine metabolism, and cell growth, we chose to focus on its regulation of autophagy. We did so particularly for autophagy's connection with mitochondrial fission and metabolism. Although it is possible that mitochondrial fission and autophagy represent separate phenomena, their concordant timing, together with TTP being an mTOR response gene with multiple mitochondrial targets, led us to hypothesize that mTOR regulates autophagy through a TTP-dependent pathway. We first performed an *in silico* analysis for the presence of TTP binding sequences (AREs), in the 3'UTRs of mRNAs involved in mitochondrial dynamics and autophagy (Fig. 7A). Eight genes with strong ARE sequences in both the mouse and human isoforms were identified (Fig. 7A, green arrows). Because TTP is an obligatory negative regulator of mRNA expression and its deletion would result in increased levels of target transcripts, we excluded *Atg32*, *Atg13* and *Atg16l*, whose repression are required to produce an autophagy phenotype [232]. On the other hand, increased expression of genes involved in mitochondrial dynamics or biogenesis could significantly alter the balance between mitochondrial fission and fusion. We measured the baseline expression of the remaining five genes in WT and *Ttp* KO MEFs. Three genes (*Opa1*, *Mfn1*, *Pgc1 $\alpha$* ) had increased expression in *Ttp* KO cells (Fig. 6A), suggesting potential direct regulation by TTP. Using RNA co-immunoprecipitation, we demonstrated that the transcripts for *Opa1* and *Mfn1*, but not *Pgc1 $\alpha$* , directly bind to TTP (Fig. 6B); thereby eliminating *Pgc1 $\alpha$*  as a target. Overexpression of WT, but not a tandem zinc finger mutant version of TTP (C124R)

incapable of binding RNA, resulted in suppression of the mRNA levels of *OPA1* and *MFN1* (Fig. 6C), confirming regulation by TTP. Consistent with the canonical role of TTP in destabilizing mRNA, *Opa1* and *Mfn1* mRNA levels were stabilized in *Ttp* KO MEFs, and DFO treatment resulted in repression of *Opa1* and *Mfn1* expression in a dose-dependent fashion in WT but not *Ttp* KO MEFs (Fig. 6D-I, 7B-C). The fission and fusion dynamics mediated by *Opa1* are also regulated by alternative splicing of the *Opa1* transcript. We did not observe any difference in splice isoforms in WT MEFs after treatment with DFO by western blot or qRT-PCR (Fig. 6H, PCR data not shown). Live confocal microscopy of MEFs exposed to iron chelation and stained with mitotracker green showed that WT mitochondria undergo extensive fission at 12 hours, while *Ttp* KO MEFs have hyper-fused mitochondria at baseline and are unable to undergo fission in response to iron deprivation (Fig. 6J-K). These results were replicated by administration rapamycin, supporting that mTORC1 inhibition and subsequent upregulation of TTP mediates the effect of iron chelation on mitochondrial dynamics (Fig. 7D-E). We also performed individual knockdown of *Opa1* and *Mfn1* to identify the primary target of TTP responsible for mitochondrial fission. *Opa1* KD restored robust mitochondria fission in *Ttp* KO MEFs with iron chelation, suggesting a central role for repression of *Opa1* mRNA in mediating altered mitochondrial dynamics during iron deprivation (Fig. 6L-M, 7F-G). On the other hand, downregulation of *Mfn1* failed to induce mitochondrial fission in *Ttp* KO MEFs after exposure to DFO (Fig. 7H-I).

To determine whether the inability to commence mitochondrial fission in *Ttp* KO cells resulted in a selective deficit in mitophagy or defective mTOR-mediated autophagy in general, we first assessed the levels of multiple markers of mitophagy in cells exposed to iron deficiency for 18 hours, 6 hours after we first observed mitochondrial fission. *Bnip3* expression, increased robustly in WT MEFs exposed to iron chelation but its induction was significantly blunted in *Ttp*

KO MEFs (Fig. 8A). Similarly, the levels of the mitochondrial membrane protein VDAC decreased in WT MEFs exposed to iron chelation but were abrogated in *Ttp* KO MEFs (Fig. 8B-C). We found that iron chelation caused induction of both mitophagy and general autophagy, indicated by increased expression and phosphorylation of BECLIN1 and decreased expression of autophagy substrates p62 and total LC3 (Fig. 8B-C, 9D). The failure to observe LC3II conversion by Western blot at 18 hours was verified by the absence of GFP<sup>+</sup> puncta in iron deficient cells overexpressing GFP-LC3 (Fig. 9A-C). In contrast, administration of doxorubicin, an mTOR independent inducer of mitophagy, significantly increased the number and size of GFP-LC3 puncta (Fig. 9A-C). Concomitant inhibition of lysosomal acidification using bafilomycin-A in iron deficient cells allowed for better visualization of total LC3 levels and brought out the conversion of LC3I to LC3II, confirming increased autophagic flux (Fig. 9D-E). Although basal levels of LC3 and p62 differed between WT and *Ttp* KO cells, the fold changes in LC3II/LC3I ratio and total p62 levels in response to iron chelation were consistent between cell types. To directly visualize mitophagy, we generated WT and *Ttp* KO MEFs stably expressing a mitochondria-targeted red fluorescent protein (mitoDS-Red) and live stained them with the lysosomal marker, lysotracker green (Fig. 8D). When exposed to iron chelation, WT MEFs had a nearly 3 fold increase in the number of mitochondria overlapping with lysosomes, while no change was observed in *Ttp* KO MEFs (Fig. 8F). Similarly, lysosomal size increased significantly in iron deficient WT MEFs only, consistent with engulfment of bulky mitochondrial fragments (Fig. 8E). Restoration of appropriate mitochondrial fission by *Opa1* KD was sufficient to rescue both mitochondrial-lysosomal colocalization and increased lysosomal size in *Ttp* KO MEFs (Fig 8D-F). Together, these data outline a fundamental pathway in which antecedent mitochondrial fission driven by TTP expression is required exclusively for mTOR-mediated mitophagy, independent of general autophagy.

## 2.5 TTP is required to sustain mitochondrial metabolism during iron deficiency.

We next investigated the role of TTP-mediated mitophagy on mitochondrial function and metabolism. Iron chelation steadily induced mitochondrial stress and activation of the mitochondrial unfolded protein response (UPR<sup>mt</sup>), as determined by the increased expression of the mitochondrial and ER stress transcription factor *Chop*, the mitochondrial protease *Lonp*, and the mitophagy marker *Bnip3* (Fig. 11A-C). Iron chelation also reduced mitochondrial membrane potential in both WT and *Ttp* KO MEFs. However, the drop in membrane potential in *Ttp* KO MEFs was significantly more severe (Fig. 10A). Furthermore, *Ttp* KO MEFs accumulated significantly more double-strand breaks in their mitochondrial DNA than WT cells in response to iron chelation (Fig. 10B). While *Ttp* KO MEFs had higher rates of proliferation under basal conditions, they demonstrated increased cell death in response to iron chelation compared to WT MEFs, consistent with exacerbated mitochondrial dysfunction (Fig. 10C-D). Since proper mitochondrial function is critical for oxidative metabolism and sustaining anabolic processes, we performed metabolomic profiling to study changes in substrate handling during iron deficiency. We observed significantly increased levels of intermediate metabolites from the TCA cycle and purine biosynthetic pathways in *Ttp* KO cells at baseline (Fig. 11D), consistent with higher rates of oxidative metabolism and cell proliferation. Iron deficiency also decreased free leucine levels while impeding *de novo* purine synthesis and purine catabolism pathways in both WT and *Ttp* KO cells (Fig. 10E, 11E-F), consistent with mTOR inactivation and cessation of cell growth. However, iron chelation led to abnormal accumulations of serine, creatine, succinate, and dihydroorotate, with correspondingly low levels of malate and fumarate, and a prominent depletion of cellular energy charge in *Ttp* KO cells compared to WT cells (Fig. 10F-H, 11G-H), indicative of a block in mitochondrial one carbon metabolism and TCA cycle dysfunction. In both genotypes, iron chelation was accompanied by the transition to anaerobic glycolytic metabolism, as evidenced by increased glucose uptake and production of glycolytic intermediates, including

G6P and lactate (Fig. 10I-J). However, *Ttp* KO cells exhibited exacerbated upregulation of glycolysis and shunting through the non-oxidative pentose phosphate pathway, likely to divert the carbon flux away from pyruvate, which cannot be oxidized efficiently in cells with dysfunctional mitochondria (Fig. 10K). In light of these findings, we decided to further our investigation and asked whether TTP protected hepatic metabolism in response to dietary iron deficiency, a condition that affects nearly 30% of the world's population [39].

## **2.6 TTP-mediated mitophagy is important for hepatic gluconeogenesis during iron deprivation**

We assessed the physiological consequences of iron deprivation on mitochondrial function and liver metabolism *in vivo* using mice with liver-specific deletion of *Ttp* (*IsTtp* KO) and WT littermates subjected to 6-9 weeks of iron deficient diet from weaning (Fig. 12A). Both WT and *IsTtp* KO mice had comparable loss of hepatic iron stores, increased hepatic *Tfr1* expression, maintained similar body weights, and developed microcytic anemia (Fig. 12B, 13A-C). Consistent with our *in vitro* data, leucine levels were reduced equally in iron deficient livers from both WT and *IsTtp* mice (Fig. 13D). Iron deficiency decreased the expression of *Lat3* and *Raptor* in both WT and *IsTtp* KO livers (Fig. 12D). *Opa1* mRNA levels were decreased, while *Bnip3* mRNA levels were increased in iron deficient WT livers but not in iron deficient *IsTtp* KO livers (Fig. 12D). Expression of UPR<sup>mt</sup> markers *Chop* and *Lonp* were also significantly higher in iron-deficient *IsTtp* KO livers compared to WT (Fig. 13F-G). Mitochondria from livers of WT mice fed iron deficient diet were smaller and rounder, consistent with mitochondrial fission (Fig 12E-F, Fig. 13E). On the other hand, mitochondria from livers of *IsTtp* KO mice remained elongated and displayed increased mitochondrial swelling, which is associated with mitochondrial stress and dysfunction (Fig. 12E-F, 13E).

Efficient gluconeogenesis from lipids and amino acids liberated by autophagy during fasting require a properly functioning TCA cycle, which we show to be impeded in *Ttp* KO cells during iron deficiency (Fig. 10G) [233]. Therefore, we assessed the capacity of livers from *IsTtp* KO mice exposed to iron deficiency to convert the amino acid alanine into glucose. We chose alanine over pyruvate to avoid potential masking of a hepatic phenotype by extrahepatic gluconeogenesis [234]. Both WT and *IsTtp* KO mice had equivalent gluconeogenic capacity when fed a control diet containing sufficient iron. Compared to control diet, injection of alanine into iron deficient WT mice resulted in a moderate increase in peak blood glucose that was sustained after 2 hours (Fig. 12G). In contrast, *IsTtp* KO mice fed iron deficient diet had lower peak blood glucose and 2 hour blood glucose compared to any other group (Fig. 12G). We confirmed this was a primary deficit in hepatic gluconeogenesis and not due to differential glucose utilization by peripheral tissue as WT and *IsTtp* KO mice fed iron deficient diet had identical glucose tolerance (Fig. 12H). These data confirm that a novel pathway involving epigenetic regulation of mTOR activity and subsequent TTP mediated mitophagy is important for the physiologic adaptation to a common nutrient deficiency *in vivo*.

## Chapter 3

### Discussion

Together, our work demonstrates that iron deficiency is a critical regulator of mTOR activity and cellular metabolism. We have identified a novel mechanism by which iron represses both cellular amino acid homeostasis and RAPTOR expression. We go on to demonstrate that the loss of mTORC1 activity engages an adaptive program, dependent on TTP, which is required to recycle damaged mitochondria via mitophagy. Failure to clear mitochondria during iron

deficiency results in altered cellular metabolism, reduced cell viability, and defective hepatic gluconeogenesis. Future investigation will be needed to shed light on how these pathways evolved and what other physiologic processes depend on the mTOR-TTP axis during iron deficiency.

### 3.1 The Requirement for Redundancy

These findings raise the question as to why such a robust and redundant system has evolved to ensure that the sensing of iron and amino acids are strictly linked. We believe this has to do with the dependence of eukaryotic organisms on the uptake of iron and certain amino acids from the extracellular environment in order to facilitate growth and reproduction. Lipids, nucleotides and cholesterol can be synthesized *de novo* and energetic substrates such as ATP and NADH can be generated from a variety of carbon sources. In contrast, iron and certain amino acids, like leucine, are the rare exception and are truly limiting. Therefore a system needed to evolve to shutdown mTOR dependent anabolic functions, such as protein synthesis, which consume large quantities of iron and amino acids, when the levels of either one are insufficient. The Jmj-C histone demethylases are perfectly suited to bridge physiologic iron sensing with amino acid homeostasis and mTOR activity as their enzymatic function depends on molecular iron and their activity at H3K27me<sup>3</sup> and H3K9me<sup>2</sup> marks allow them to regulate a pathway at multiple levels simultaneously, ensuring tight control. Further work will be needed to identify which Jmj-C histone demethylase(s) specifically are required for regulation of *LAT3* and *RAPTOR* by iron. While EZH1 and EZH2 are the dominant methyltransferases with activity at H3K27, multiple methyltransferases in addition to G9a and GLP have been implicated to methylate H3K9 [235, 236]. Our data demonstrates that other histone methyltransferases are responsible for regulating H3K9me<sup>2</sup> at the *LAT3* and *RAPTOR* promoters. In addition to regulation of mTORC1 signaling at the epigenetic level, iron deprivation can indirectly modulate

mTORC1 activity multiple ways by engaging the HIF1/2 pathway, inducing REDD1 expression, and activating AMPK through loss of cellular ATP pools. The redundancy afforded by these converging pathways is reflected in our data by demonstrating that modulation of any one pathway is unable to fully restore mTORC1 activity in the presence of iron deficiency.

### **3.2 Histone Methylation and Cancer**

Alterations in global H3K27me<sup>3</sup> and H3K9me<sup>2</sup> marks are associated with tumor progression and patient survival in ovarian, pancreatic and breast cancer [237-240]. At the same time, malignant cells require great quantities of iron to sustain metabolic activity and proliferation. The inhibitors of histone demethylation used in this study, JIB-04 and GSK-J4, have both been used pre-clinically to inhibit tumor growth and block cancer-stem cell self-renewal, although the specific mechanisms underlying these phenomena have yet to be determined [241, 242]. Our study implicates the mTOR-TTP axis as a potential therapeutic target through its influence on mitochondrial quality control and cellular metabolism. Although mTOR inhibitors such as sirolimus and evirolimus are approved for the treatment of certain cancers and 2<sup>nd</sup> generation mTOR inhibitors are currently being tested in clinical trials, the overall success of these drugs has been limited [243, 244]. This is due, in part, to robust upregulation of autophagy which enables cancer cells to survive periods of cytostatic and cytotoxic stress [245]. The subsequent goal should be to design combinatorial therapies that simultaneously disrupt mTOR activity and TTP mediated mitophagy so that cancer cells will be less able to compensate by rewiring their metabolism. This synthetic lethality approach is the same principle underlying the use of PARP inhibitors in BRCA1/2 mutated breast and ovarian cancers, which have achieved remarkable success in phase II clinical trials [246, 247].

### **3.3 Connections Linking Mitophagy and Autophagy**

At least two pathways facilitating mitophagy have been identified. Both the canonical and alternative mitophagy pathways depend on ULK1, linking them to cellular nutrient availability and mTOR activity [248]. The presence of LC3I to LC3II conversion after bafilomycin A treatment indicates that iron deficiency mediated mitophagy utilizes, at least in part, the canonical pathway. However, we cannot rule out participation of the alternative pathways in which vesicles are derived from Rab9<sup>+</sup> trans-golgi. Our data confirms that antecedent mitochondrial fission mediated by TTP is required to generate cargo small enough for autophagosomal engulfment. However, our observation of LC3II conversion and loss of p62 in *Ttp* KO MEFs also suggests that concurrent mitochondrial fission is not strictly required for proper lysosomal maturation and progression of autophagy. Further work will be needed to understand the regulatory mechanisms linking lysosomal and mitochondrial dynamics and why certain conditions, like iron deficiency, disrupt that connection. After fission, multiple adaptor proteins can bridge damaged mitochondria with the autophagosome, including PARKIN/PINK1, BNIP3, FUNDC1, and ATG32 [224]. Although it is still unclear which adaptor proteins mediate mitophagy during iron deficiency, our data suggests that BNIP3 might play a significant role. Supporting this hypothesis, OPA1 has been shown to directly complex with BNIP3 and this interaction is required to counteract BNIP3 mediated mitochondrial fission [249]. This fits our model as we show TTP-mediated repression of *Opa1* mRNA reduces OPA1 protein levels and facilitates BNIP3 expression and mitochondrial fission. Importantly, our study is the first to identify a pre-translational role for RNA destabilization by TTP as a unified gatekeeper for selective-autophagy, prior to protein-level regulation.

### **3.4 Physiologic Limitations of Hepatic Mitophagy**

Defects in autophagy and mitophagy have profound effects on systemic health and contribute to anemia, hepatosteatosis, and neurodegenerative diseases such as Parkinson's disease [250-

252]. We chose to investigate hepatic gluconeogenesis as a proof of principle that TTP is a bona fide mediator of mitophagy and mitochondrial function *in vivo*. We utilized a prolonged iron deficiency protocol to ensure adequate depletion of liver iron stores. Therefore, we did not expect to directly observe lysosomes containing mitochondrial fragments in our TEM images from iron deficient WT livers. By 6 weeks, we expect the initial wave of mitophagic clearance to have resolved and given way to long-term changes in mitochondrial biogenesis, similar to what has been observed in other organs [253]. It is also not surprising the fasting glucose levels were not different between Is *Ttp* WT and KO mice fed iron deficient diet because hepatic gluconeogenesis is not required for maintenance of euglycemia during fasting [254]. Gluconeogenesis from glutamine, but not alanine, in the kidneys and intestines is sufficient to compensate for loss of hepatic gluconeogenesis in liver-specific *G6pc*<sup>-/-</sup> mice.

### 3.5 Human Genetics and TTP

While homozygous deletion of *Ttp* causes significant inflammation and autoimmune disease due to its regulation of *Tnfa* in macrophages, thus far, no function-modifying SNPs or loss of heterozygosity have been linked to disorders of iron in humans. One possible reason for this is that current genome wide association studies or exome-sequencing analyses in iron deficient populations have sought to identify loci associated with the regulation of iron itself. Instead, we propose that future studies should focus on the association of iron with metabolic outcomes and specific organ function. Based on our data, it is interesting to speculate that mutations which would generate hypomorphic TTP protein may have been selected against over the course of human evolution due to poor metabolic fitness in the setting of a common nutrient deficiency.

## Chapter 4

### Summary and Future Directions

#### 4.1 Summary

We have identified and characterized a novel pathway by which iron, an essential nutrient, controls mTOR activity through the regulation of global histone methylation. Additionally, we have uncovered a previously unknown checkpoint in selective-autophagy in which mTOR regulates mitophagy through TTP-mediated mRNA degradation of a mitochondrial fusion gene. Loss of TTP in iron deficiency prevents normal mitochondrial quality control and results in aberrant glucose metabolism *in vitro* and blockage of hepatic gluconeogenesis *in vivo*. We believe these findings will be of great value to the field for two reasons 1) they describe an entirely novel mechanism of iron sensing leading to epigenetic control of mTOR activity and 2) they clearly show that mitochondrial fission is not required for general autophagy. We also believe that the pathways we identified have profound implications for diseases with high utilization of iron and mTOR, including cancer and neurodegeneration.

#### 4.2 Future Directions

In light of this work, several important questions that could form the basis of future investigation.

1. Which Jmj-C domain-containing histone demethylase(s) are the primary drivers of the adaptive response to iron deprivation?
2. In addition to LAT3 and RAPTOR, what is the complete gene set that is regulated through DNA hypermethylation in response to iron chelation?

3. Can the connection between histone demethylases and mTOR be exploited for the generation of novel cancer therapies?
4. Does TTP regulate additional mTOR dependent pathways during iron deficiency, such as protein translation?
5. Which mitophagy receptors are sufficient to engage LC3II during iron deprivation?
6. Does TTP mediated mitophagy truly liberate mitochondrial iron and amino acids for utilization?
7. Could use of a TTP inhibitor sensitize tumors to mTOR inhibitors which have limited clinical efficacy?

## Chapter 5

### Materials and Methods

**5.1 Cell culture, gene downregulation, and overexpression.** MEFs and HepG2 cells (ATCC) were grown in Dulbecco's Modified Eagle's Medium (Corning) supplemented with 10% FBS (Atlanta Biologicals). HEK293T cells (ATCC) were grown in Modified Eagle's Medium (Corning) supplemented with 10% FBS and 1% sodium pyruvate (Sigma). *Ttp* KO MEFs were generated and generously gifted by Dr. Perry Blackshear (NIEHS). *Tsc2* KO were described previously [255] and *Ampk $\alpha$ 1/ $\alpha$ 2* dKO MEFs were generous gifts from Dr. Navdeep Chandel (Northwestern University). siRNAs against mouse *Opa1* and human *REDD1* (Dharmacon) were transfected using Dharmafect I Transfection Reagent (Dharmacon) according to the manufacturer's protocols. The siRNA concentrations of 6.25nM and 25nM were used to achieve either moderate or robust knockdown, respectively. Lentivirus encoding shRNA against mouse *Mfn1*

was purchased from Northwestern University's DNA/RNA Delivery Core (<http://skinresearch.northwestern.edu/research/dna-rna-core/index.html>) and packaged in HEK293T cells co-transfected with pPAX2 and pMDG2 packaging vectors using standard protocols. Wildtype or tandem zinc finger TTP mutant plasmids were gifts from Dr. Perry Blackshear (NIEHS) and transfected into HepG2 cells using Lipofectamine 2000 (Life Technologies) according to manufacturer's instructions. LC3-GFP and MitoDSRED plasmids (Addgene) were transfected into MEFs using the same method. All other transfections were performed in HEK293T cells using either Lipofectamine 2000 or the CaPO<sub>4</sub> method. Plasmids encoding RAP2A, RHEB, RAGB<sup>Q99L</sup>, RAGC<sup>S75N</sup>, RAPTOR, and RAPTOR-RHEB15 were all purchased from Addgene. Transient transfections was performed 24 hours before adding iron chelator when indicated. Stable cell lines were generated by growing transfected cells in 1-10 µg/ml puromycin (Sigma) for 2 or more passages or by FACS sorting RFP<sup>+</sup> cells in the case of MitoDSRED.

**5.2 Drug treatments.** The iron chelators deferoxamine (DFO) and 2,2'-bipyridyl (BPD) were purchased from Sigma and used at the indicated concentrations. mTOR inhibitors rapamycin (Sigma) and torin1 (Sigma) were used at 50 nM and 250 nM respectively. Leucine (Sigma) and L-leucyl-L-leucine-methyl-ester (LLOME; Cayman Chemical) were both used at 400µM. Histone demethylase inhibitors JIB-04 (Tocris) and GSK-J4 (Sigma) were used at 2µM and 5µM, respectively. Histone methyltransferase inhibitors 3-Deazaneplanocin A (DZNep; Sigma) and UNC-0641 (Sigma) were used at 20µM and 500µM, respectively. Doxorubicin was purchased from Sigma and used at 5µM. All treatments began when cells reached approximately 60% confluency unless otherwise noted.

**5.3 *In silico* analysis of AU-rich elements.** AREs were identified by either of the following two criteria: 1) curated ARE entry in the AREsite Database (<http://nibiru.tbi.univie.ac.at/cgi-bin/AREsite/AREsite.cgi>), or 2) presence of (U)AUUUA(U) sequence in the 3'UTR region of reference mRNA sequences by manual search using the UCSC genome browser (<https://genome.ucsc.edu/>).

**5.4 RNA isolation, reverse transcription and quantitative RT-PCR.** RNA was isolated from cells or tissues using RNA-STAT60 (Teltest). Reverse transcription was carried out using qScript Reverse Transcription Kit (Quanta). The resulting cDNA was amplified quantitatively using PerfeCTa SYBR Green Mix (Quanta) on a 7500 Fast Real-time PCR System (Applied Biosystems). The relative gene expression was determined using differences in Ct values between gene of interest and house-keeping control genes. A complete list of primers is included in a supplementary table.

**5.5 mRNA stability assay and RNA co-IP.** For mRNA stability experiments cells were treated with 7.5 $\mu$ M actinomycin D (Sigma) for indicated times and RNA was harvested and processed as described above. For RNA co-IP, MEF cells were resuspended in IP lysis buffer (10mMTris-HCl [pH 7.6], 1 mM KAc, 1.5 mM MgAc, 2 mM DTT, 10 ml/ml ProteaseArrest inhibitors) and mechanically lysed with a Power Gen 500 homogenizer (Fisher), followed by centrifugation at 12,000g for 10 min at 4<sup>o</sup> C to remove debris. Lysates were then incubated with human TTP (kindly provided by Dr. William Rigby, Dartmouth University) or IgG antibody at 4<sup>o</sup> C with continuous rotation O/N. Protein G Sepharose Fast Flow beads (Sigma) were washed with IP buffer (10 mM Tris-HCl [pH 7.6], 1.5 mM MgCl<sub>2</sub>, 100 mM NaCl, 0.5% Triton X-100, 10 ml/ml ProteaseArrest inhibitors) and incubated with cell lysate/antibody at 4<sup>o</sup> C with continuous rotation again for O/N. Beads were then washed six times with cold IP buffer and RNA was

collected. Equal amounts of RNA were amplified by qRT-PCR and the expression of each gene was normalized to that of 18S. Data were represented as the fold enrichment over IgG control.

**5.6 Western blots.** Cells and tissue were lysed in radioimmunoprecipitation assay (RIPA) buffer supplemented with protease inhibitor (Pierce), and phosphatase inhibitors sodium vanadate (Sigma) and sodium pyrophosphate (Sigma). Protein concentration in samples was determined using the BCA Protein Quantification Kit (Pierce). Equal amounts of protein were loaded on a tris-glycine polyacrylamide gel (Life Technologies) and transferred to nitrocellulose membrane. After blocking with TBS containing 0.005% Tween 20 (Fisher) and 5% BSA, the membrane was incubated with primary antibody against indicated proteins. A complete list of antibodies is included in a supplementary table.

**5.7 Iron quantification.** Cells or liver tissue were homogenized in RIPA buffer, spun at 16,000g for 15 minutes and the supernatant collected. Equal amounts of protein were mixed with protein precipitation solution (1:1 1 N HCl and 10% trichloroacetic acid) and heated to 95° C for 1 hour to release iron. Precipitated protein was removed by centrifugation at 4° C at 16,000g for 10 min, the supernatant was mixed with the equal volume of chromogen solution (0.5 mM ferrozine, 1.5 M sodium acetate, 0.1% [v/v] thioglycolic acid), and the absorbance was measured on a Spectra Max Plus microplate reader at 562nm. Absolute iron values were determined was based on a standard curve generated using Fe-acetate.

**5.8 Amino acid profiling.** Amino acid levels in muscle were determined using a Beckman 121 MB amino acid analyzer using a previously established protocol. Briefly, cell pellets or whole-liver tissue were hydrolyzed with 6 mol l<sup>-1</sup> HCl for 24 h at 110 °C in sealed tubes after replacing

oxygen with nitrogen. The solution obtained was filtered through a 25- $\mu$ m membrane filter and then analyzed for amino acids.

**5.9  $^3\text{H}$ -leucine and  $^{14}\text{C}$ -glucose uptake.** For leucine uptake, MEFs were subjected iron chelation or rapamycin for 24hrs and then incubated with  $^3\text{H}$ -leucine (Sigma) for 5 minutes, washed three times with cold PBS to remove residual extracellular  $^3\text{H}$ -leucine, and immediately lysed in RIPA buffer. Glucose uptake was measured the same way except incubation with  $^{14}\text{C}$ -glucose (Sigma) lasted for 10 minutes. Protein content of each sample was determined by BCA assay. Radioactivity of the lysate was determined by scintillation counting and normalized to the protein concentration of each sample.

**5.10  $^{35}\text{S}$ -methionine based measurement of protein synthesis.** HEK293T cells were preloaded with  $^{35}\text{S}$ -methionine (Sigma) for two passages and then plated in 10cm dishes at 60% confluency. At the start of the experiment, cells were washed 3x with PBS and chased for 24 hours in normal growth media containing either iron chelator or vehicle control. Cells were washed 1x with PBS and immediately lysed in RIPA buffer. Protein content of each sample was determined by BCA assay. Radioactivity of the lysate was determined by scintillation counting and normalized to the protein concentration of each sample.

**5.11 Luciferase assay.** A plasmid containing the promoter and whole sequence of human *TTP* was generously gifted by Dr. Perry Blackshear (NIEHS). We then subcloned the promoter, first exon and intron into the pGL3basic vector containing the gene for firefly luciferase (Ambion). We performed site directed mutagenesis to remove the start codon in the first exon rendering only the regulatory sequences in the promoter and first intron functional. HEK293T cells were transfected in 10cm dishes with both the *TTP-firefly* and *Renilla* luciferase constructs using

Lipofectamine 2000, following incubation in complete medium for 20 hours. Cells were then lifted and plated into 24 well dishes and exposed to iron chelation for 24 hours and harvested in passive lysis buffer (Promega). The luminescence was quantified using the Dual-Luciferase Reporter Assay System (Promega) on a luminometer (Turner Biosystems, Modulus Microplate) according to the manufacturer's protocol. *Renilla* luminescence was used as normalization control for variations in transfection efficiency.

**5.12 Confocal imaging.** For immunocytochemistry, HEK293T cells were plated on 18x18mm coverglass coated with .5% fibronectin (Sigma) in .02% gelatin (Sigma) and treated as described. At the end of the experiment, cells were fixed using 4% paraformaldehyde for 10 min and subsequently washed 3x in 1X PBS. Cells were permeabilized in 1X PBS-T (PBS + 0.1% triton x-100 (Sigma)) for 1 hour and then incubated with designated primary antibodies O/N at 4° C in PBST+ (PBS-T+ 5% donkey serum (Sigma)). Coverslips were then washed 3x in 1X PBST and stained with secondary antibodies in PBST+ for 2 hours, washed 3x in 1X PBS, and then mounted on slides using Prolong Diamond mounting media (Life Technologies). A list of all primary and secondary antibodies is provided in a supplemental table. For imaging of lysosomal permeability, cells were incubated with acridine orange (Invitrogen) at 2µg/ml for 15minutes and washed 1x with HBSS (Gibco) before imaging in 1X HBSS supplemented with 5mM HEPES (HBSS-H; Sigma). For imaging of mitochondrial morphology and membrane potential, cells were stained with 250 nM of Mitotracker Green (Life Technologies) and 10 nM of TMRE (Life Technologies) for 15 min, washed 1x with HBSS and imaged in 1x HBSS-H. Analyses of autophagy and mitophagy were performed in mitoDSRED expressing MEFs stained with 500nM lysotracker green (Life Technologies) in 1X HBSS-H and directly imaged. Cells expressing LC3-GFP were switched from regular growth media to 1X HBSS-H and imaged. All images were acquired on a Zeiss LSM 510 Meta confocal microscope. Images were quantified using ImageJ.

**5.13 Mitochondrial DNA content determination.** Total cellular DNA from cells and tissue were isolated using GeneJet Genomic DNA Purification Kit (ThermoFisher) according to manufacturer's instructions. Following isolation, nuclear and mitochondrial DNA were quantified using quantitative realtime PCR with primers specific for gen*Polb* genomic DNA or mt*Cox1* locus on mitochondrial chromosome, as described above.

**5.14 Cell growth and apoptosis analysis.** For quantification of cell growth, cells were stained with 5 µg/ml PI (Thermofisher) and 10 µg/ml Hoechst 33342 (Invitrogen) in 1X HBSS. Images were acquired on a Zeiss AxioObserver.Z1 microscope and live cells were defined as the number of PI-negative/Hoechst 33342-positive nuclei. Apoptosis was quantified using a FACS Canto Flow Cytometer (BD) and data were gated and analyzed using FloJo software. Cells were treated with iron chelator or vehicle control, lifted and stained in annexin binding buffer containing Annexin-V conjugated to Alexafluor 350 (Life Technologies) and 1µM ToPRO3-Iodide (Life Technologies) according to manufacturer's instructions and. Apoptotic cells were defined as the AnnexinV-positive/ToPRO3-positive population.

**5.15 Metabolomics.** Metabolomics services were performed by the Metabolomics Core Facility at Robert H. Lurie Comprehensive Cancer Center of Northwestern University. Samples were analyzed by High-Performance Liquid Chromatography and High-Resolution Mass Spectrometry and Tandem Mass Spectrometry (HPLC-MS/MS). Specifically, system consisted of a Thermo Q-Exactive in line with an electrospray source and an Ultimate3000 (Thermo) series HPLC consisting of a binary pump, degasser, and auto-sampler outfitted with a Xbridge Amide column (Waters; dimensions of 4.6 mm x 100 mm and a 3.5 µm particle size). The mobile phase A contained 95% (vol/vol) water, 5% (vol/vol) acetonitrile, 20 mM ammonium

hydroxide, 20 mM ammonium acetate, pH = 9.0; B was 100% Acetonitrile. The gradient was as following: 0 min, 15% A; 2.5 min, 30% A; 7 min, 43% A; 16 min, 62% A; 16.1-18 min, 75% A; 18-25 min, 15% A with a flow rate of 400  $\mu$ L/min. The capillary of the ESI source was set to 275 °C, with sheath gas at 45 arbitrary units, auxiliary gas at 5 arbitrary units and the spray voltage at 4.0 kV. In positive/negative polarity switching mode, an m/z scan range from 70 to 850 was chosen and MS1 data was collected at a resolution of 70,000. The automatic gain control (AGC) target was set at  $1 \times 10^6$  and the maximum injection time was 200 ms. The top 5 precursor ions were subsequently fragmented, in a data-dependent manner, using the higher energy collisional dissociation (HCD) cell set to 30% normalized collision energy in MS2 at a resolution power of 17,500. The sample volumes of 10  $\mu$ L were injected. Data acquisition and analysis were carried out by Xcalibur 4.0 software and Tracefinder 2.1 software, respectively (both from Thermo Fisher Scientific).

**5.16 Mouse strain and iron deficiency diet.** C57Bl/6 *Ttp<sup>ff</sup>* mice (a kind gift from Dr. Perry Blakeshear, NIEHS) were engineered with flox sites flanking exon 2 of *Ttp*. Liver-specific *Ttp* knockout (*lsTtp* KO) mice were generated by breeding *Ttp<sup>ff</sup>* mice with albumin-Cre transgenic mice (a kind gift from Dr. Joseph Bass, Northwestern). Mice were housed in the barrier facility at Northwestern University with 12 h light and 12 h dark cycle, and received either normal chow or iron deficient diet containing 2-6 ppm of iron (TD 80394, Harlan-Teklad), which was started on the day of weaning and continued for 6 weeks. All animal studies were approved by the Institutional Animal Care and Use Committee at Northwestern University and were performed in accordance with guidelines from the National Institutes of Health.

**5.17 *In vivo* metabolic studies.**

For all *in vivo* metabolic studies, age-matched male WT and *IsTtp* KO littermates were used. For the alanine tolerance test (ATT), mice were fasted for 24 hours and injected intraperitoneally at 10 $\mu$ l/g body weight with 20% L-alanine (Sigma) dissolved in sterile PBS. For the glucose tolerance test (GTT) mice were fasted for 16 hours and injected at 10 $\mu$ l/g body weight with a 20% dextrose (Sigma) solution in PBS.

**5.18 Blood count and red blood cell measurements.** For measurement of blood parameters, whole blood was collected and anti-coagulated with EDTA. Counting was performed on a Hemavet 950 analyzer (Drew Scientific).

**5.19 Organ harvest, and histological analysis.** At the time of tissue harvest, mice were anesthetized with 250 mg/kg dose of freshly prepared Tribromoethanol (Avertin; Sigma) and tissue was excised and rinsed in phosphate buffered saline to remove excess blood. The liver tissue for biochemical assays was then freshly frozen in liquid nitrogen and stored at -80 °C until the assay. For histological analysis, the liver tissue was fixed overnight in 4% paraformaldehyde before graded dehydration in 70%, 80%, 90% and 100% ethanol. The tissue sample was further dehydrated with xylene and embedded into paraffin. Sections were stained with hematoxylin and eosin for evaluation of general morphology and tissue organization.

**5.20 Transmission Electron Microscopy.** Sample preparation and electron microscopy was performed by the Center for Advanced Microscopy core facility at Northwestern University (<https://cam.facilities.northwestern.edu/>). In brief, liver tissue was harvested and finely dissected to approximately 1-2mm<sup>3</sup> and samples were fixed and processed according to the protocol available on the CAM's website. Processed sections were imaged using a FEI Tecnai Spirit G2

120kV transmission electron microscope. Hepatocyte mitochondria were analyzed for size parameters using ImageJ software.

**5.21 Statistical analysis.** Experiments in immortalized cell lines (MEFs, HepG2, and HEK293T) were performed in triplicate for each condition, and each experiment was replicated at least once. For *in vivo* experiments, animals were assigned to experimental groups using simple randomization, without investigator blinding. No statistical methods were used to predetermine sample size. Unpaired two-tailed Student's t-tests,  $\chi^2$  test, or one-way ANOVA were used to determine statistical significance when appropriate.  $P < 0.05$  was considered to be statistically significant, as indicated by an asterisk. Significant one-way ANOVA were followed by Tukey post hoc analysis.

**Tables and Figures**

Table 1.

<b><u>System</u></b>	<b><u>Gene</u></b>	<b><u>GTEx</u></b>	<b><u>HPA</u></b>	<b><u>Average</u></b>
y <sup>+</sup> Lat1	SLC7A7	1.1	7.9	4.5
y <sup>+</sup> Lat2	SLC7A6	0.4	0.6	0.5
Lat1	SLC7A5	6.685	1.8	4.2425
Lat2	SLC7A8	0.76	3.8	2.28
4F2hc	SLC3A2	10.102	27.4	18.751
<b>Lat3</b>	<b>SLC43A1</b>	<b>36.297</b>	<b>50</b>	<b>43.1485</b>
Lat4	SLC43A2	-0.385	0.5	0.0575
ATB <sup>0,+</sup>	SLC6A14	0	0	0
B <sup>0</sup> AT1	SLC6A19	0.4	0.1	0.25
B <sup>0</sup> AT2	SLC6A15	0	0	0

Figure 1.

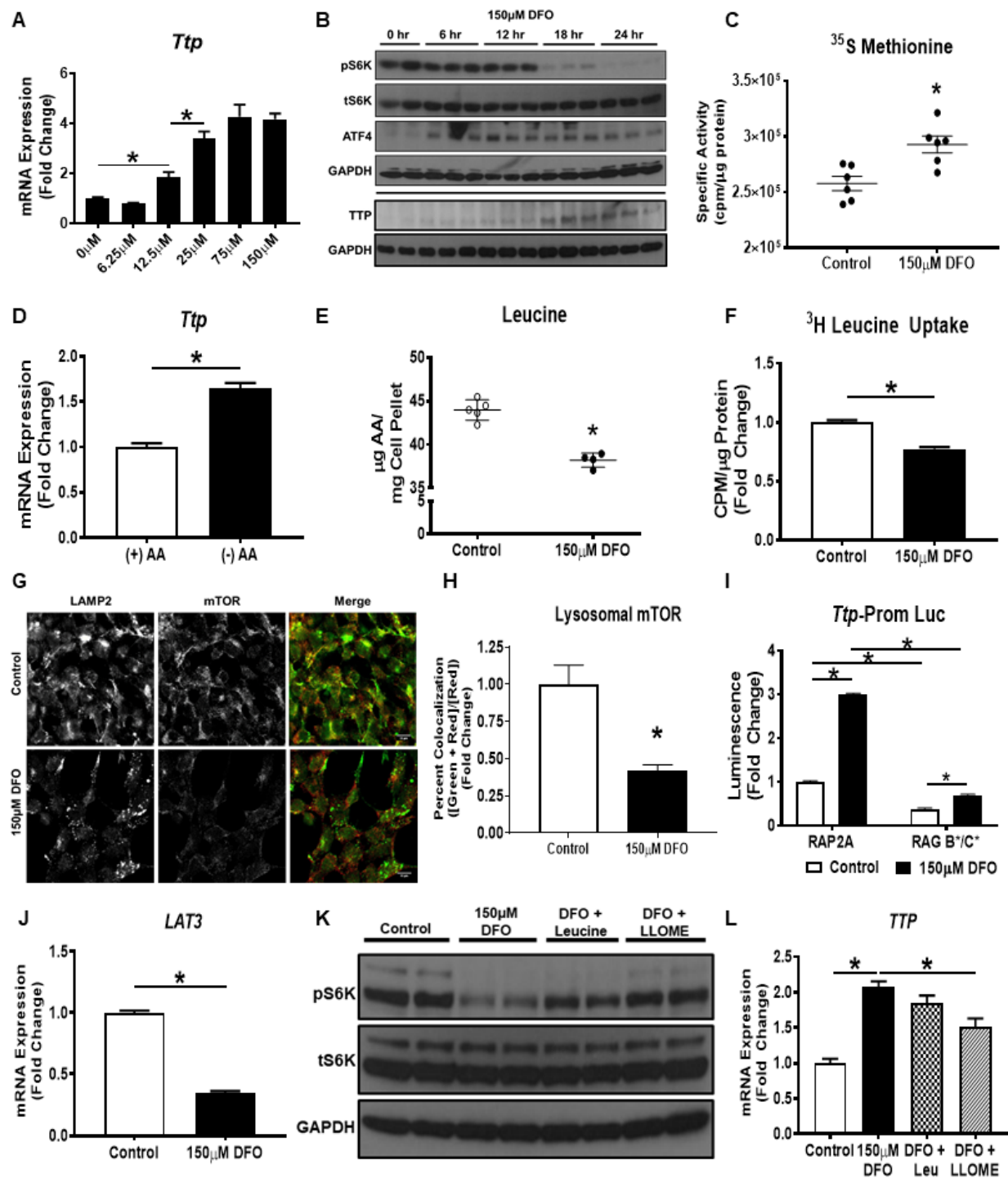


Figure 2.

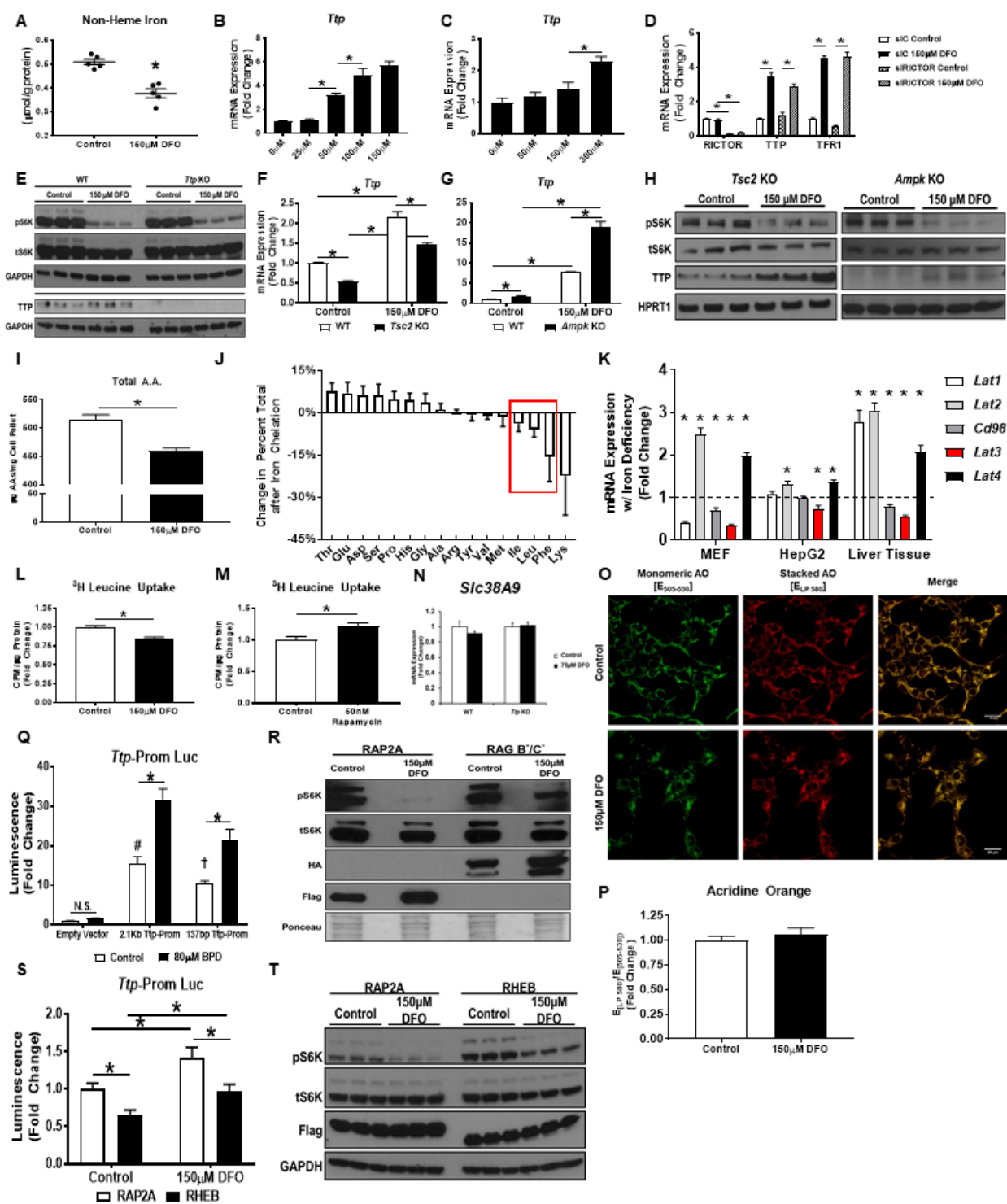


Figure 3.

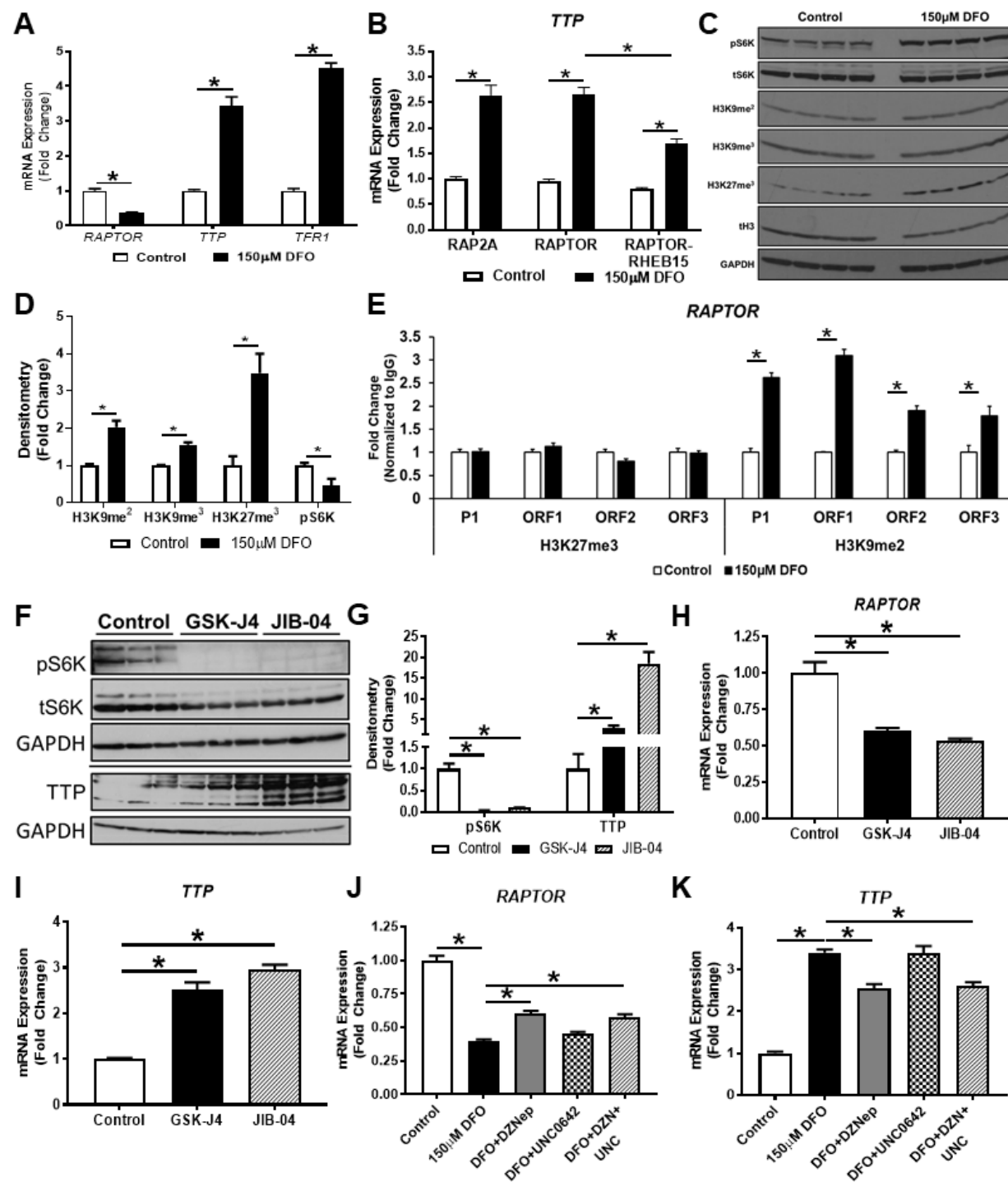


Figure 4.

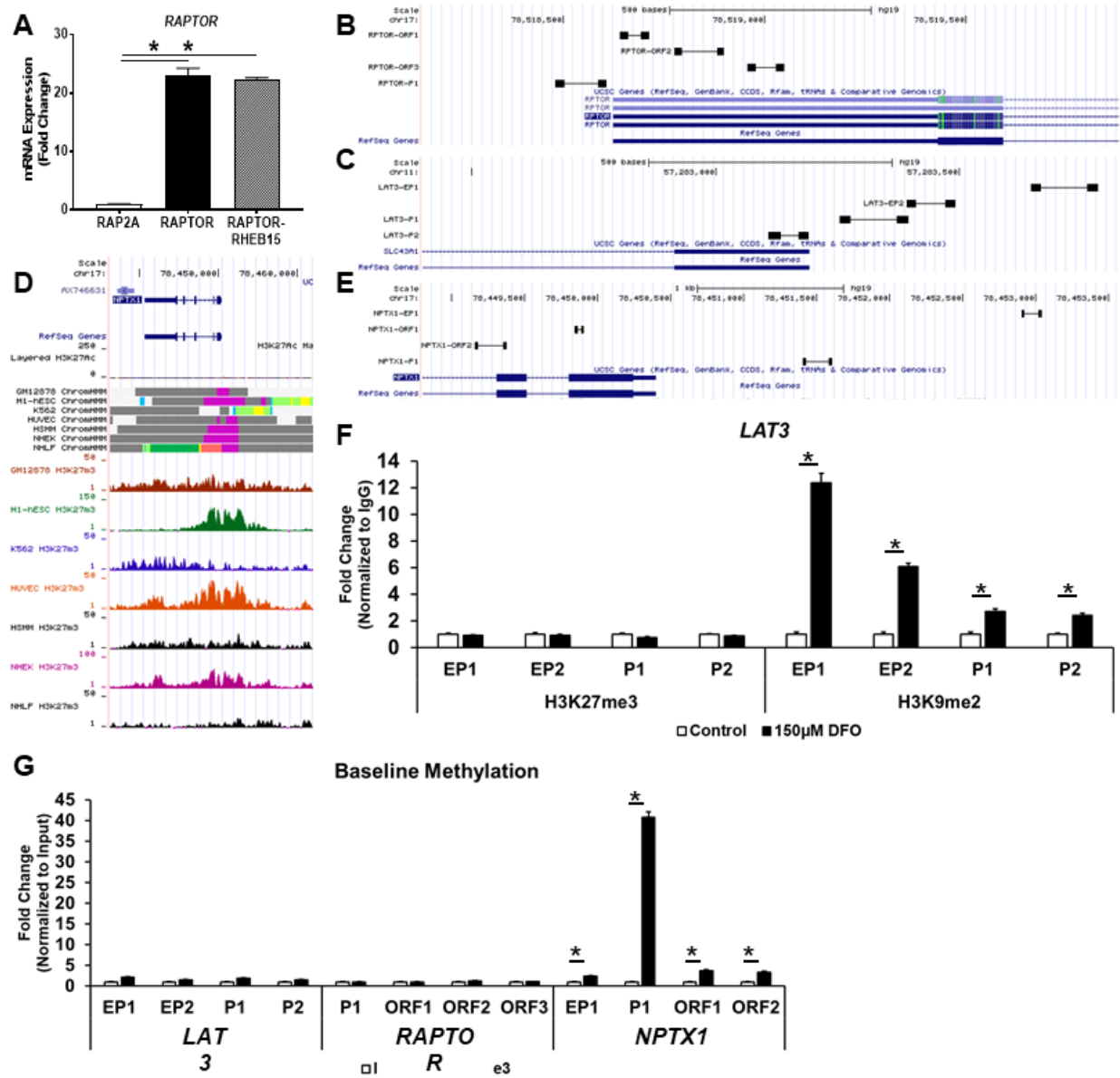


Figure 5.

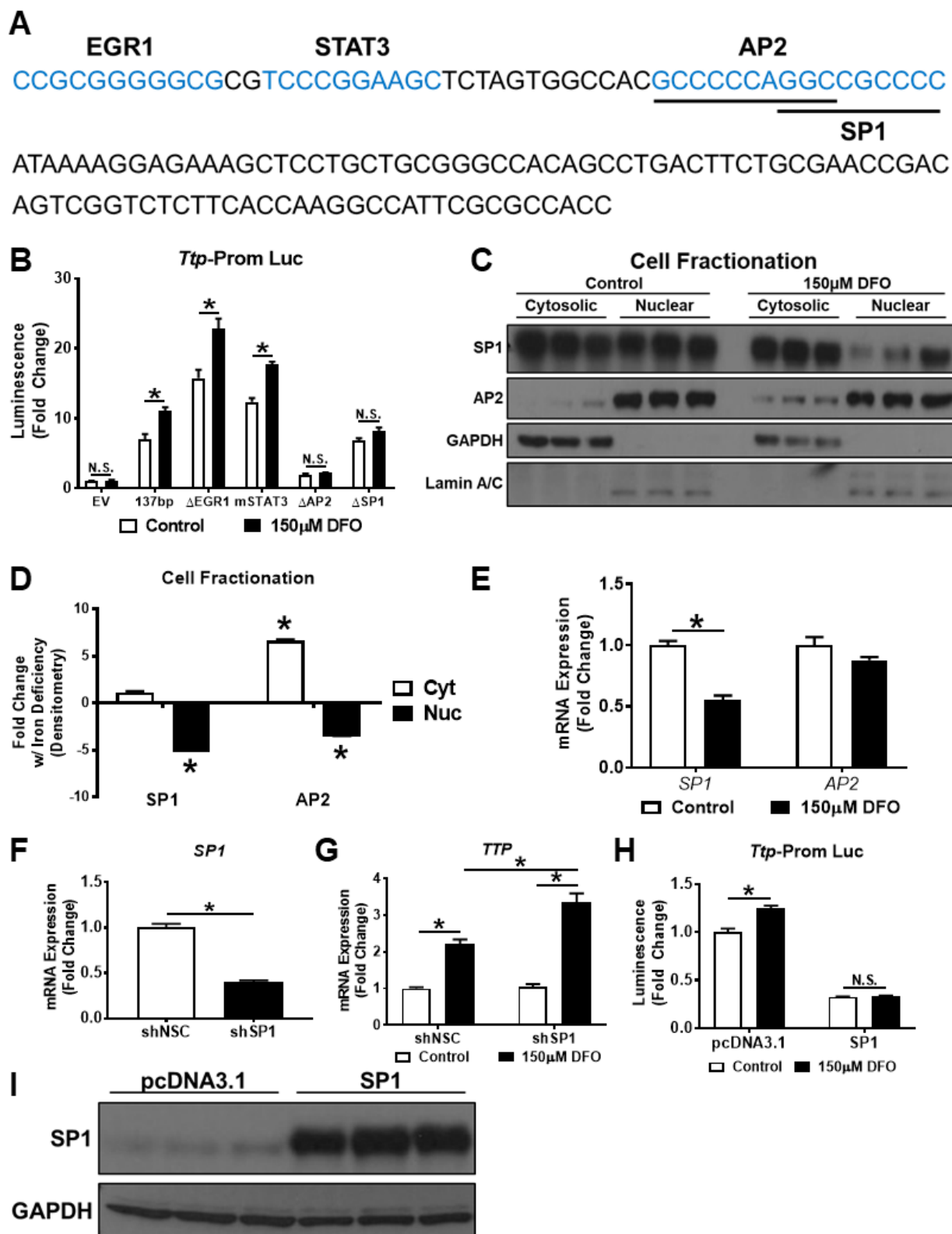


Figure 6.

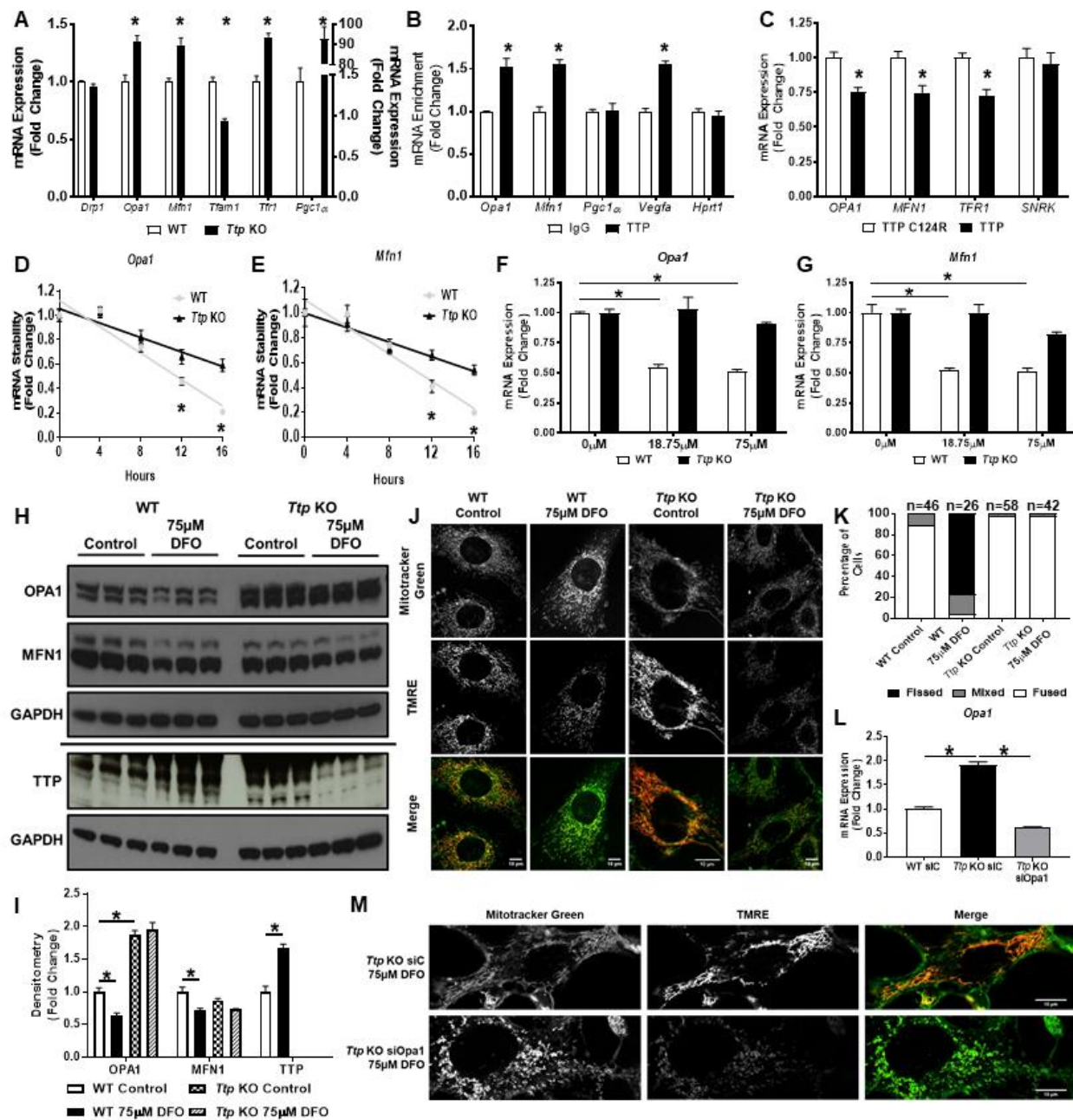


Figure 7.

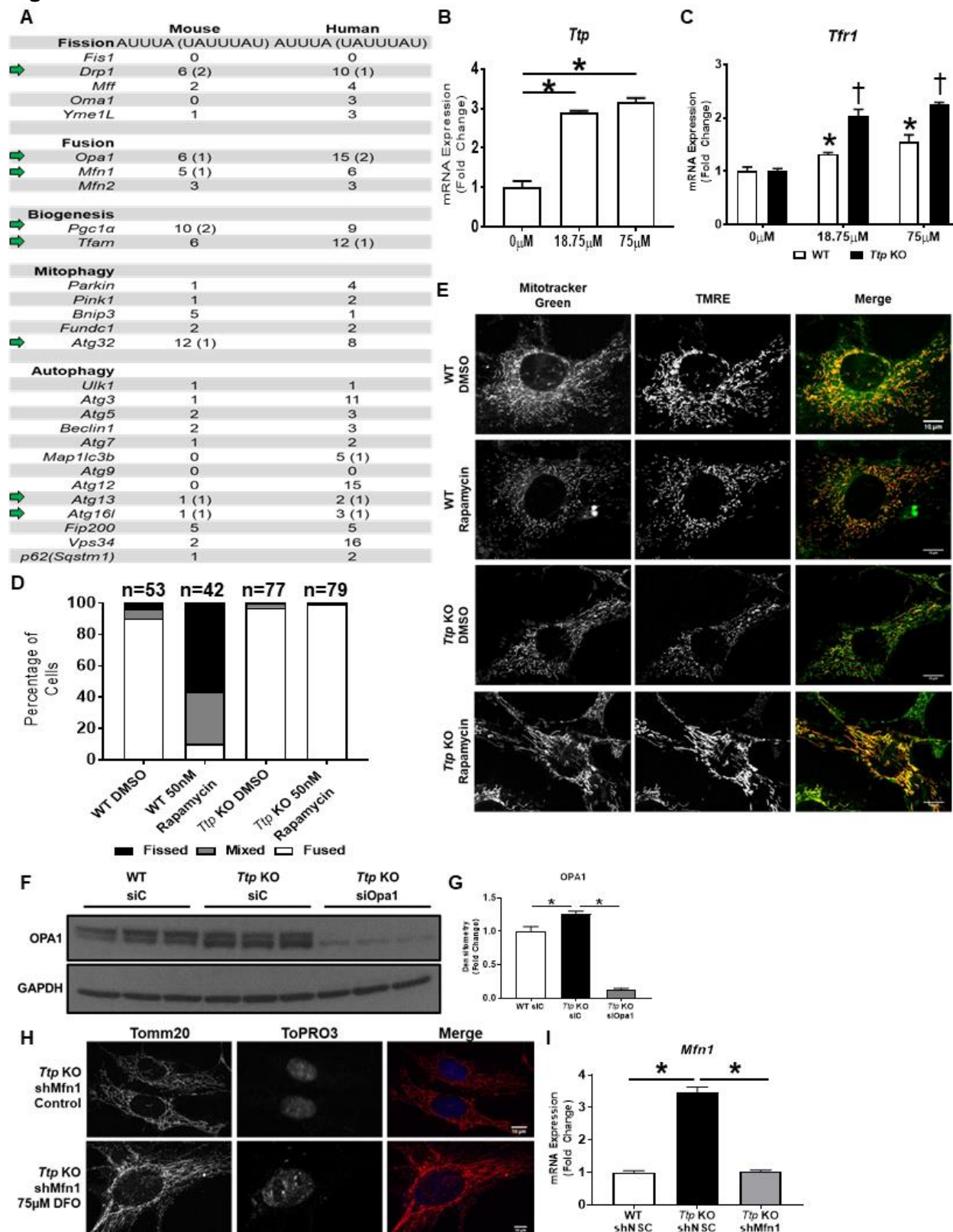


Figure 8.

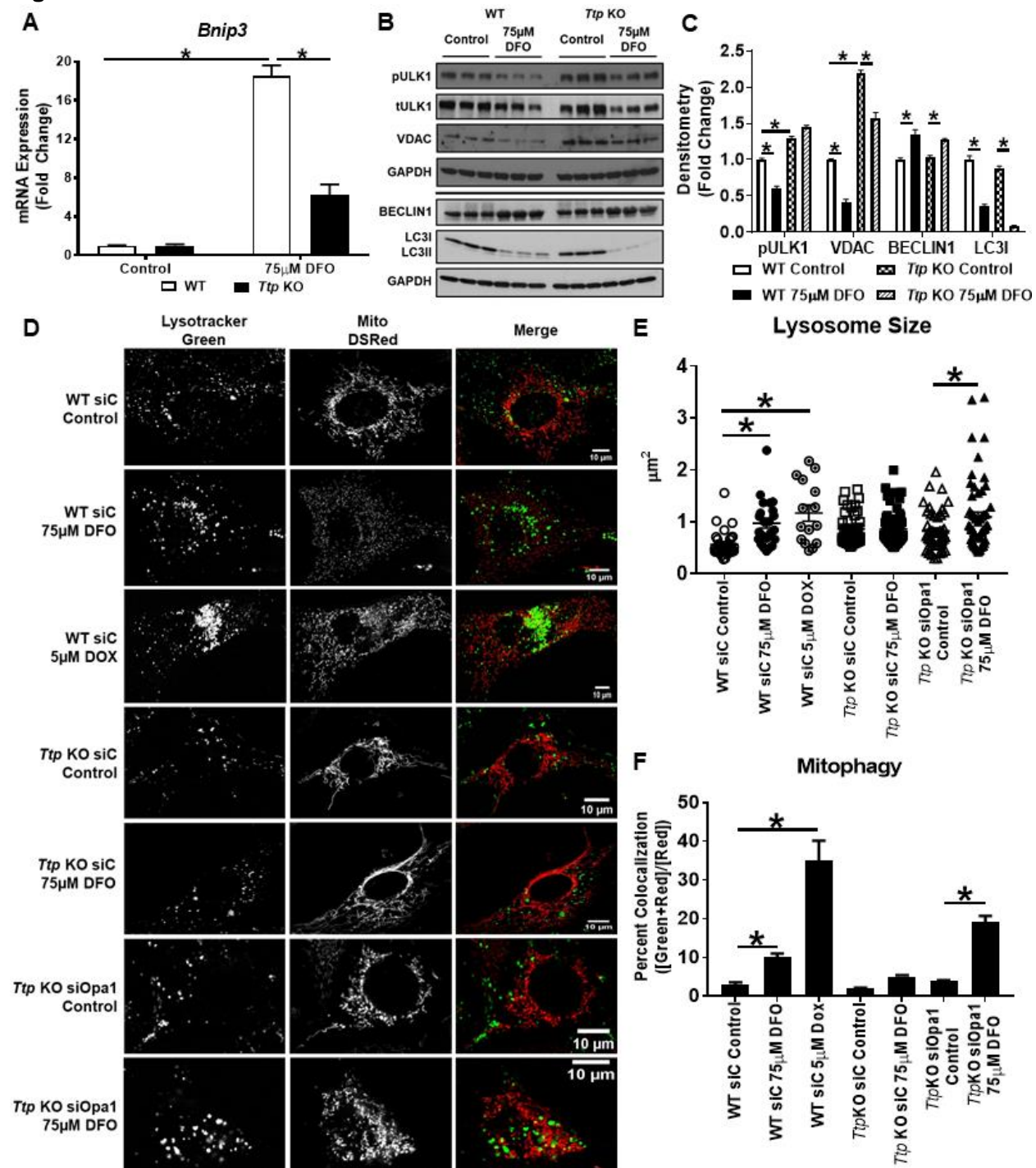


Figure 9.

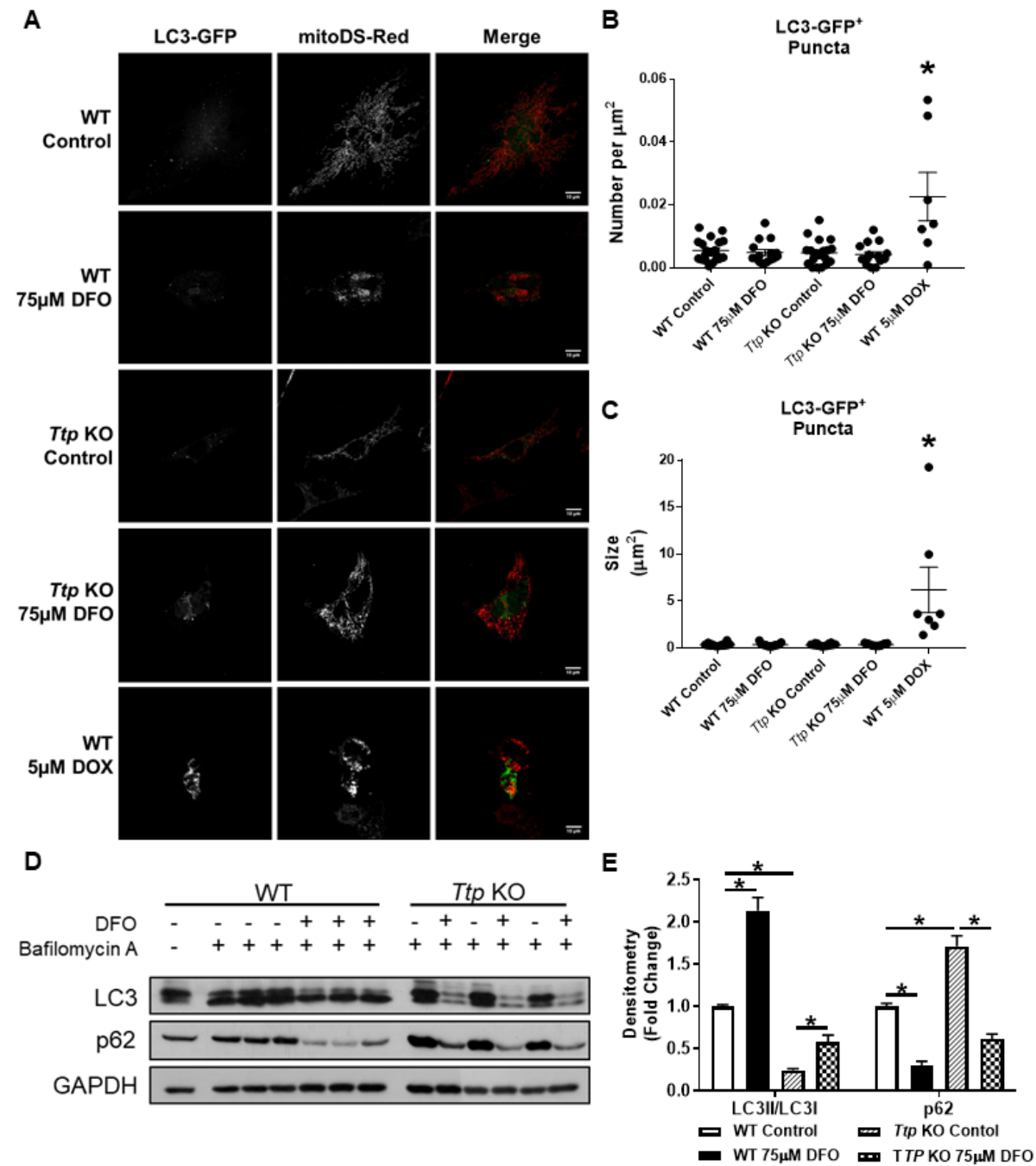


Figure 10.

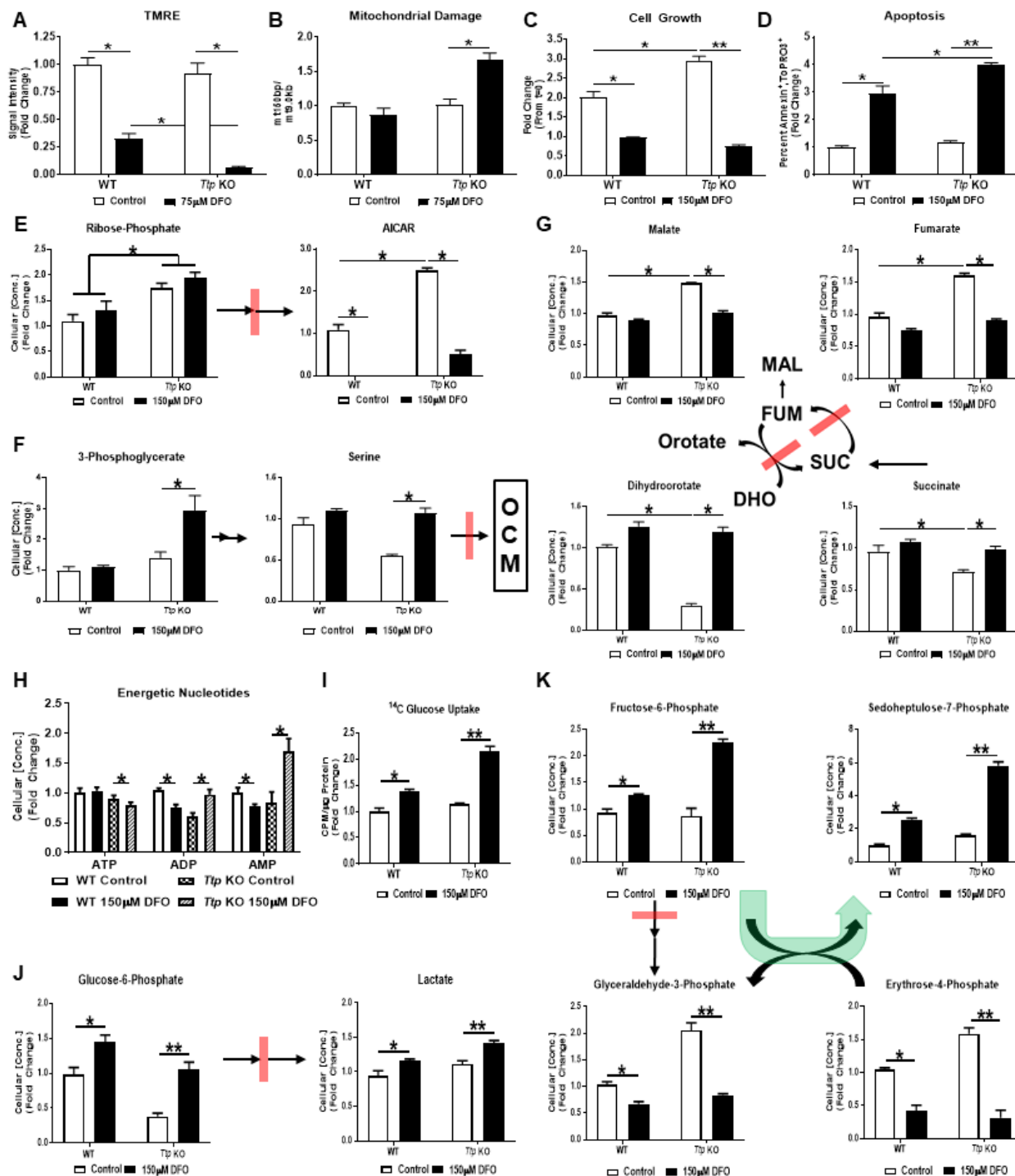


Figure 11.

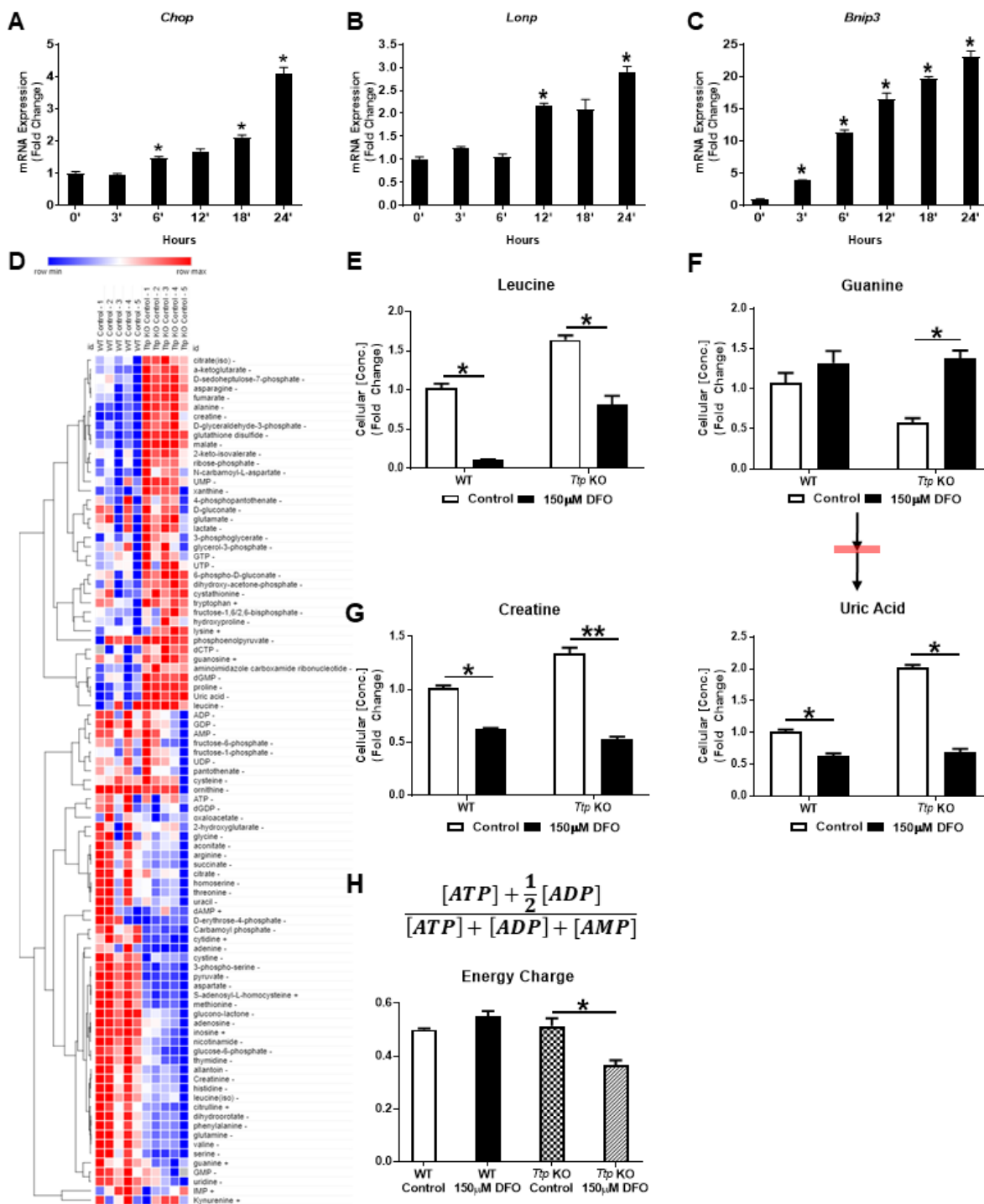


Figure 12.

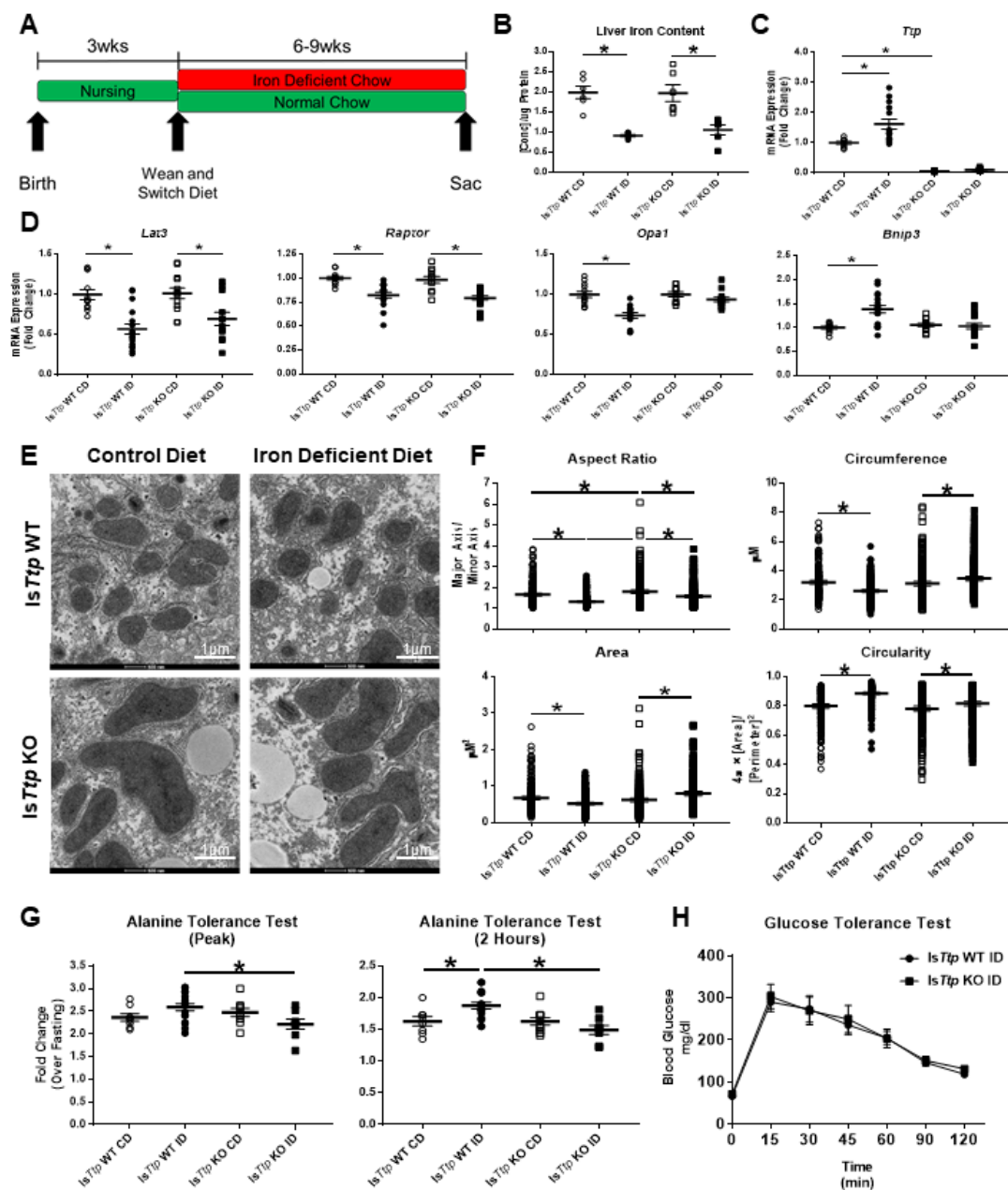


Figure 13.

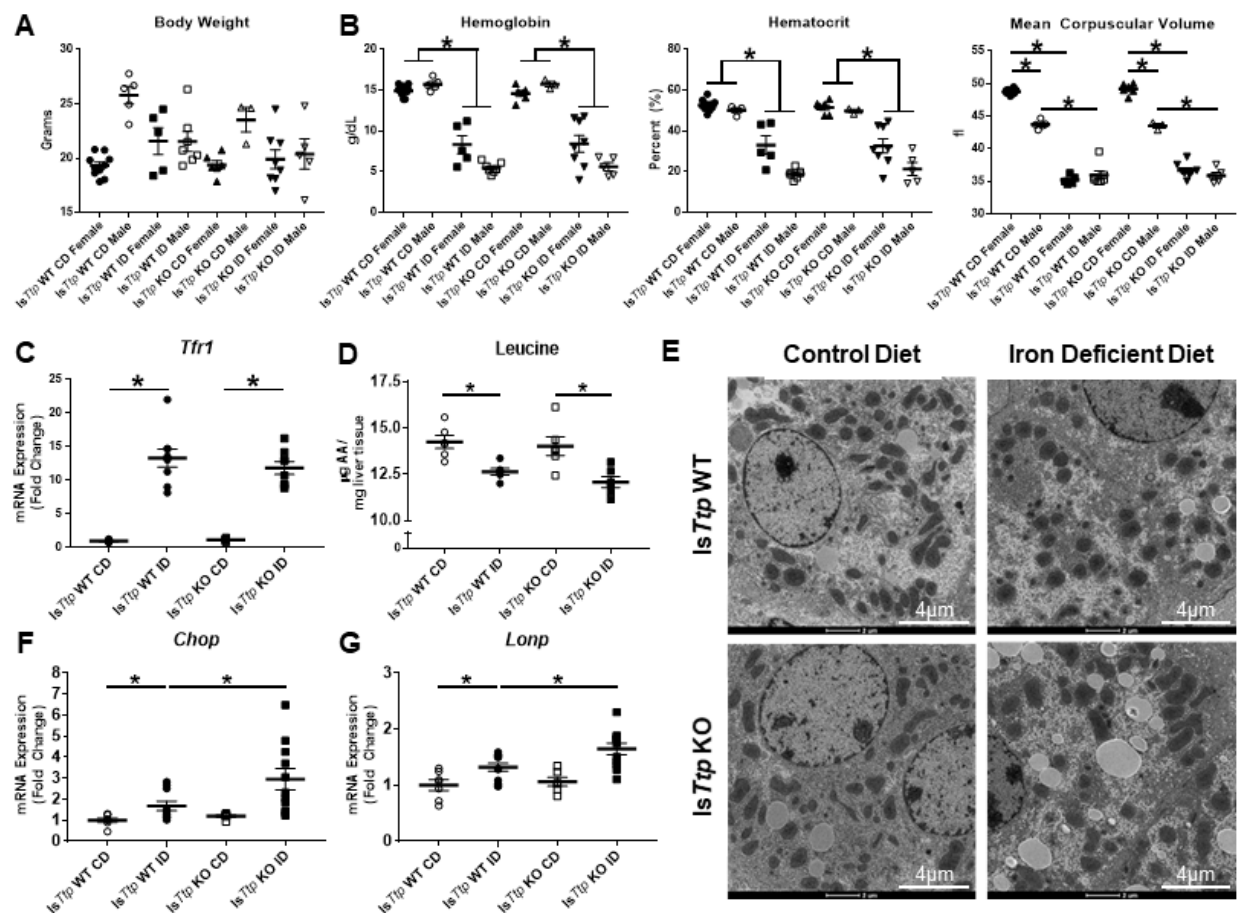
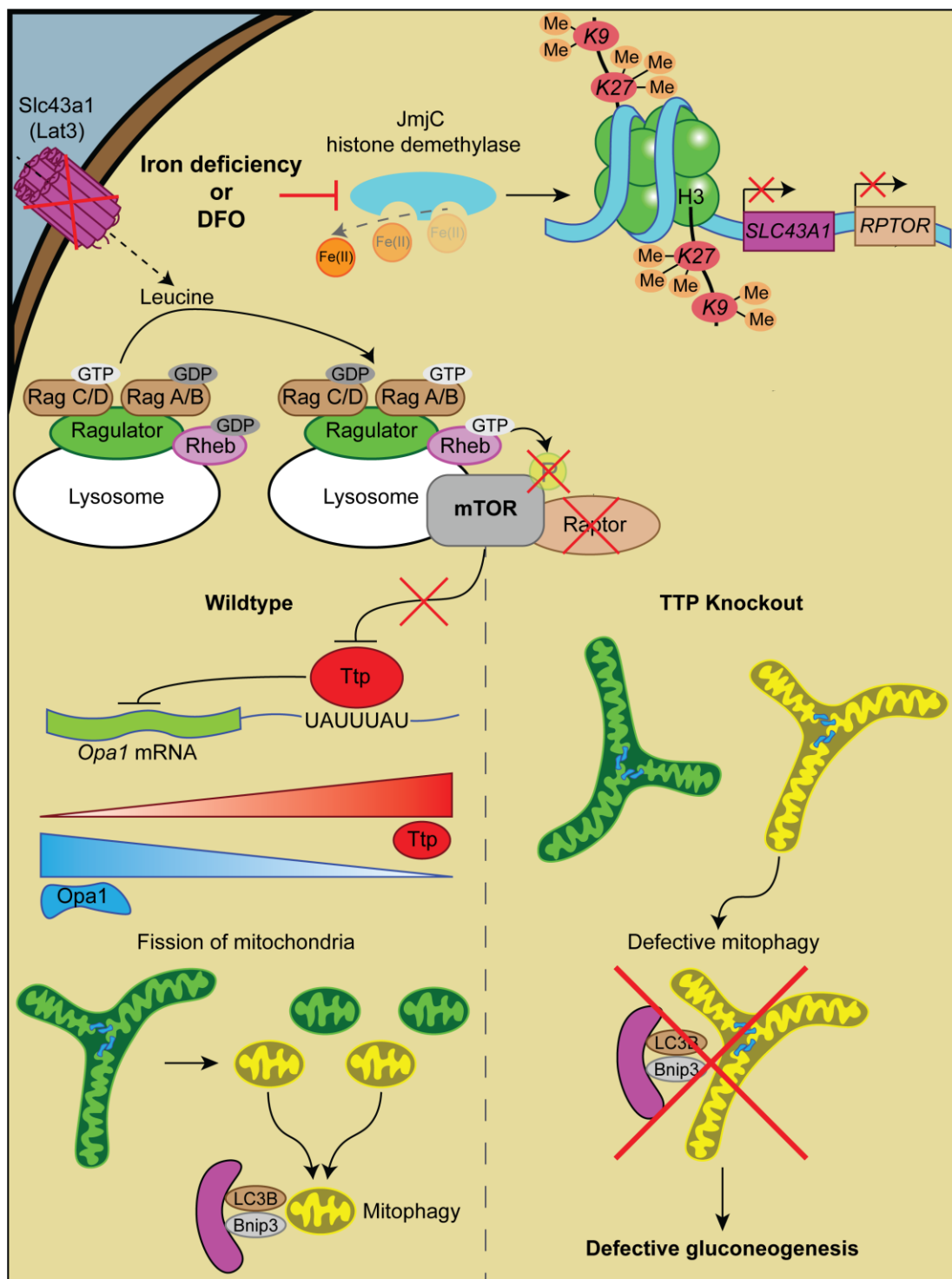


Figure 14.



## **Figure Legends**

### **Table 1. Hepatic Expression of Major Leucine Transporters.**

Gene expression values in TPM from two open source RNA-seq databases of human tissues.

(<https://www.gtexportal.org/home/>) (<https://www.proteinatlas.org/>)

**Figure 1. Iron chelation inhibits mTOR activity by altering amino acid homeostasis.** (A) qRT-PCR for *Ttp* in MEFs ( $p < 0.05$ , ANOVA with multiple comparisons). (B) Western blot analysis of S6K phosphorylation, ATF4 and TTP expression in MEFs treated with DFO. Same samples ran on two separate gels. GAPDH; loading control. (C) Radioactive methionine levels in the protein fraction of HEK293T cells ( $p < 0.05$ , two-sided t-test). (D) qRT-PCR for *Ttp* in MEFs deprived of total amino acids for 1hr ( $p < 0.05$ , two-sided t-test). (E) Total cellular leucine concentration in HEK293T cells ( $p < 0.05$ , two-sided t-test). (F) Radioactive leucine uptake in MEFs ( $p < 0.05$ , two-sided t-test). (G) Representative confocal imaging showing LAMP2 and mTOR subcellular localization in HEK293T cells. (H) Quantification of mTOR subcellular localization at the lysosome from images in G. (I) *Ttp*-promoter driven luciferase assay in HEK293T cells transfected with RAP2A (control) or RAGB<sup>Q99L</sup>/RAGC<sup>S75N</sup> (constitutively active RAG complex) ( $p < 0.05$ , ANOVA with multiple comparisons). (J) qRT-PCR for *Lat3* (*Slc43A1*) in MEFs ( $p < 0.05$ , two-sided t-test). (K) Western blot analysis of S6K phosphorylation in HEK293T cells. GAPDH; loading control (L) qRT-PCR for *TTP* in HEK293T cells ( $p < 0.05$ , ANOVA with multiple comparisons). Treatment times for all experiments were 24hrs unless otherwise specified.

### **Figure 2. Iron chelation inhibits mTOR activity by altering amino acid homeostasis**

**(Cont.).** (A) Cellular non-heme iron content in HEK293T cells ( $p < 0.05$ , two-sided t-test). (B-C)

qRT-PCR in MEFs (B) and primary murine hepatocytes (C) treated with DFO ( $p < 0.05$ , ANOVA with multiple comparisons). (D) qRT-PCR for *TTP* in HEK293T cells transfected with control or *RICTOR*-targeted siRNA and then treated with DFO. *RICTOR* and *TFR1*; positive controls confirming effective knockdown and iron chelation ( $p < 0.05$ , ANOVA with multiple comparisons). (E) Western blot analysis of S6K phosphorylation and TTP expression in WT and *Ttp* KO MEFs. (F-G) qRT-PCR for *Ttp* in WT and *Tsc2* KO (F), or *Ampk* KO (G) MEFs ( $p < 0.05$ , ANOVA with multiple comparisons). (H) Western blot analysis of TTP expression in *Tsc2* KO and *Ampk* KO MEFs. (I) Intracellular concentration of total amino acids (free + peptidyl) in HEK293T cells ( $p < 0.05$ , two-sided t-test). (J) Change in the percent total composition of selected amino acids after iron chelation. Samples are the same from I. (K) qRT-PCR for the LAT family of leucine transporters in MEFs, the human hepatocellular carcinoma cell line HepG2, and murine liver tissue. ( $p < 0.05$ , two-sided t-test). (L-M) Radioactive leucine uptake in *Ttp* KO MEFs treated with DFO (L), and WT MEFs treated with rapamycin (M) ( $p < 0.05$ , two-sided t-test). (N) qRT-PCR for the arginine dependent lysosomal leucine exporter, *SLC38A9* in HEK293T cells ( $p < 0.05$ , two-sided t-test). (O) Representative confocal images of HEK293T cells stained with acridine orange to visualize lysosomal permeability. (P) Quantification of acridine orange intensity from images in O (Q) Luciferase assay in HEK293T cells transfected with a 2.1kb or 137bp *Ttp*-promoter driven luciferase. A minimal promoter was sufficient in conferring full responsiveness to iron deprivation. Empty vector; negative control ( $p < 0.05$ , two-sided t-test). (R) Representative western blot analysis of HEK293T cells transfected with RAP2A (control) or RAGB<sup>Q99L</sup>/RAGC<sup>S75N</sup> (constitutively active RAG complex). Paired samples with Fig.1I. (S) *Ttp*-promoter driven luciferase assay in HEK293T cells transfected with RAP2A (control) or RHEB (confers growth factor insensitivity to mTOR) ( $p < 0.05$ , ANOVA with multiple comparisons). (T) Western blot analysis of paired samples with (S) demonstrating equivalent loss of S6K phosphorylation and FLAG expression.

**Figure 3. Iron chelation causes H3 hypermethylation and represses RAPTOR expression.**

(A) qRT-PCR for *RAPTOR* and *TTP*. *TFR1*; positive control confirming effective iron chelation ( $p < 0.05$ , two-sided t-test). (B) qRT-PCR for *TTP* in cells stably expression WT RAPTOR or RAPTOR-RHEB15 (amino acid insensitive). RAP2A; negative control ( $p < 0.05$ , two-sided t-test). (C) Western blot analysis of mTOR activity and H3 methyl marks. GAPDH; loading control. (D) Densitometry analysis of the western blot in C. ( $p < 0.05$ , two-sided t-test). (E) Chromatin immunoprecipitation (ChIP)-PCR of *RPTOR* gene locus using antibodies against H3K27me<sup>3</sup> and H3K9me<sup>2</sup>.  $n = 6$  per group ( $p < 0.05$ , two-sided t-test). (F) Western blot analysis of mTOR activity and TTP expression in cells treated with Jumonji-C domain containing demethylase inhibitors. Same samples ran on two separate gels. GAPDH; loading control. (G) Densitometry analysis of the western blot in F ( $p < 0.05$ , two-sided t-test). (H) qRT-PCR for *RAPTOR* in cells treated with histone demethylase inhibitors ( $p < 0.05$ , one way ANOVA). (I) qRT-PCR for *TTP* from the same samples in H ( $p < 0.05$ , one way ANOVA). (J) qRT-PCR for *RAPTOR* in cells treated with histone methyltransferase inhibitors ( $p < 0.05$ , ANOVA with multiple comparisons). (K) qRT-PCR for *TTP* from the same samples in J ( $p < 0.05$ , ANOVA with multiple comparisons). All treatments were performed in HEK293T cells for 24hrs unless otherwise specified.

**Figure 4. Iron chelation causes H3 hypermethylation and represses RAPTOR expression**

**(Cont.)** (A) qRT-PCR from the same samples in Fig. 3B confirming successful overexpression of RAPTOR ( $p < 0.05$ , one way ANOVA). (B) Images generated from the UCSC genome browser, build GRCh38/hg38 (<http://genome.ucsc.edu>) depicting the locations of the primers targeted around the *RPTOR* gene locus. (C) Primer locations targeted around the *SLC43A1* gene locus. (D) Images generated from the UCSC genome browser, build GRCh38/hg38 (<http://genome.ucsc.edu>) using the Track Data Hub to visualize H3K27me<sup>3</sup> marks at the *NPTX1*

promoter. *NPTX1* is a gene neighboring *RPTOR* that is hypermethylated at baseline. (E) Primer locations targeted around the *NPTX1* gene promoter. (F) ChIP-PCR of *SLC43A1* gene locus using antibodies against H3K27me<sup>3</sup> and H3K9me<sup>2</sup> ( $p < 0.05$ , two-sided t-test). (G) ChIP-PCR confirming effective pull-down with the H3K27me<sup>3</sup> antibody. The data from the ChIP-PCR experiments in Fig. 3E and Fig. 4F-G were generated from the same samples.

**Figure 5. Transcription factors SP1 and AP2 regulate *TTP* expression during Iron**

**deficiency.** (A) Sequence of the 137bp minimal mouse *Ttp* promoter with putative transcription factor binding sites labelled in blue. (B) *Ttp*-promoter luciferase assay in HEK293T cells transfected with constructs in which individual transcription factor binding sites were deleted or mutated. EV; empty vector, negative control, 137bp; WT minimal promoter, positive control ( $p < 0.05$ , one way ANOVA with multiple comparison). (C-D) Western blot and corresponding densitometry of subcellular localization of SP1 and AP2 in HEK293T cells exposed to iron chelation. ( $p < 0.05$ , two-sided t-test). (E) qRT-PCR for *SP1* and *AP2* expression in HEK293T cells. ( $p < 0.05$ , two-sided t-test). (F) qRT-PCR for *SP1* expression in HEK293T confirming successful *SP1* knockdown via transfection with shRNA. ( $p < 0.05$ , two-sided t-test). (G) qRT-PCR for *TTP* expression in same cells as (F) exposed to iron deficiency. ( $p < 0.05$ , one way ANOVA with multiple comparison). (H) *Ttp*-promoter luciferase assay in HEK293T cells overexpressing SP1 or empty vector. ( $p < 0.05$ , one way ANOVA with multiple comparison). (I) Western blot confirming successful SP1 overexpression. Parallel samples with (H).

**Figure 6. TTP mediated degradation of *Opa1* mRNA is required for mitochondrial fission**

**in response to iron chelation.** (A) qRT-PCR for genes involved in mitochondrial dynamics ( $p < 0.05$ , two-sided t-test). (B) RNA coimmunoprecipitation-PCR using a TTP antibody. *Vegf* and *Hprt1*; positive and negative controls, respectively ( $p < 0.05$ , two-sided t-test). (C) qRT-PCR in

HEPG2 cells overexpressing WT TTP or TTP<sup>C124R</sup> (tandem zinc-finger (TZF) mutant incapable of binding RNA). *TFR1* and *SNRK*; positive and negative controls, respectively ( $p < 0.05$ , two-sided t-test). (D-E) qRT-PCR in MEFs treated with 7.5 $\mu$ M Actinomycin-D ( $p < 0.05$ , two-sided t-test). (F-G) qRT-PCR in MEFs treated with DFO for 24hrs ( $p < 0.05$ , one way ANOVA). (H) Western blot analysis in MEFs treated with DFO for 12hrs. Same samples ran on two separate gels. GAPDH; loading control. (I) Densitometry analysis of western blot in H ( $p < 0.05$ , two-sided t-test). (J) Representative confocal imaging of MEFs treated with DFO for 12hrs. (K) Quantification of mitochondrial fission and fusion from images in J.  $n = \#$  of cells scored. ( $p < 0.05$ ,  $\chi^2$  test). (L) qRT-PCR in MEFs transfected with control (siC) or *Opa1*-targeted (si*Opa1*) siRNA ( $p < 0.05$ , one way ANOVA). (M) Representative confocal imaging of *Ttp* KO MEFs treated with DFO for 12hrs and either control or *Opa1*-targeted siRNA.

**Figure 7. TTP mediated degradation of *Opa1* mRNA is required for mitochondrial fission in response to iron chelation (Cont.).** (A) Table of candidate genes involved in mitochondrial dynamics and autophagy that could be potential targets of TTP. *In silico* analysis of ARE sites was performed using the University of Vienna's AREsite (<http://nibiru.tbi.univie.ac.at/cgi-bin/AREsite/AREsite.cgi>) (B-C) qRT-PCR for *Ttp* (B) and *Tfr1* (C) in the same samples as Fig. 5F-G confirming effective iron chelation. Asterisk (\*) indicates statistical significance when compared to 0 $\mu$ M within the same genotype; cross (†) indicates statistical significance when compared to WT within the same dose of DFO ( $p < 0.05$ , ANOVA with multiple comparisons). (D) Representative confocal imaging of MEFs treated with 50nM Rapamycin for 12hrs. (E) Quantification of mitochondrial fission and fusion from images in D.  $n = \#$  of cells scored. ( $p < 0.05$ ,  $\chi^2$  test). (F-G) Western blot analysis and corresponding densitometry of WT and *Ttp* KO MEFs transfected with either control or *Opa1*-targeted siRNA. ( $p < 0.05$ , ANOVA with multiple

comparisons). (H) Western blot analysis and corresponding densitometry of WT and *Ttp* KO MEFs transfected with either control or *Opa1*-targeted siRNA. ( $p < 0.05$ , ANOVA with multiple comparisons). (I) Densitometry analysis of western blot in H ( $p < 0.05$ , two-sided t-test). (J) Representative confocal imaging of MEFs treated with DFO for 12hrs. (K) Quantification of mitochondrial fission and fusion from images in J.  $n = \#$  of cells scored. ( $p < 0.05$ ,  $\chi^2$  test). (L) qRT-PCR in MEFs transfected with control (siC) or *Opa1*-targeted (si*Opa1*) siRNA ( $p < 0.05$ , one way ANOVA). (M) Representative confocal imaging of *Ttp* KO MEFs treated with DFO for 12hrs and either control or *Opa1*-targeted siRNA.

comparisons). (H) Representative confocal imaging of *Ttp* KO MEFs expressing *Mfn1*-targeted (shMfn1) shRNA and treated with DFO for 12hrs. Tomm20; mitochondrial inner-membrane protein, ToPRO3; nuclear stain. (I) qRT-PCR in MEFs stably infected with lentiviruses containing either control (shNSC) or *Mfn1*-targeted (shMfn1) shRNA ( $p < 0.05$ , ANOVA with multiple comparisons).

**Figure 8. Iron deficiency induces conventional mitophagy that is dependent on TTP-**

**mediated mitochondrial fission.** (A) Western blot analysis of proteins involved in autophagy/mitophagy in MEFs treated with DFO for 18hrs. Identical samples run on separate gels. GAPDH; loading control (B) Densitometry analysis of the western blot in B ( $p < 0.05$ , ANOVA with multiple comparisons). (C) qRT-PCR of the mitophagy marker *Bnip3* in WT and *Ttp* KO MEFs treated with DFO for 18hr ( $p < 0.05$ , ANOVA with multiple comparisons). (D) Representative confocal images of MEFs transfected with either control or *Opa1*-targeted siRNA and then treated with DFO for 18hrs. Lysosomes were labelled with lysotracker green dye. Doxorubicin – an mTOR independent inducer of mitophagy; positive control. (E) Quantification of lysosomal size from the images presented in D.  $n = 5-9$  cells per condition ( $p < 0.05$ , ANOVA with multiple comparisons) (F) Quantification of lysosomal and mitochondrial signal colocalization from the images presented in D.  $n = 5-9$  cells per condition ( $p < 0.05$ , ANOVA with multiple comparisons).

**Figure 9. Iron deficiency induces conventional mitophagy that is dependent on TTP-**

**mediated mitochondrial fission (Cont.).** (A) Representative confocal imaging of WT and *Ttp* KO MEFs. MEFs stably expressing mitochondria-targeted dsRED were transfected with a LC3-GFP plasmid to visualize autophagy and then treated with DFO for 18hrs. Doxorubicin; positive control. (B) Quantification of LC3-GFP<sup>+</sup> puncta density from the images presented in A.  $n = 5-9$

cells per condition ( $p < 0.05$ , ANOVA with multiple comparisons) (C) Quantification of LC3-GFP<sup>+</sup> puncta size from the images presented in A.  $n = 5-9$  cells per condition ( $p < 0.05$ , ANOVA with multiple comparisons). (D-E) Western blot and corresponding densitometry of WT and *Ttp* KO MEFs treated with bafilomycin-A to block lysosomal acidification and degradation of LC3II. ( $p < 0.05$ , ANOVA with multiple comparisons).

**Figure 10. Failure of mitochondrial fission in iron deficient *Ttp* KO MEFs causes mitochondrial dysfunction and altered metabolism.** (A) Quantification of TMRE signal intensity from images represented in Fig. 3J.  $n = 13-33$  cells per condition ( $p < 0.05$ , ANOVA with multiple comparisons). (B) qRT-PCR in MEFs treated with DFO for 24hrs. Damage induced double-strand breaks in mtDNA causes selective reduction in amplification of the 9.0kb amplicon ( $p < 0.05$ , ANOVA with multiple comparisons). (C) Quantification of cell growth in MEFs exposed to DFO for 24hrs. Live cells were quantified by counting adherent Hoechst<sup>(+)</sup>, propidium iodide<sup>(-)</sup> nuclei using fluorescent microscopy ( $p < 0.05$ , ANOVA with multiple comparisons). (D) Quantification of apoptosis in MEFs exposed to DFO for 24hrs. Apoptotic cells were quantified using flow cytometry as annexin<sup>+</sup>, ToPRO3<sup>+</sup> cell population. ( $p < 0.05$ , ANOVA with multiple comparisons). (E-H,J-K) Metabolomic profiling in WT and *Ttp* KO MEFs treated with DFO for 24hrs. levels of metabolites involved in de novo purine synthesis (E), one-carbon metabolism (F), the TCA-cycle (G), and energy production (H) are shown with points of disruption during iron deficiency signified by red bars. (I) Quantification of radioactive glucose uptake in WT and *Ttp* KO MEFs. ( $p < 0.05$ , ANOVA with multiple comparisons). (J-K) Metabolomic data showing increased glycolysis (J), and carbon shunting through the non-oxidative branch of the pentose-phosphate pathway (K) as highlighted by a green arrow. A single asterisk (\*) indicates statistical significance. Double asterisks (\*\*) designates significance and a greater fold change between

DFO and control in *Ttp* KO MEFs compared to WT MEFs. ( $p < 0.05$ , ANOVA with multiple comparisons).

**Figure 11. Failure of mitochondrial fission in iron deficient *Ttp* KO MEFs causes mitochondrial dysfunction and altered metabolism (Cont.).** (A-C) qRT-PCR for markers of UPR<sup>mt</sup> (A-B) and mitophagy (C) overtime after treatment with 150 $\mu$ M DFO. Asterisks (\*) indicates statistical significance compared to the preceding time point ( $p < 0.05$ , ANOVA with multiple comparisons). (D) Heat map and hierarchical clustering of metabolomics data using the Broad Institute's open source Morpheus software (<https://software.broadinstitute.org/morpheus/>). (E) Intracellular concentration of free leucine confirming effective iron chelation ( $p < 0.05$ , ANOVA with multiple comparisons). (F) Concentrations of key metabolites involved in purine catabolism. Blockage during iron deficiency signified by red bar ( $p < 0.05$ , ANOVA with multiple comparisons). (G) Intracellular concentration of creatine. A single asterisk (\*) indicates statistical significance. Double asterisks (\*\*) designates significance and a greater fold change between DFO and control in *Ttp* KO MEFs compared to WT MEFs. ( $p < 0.05$ , ANOVA with multiple comparisons). (H) Calculation of cellular energy charge using the indicated equation and the concentrations of AMP, ADP, and ATP ( $p < 0.05$ , ANOVA with multiple comparisons). The data from Fig. 9E-K and Fig. 10D-H were generated from the same experiment.

**Figure 12. Liver-specific deletion of *Ttp* causes failure of mitochondrial fission and mitophagy and defective gluconeogenesis during iron deficiency *in vivo*.** (A) Schematic depicting *in vivo* iron deficiency protocol. (B-D) Hepatic iron content and qRT-PCR demonstrating iron deficiency induced mTOR inactivation and mitophagy. CD = control diet, ID = iron deficient diet.  $n = 6-19$  mice per group ( $p < 0.05$ , ANOVA with multiple comparisons). (E)

Representative transmission electron micrographs of CD and ID hepatocyte mitochondria from WT and *IsTtp* KO mice. 9300x magnification (F) Mitochondrial morphology measurements from the images presented in E.  $n = 204-255$  mitochondria per group ( $p < 0.05$ , ANOVA with multiple comparisons). (G) Alanine tolerance tests from WT and *IsTtp* KO mice subjected to CD or ID. Peak values occurred within 60-90min of injection.  $n = 8-17$  mice per group ( $p < 0.05$ , ANOVA with multiple comparisons). (H) Glucose tolerance test from ID WT and *IsTtp* KO mice.  $n = 9-12$  mice per group.

**Figure 13. Liver-specific deletion of *Ttp* causes failure of mitochondrial fission and mitophagy and defective gluconeogenesis during iron deficiency *in vivo* (Cont.).** (A-B)

Body weight and red blood cell profiling from WT and *IsTtp* KO mice subjected to CD or ID. No genotype specific differences were observed in body weight or parameters of system anemia. CD = control diet, ID = iron deficient diet.  $n = 6-19$  mice per group ( $p < 0.05$ , ANOVA with multiple comparisons). (C) qRT-PCR of hepatic *Tfr1* expression in WT and *IsTtp* KO mice subjected to CD or ID.  $n = 6-19$  mice per group ( $p < 0.05$ , ANOVA with multiple comparisons). (D) Hepatic concentration of free leucine in WT and *IsTtp* KO mice subjected to CD or ID.  $n = 6$  samples per group ( $p < 0.05$ , ANOVA with multiple comparison). (E) Representative transmission electron micrographs of CD and ID hepatocyte mitochondria from WT and *IsTtp* KO mice. 2900x magnification. Images taken together with images shown in Fig. 6D (F) qRT-PCR of hepatic *Chop* and *Lonp* expression in WT and *IsTtp* KO mice subjected to CD or ID.  $n = 6-19$  mice per group ( $p < 0.05$ , ANOVA with multiple comparisons).

**Figure 14. Graphical Summary.**

Iron chelation results in histone hypermethylation and epigenetic silencing of the leucine transporter *LAT3* and mTORC1 cofactor *RAPTOR*. Loss of mTORC1 activity promotes

mitochondrial fission and mitophagy through the induction of the mRNA binding protein TTP which post-transcriptionally represses *OPA1* expression. Genetic deletion of *TTP* results in dysfunction of mitochondrial metabolism and impaired hepatic gluconeogenesis in response to iron deficiency. Image generated in collaboration with Jonathan Anker.

1. Yi, C., et al., *Iron-catalysed oxidation intermediates captured in a DNA repair dioxygenase*. Nature, 2010. **468**(7321): p. 330-3.
2. Beinert, H., *Spectroscopy of succinate dehydrogenases, a historical perspective*. Biochim Biophys Acta, 2002. **1553**(1-2): p. 7-22.
3. Ohmura, N., et al., *Anaerobic respiration using Fe(3+), S(0), and H(2) in the chemolithoautotrophic bacterium Acidithiobacillus ferrooxidans*. J Bacteriol, 2002. **184**(8): p. 2081-7.
4. Fleming, M.D., et al., *Microcytic anaemia mice have a mutation in Nramp2, a candidate iron transporter gene*. Nat Genet, 1997. **16**(4): p. 383-6.
5. Gunshin, H., et al., *Cloning and characterization of a mammalian proton-coupled metal-ion transporter*. Nature, 1997. **388**(6641): p. 482-8.
6. Shayeghi, M., et al., *Identification of an intestinal heme transporter*. Cell, 2005. **122**(5): p. 789-801.
7. Qiu, A., et al., *Identification of an intestinal folate transporter and the molecular basis for hereditary folate malabsorption*. Cell, 2006. **127**(5): p. 917-28.
8. Hentze, M.W., et al., *Two to tango: regulation of Mammalian iron metabolism*. Cell, 2010. **142**(1): p. 24-38.
9. McKie, A.T., et al., *A novel duodenal iron-regulated transporter, IREG1, implicated in the basolateral transfer of iron to the circulation*. Mol Cell, 2000. **5**(2): p. 299-309.
10. Ganz, T., *Systemic iron homeostasis*. Physiol Rev, 2013. **93**(4): p. 1721-41.
11. Vulpe, C.D., et al., *Hephaestin, a ceruloplasmin homologue implicated in intestinal iron transport, is defective in the sla mouse*. Nat Genet, 1999. **21**(2): p. 195-9.
12. Park, C.H., et al., *Hepcidin, a urinary antimicrobial peptide synthesized in the liver*. J Biol Chem, 2001. **276**(11): p. 7806-10.

13. Nemeth, E., et al., *Hepcidin regulates cellular iron efflux by binding to ferroportin and inducing its internalization*. Science, 2004. **306**(5704): p. 2090-3.
14. Santos, P.C., J.E. Krieger, and A.C. Pereira, *Molecular diagnostic and pathogenesis of hereditary hemochromatosis*. Int J Mol Sci, 2012. **13**(2): p. 1497-511.
15. Knutson, M.D., et al., *Iron release from macrophages after erythrophagocytosis is up-regulated by ferroportin 1 overexpression and down-regulated by hepcidin*. Proc Natl Acad Sci U S A, 2005. **102**(5): p. 1324-8.
16. Babitt, J.L. and H.Y. Lin, *Molecular mechanisms of hepcidin regulation: implications for the anemia of CKD*. Am J Kidney Dis, 2010. **55**(4): p. 726-41.
17. Babitt, J.L., et al., *Bone morphogenetic protein signaling by hemojuvelin regulates hepcidin expression*. Nat Genet, 2006. **38**(5): p. 531-9.
18. Pietrangelo, A., *Hereditary hemochromatosis: pathogenesis, diagnosis, and treatment*. Gastroenterology, 2010. **139**(2): p. 393-408, 408 e1-2.
19. Wang, R.H., et al., *A role of SMAD4 in iron metabolism through the positive regulation of hepcidin expression*. Cell Metab, 2005. **2**(6): p. 399-409.
20. Du, X., et al., *The serine protease TMPRSS6 is required to sense iron deficiency*. Science, 2008. **320**(5879): p. 1088-92.
21. Silvestri, L., et al., *The serine protease matriptase-2 (TMPRSS6) inhibits hepcidin activation by cleaving membrane hemojuvelin*. Cell Metab, 2008. **8**(6): p. 502-11.
22. Gao, J., et al., *Interaction of the hereditary hemochromatosis protein HFE with transferrin receptor 2 is required for transferrin-induced hepcidin expression*. Cell Metab, 2009. **9**(3): p. 217-27.
23. Schmidt, P.J., et al., *The transferrin receptor modulates Hfe-dependent regulation of hepcidin expression*. Cell Metab, 2008. **7**(3): p. 205-14.

24. D'Alessio, F., M.W. Hentze, and M.U. Muckenthaler, *The hemochromatosis proteins HFE, Tfr2, and HJV form a membrane-associated protein complex for hepcidin regulation*. J Hepatol, 2012. **57**(5): p. 1052-60.
25. Burger, P., et al., *CD47 functions as a molecular switch for erythrocyte phagocytosis*. Blood, 2012. **119**(23): p. 5512-21.
26. Oldenborg, P.A., H.D. Gresham, and F.P. Lindberg, *CD47-signal regulatory protein alpha (SIRPalpha) regulates Fc gamma and complement receptor-mediated phagocytosis*. J Exp Med, 2001. **193**(7): p. 855-62.
27. White, C., et al., *HRG1 is essential for heme transport from the phagolysosome of macrophages during erythrophagocytosis*. Cell Metab, 2013. **17**(2): p. 261-70.
28. Wilks, A. and G. Heinzl, *Heme oxygenation and the widening paradigm of heme degradation*. Arch Biochem Biophys, 2014. **544**: p. 87-95.
29. Epstein, A.C., et al., *C. elegans EGL-9 and mammalian homologs define a family of dioxygenases that regulate HIF by prolyl hydroxylation*. Cell, 2001. **107**(1): p. 43-54.
30. Bruick, R.K. and S.L. McKnight, *A conserved family of prolyl-4-hydroxylases that modify HIF*. Science, 2001. **294**(5545): p. 1337-40.
31. Maxwell, P.H., et al., *The tumour suppressor protein VHL targets hypoxia-inducible factors for oxygen-dependent proteolysis*. Nature, 1999. **399**(6733): p. 271-5.
32. Tacchini, L., et al., *Transferrin receptor induction by hypoxia. HIF-1-mediated transcriptional activation and cell-specific post-transcriptional regulation*. J Biol Chem, 1999. **274**(34): p. 24142-6.
33. Qian, Z.M., et al., *Divalent metal transporter 1 is a hypoxia-inducible gene*. J Cell Physiol, 2011. **226**(6): p. 1596-603.
34. Liu, Q., et al., *Hypoxia-inducible factor regulates hepcidin via erythropoietin-induced erythropoiesis*. J Clin Invest, 2012. **122**(12): p. 4635-44.

35. Braliou, G.G., et al., *2-Oxoglutarate-dependent oxygenases control hepcidin gene expression*. J Hepatol, 2008. **48**(5): p. 801-10.
36. Verga Falzacappa, M.V., et al., *STAT3 mediates hepatic hepcidin expression and its inflammatory stimulation*. Blood, 2007. **109**(1): p. 353-8.
37. Holden, V.I. and M.A. Bachman, *Diverging roles of bacterial siderophores during infection*. Metallomics, 2015. **7**(6): p. 986-95.
38. Weiss, G. and L.T. Goodnough, *Anemia of chronic disease*. N Engl J Med, 2005. **352**(10): p. 1011-23.
39. World Health, O., *Conclusions and recommendations of the WHO Consultation on prevention and control of iron deficiency in infants and young children in malaria-endemic areas*. Food Nutr Bull, 2007. **28**(4 Suppl): p. S621-7.
40. Kassebaum, N.J., et al., *A systematic analysis of global anemia burden from 1990 to 2010*. Blood, 2014. **123**(5): p. 615-24.
41. Baltussen, R., C. Knai, and M. Sharan, *Iron fortification and iron supplementation are cost-effective interventions to reduce iron deficiency in four subregions of the world*. J Nutr, 2004. **134**(10): p. 2678-84.
42. WHO, M.H.a.S.M.P., Division of Family Health, *World Health Organization. The prevalence of anaemia in women: a tabulation of available information*. WHO/MCH/MSM/92, 1992. **2nd ed.**
43. Haider, B.A., et al., *Anaemia, prenatal iron use, and risk of adverse pregnancy outcomes: systematic review and meta-analysis*. BMJ, 2013. **346**: p. f3443.
44. Lozoff, B., et al., *Long-lasting neural and behavioral effects of iron deficiency in infancy*. Nutr Rev, 2006. **64**(5 Pt 2): p. S34-43; discussion S72-91.
45. Choudhury, V., et al., *Latent iron deficiency at birth influences auditory neural maturation in late preterm and term infants*. Am J Clin Nutr, 2015. **102**(5): p. 1030-4.

46. Okon, E., I.S. Levij, and E.A. Rachmilewitz, *Splenectomy, iron overload and liver cirrhosis in beta-thalassemia major*. Acta Haematol, 1976. **56**(3): p. 142-50.
47. Tangvarasittichai, S., et al., *Association of iron overload and oxidative stress with insulin resistance in transfusion-dependent beta-thalassemia major and beta-thalassemia/HbE patients*. Clin Lab, 2013. **59**(7-8): p. 861-8.
48. Ichikawa, Y., et al., *Cardiotoxicity of doxorubicin is mediated through mitochondrial iron accumulation*. J Clin Invest, 2014. **124**(2): p. 617-30.
49. Chang, H.C., et al., *Reduction in mitochondrial iron alleviates cardiac damage during injury*. EMBO Mol Med, 2016. **8**(3): p. 247-67.
50. Khechaduri, A., et al., *Heme levels are increased in human failing hearts*. J Am Coll Cardiol, 2013. **61**(18): p. 1884-93.
51. Olson, L.J., et al., *Cardiac iron deposition in idiopathic hemochromatosis: histologic and analytic assessment of 14 hearts from autopsy*. J Am Coll Cardiol, 1987. **10**(6): p. 1239-43.
52. Kra, S.J., J.W. Hollingsworth, and S.C. Finch, *Arthritis with Synovial Iron Deposition in a Patient with Hemochromatosis*. N Engl J Med, 1965. **272**: p. 1268-71.
53. Gan, E.K., L.W. Powell, and J.K. Olynyk, *Natural history and management of HFE-hemochromatosis*. Semin Liver Dis, 2011. **31**(3): p. 293-301.
54. Simcox, J.A. and D.A. McClain, *Iron and diabetes risk*. Cell Metab, 2013. **17**(3): p. 329-41.
55. Uitz, P.M., et al., *Pituitary function in patients with hereditary haemochromatosis*. Horm Metab Res, 2013. **45**(1): p. 54-61.
56. Bardou-Jacquet, E. and P. Brissot, *Diagnostic evaluation of hereditary hemochromatosis (HFE and non-HFE)*. Hematol Oncol Clin North Am, 2014. **28**(4): p. 625-35, v.

57. Kato, J., et al., *A mutation, in the iron-responsive element of H ferritin mRNA, causing autosomal dominant iron overload*. Am J Hum Genet, 2001. **69**(1): p. 191-7.
58. Schieber, M. and N.S. Chandel, *ROS function in redox signaling and oxidative stress*. Curr Biol, 2014. **24**(10): p. R453-62.
59. Motohashi, N. and I. Mori, *Superoxide-dependent formation of hydroxyl radical catalyzed by transferrin*. FEBS Lett, 1983. **157**(1): p. 197-9.
60. Murphy, M.P., *How mitochondria produce reactive oxygen species*. Biochem J, 2009. **417**(1): p. 1-13.
61. Winterbourn, C.C., *Toxicity of iron and hydrogen peroxide: the Fenton reaction*. Toxicol Lett, 1995. **82-83**: p. 969-74.
62. Dixon, S.J., et al., *Ferroptosis: an iron-dependent form of nonapoptotic cell death*. Cell, 2012. **149**(5): p. 1060-72.
63. Yang, W.S. and B.R. Stockwell, *Ferroptosis: Death by Lipid Peroxidation*. Trends Cell Biol, 2016. **26**(3): p. 165-176.
64. Vanden Berghe, T., et al., *Regulated necrosis: the expanding network of non-apoptotic cell death pathways*. Nat Rev Mol Cell Biol, 2014. **15**(2): p. 135-47.
65. Jiang, L., et al., *Ferroptosis as a p53-mediated activity during tumour suppression*. Nature, 2015. **520**(7545): p. 57-62.
66. Klausner, R.D., J. Harford, and J. van Renswoude, *Rapid internalization of the transferrin receptor in K562 cells is triggered by ligand binding or treatment with a phorbol ester*. Proc Natl Acad Sci U S A, 1984. **81**(10): p. 3005-9.
67. Klausner, R.D., et al., *Receptor-mediated endocytosis of transferrin in K562 cells*. J Biol Chem, 1983. **258**(8): p. 4715-24.
68. Liu, A.P., et al., *Local clustering of transferrin receptors promotes clathrin-coated pit initiation*. J Cell Biol, 2010. **191**(7): p. 1381-93.

69. Guo, B., et al., *Iron regulates the intracellular degradation of iron regulatory protein 2 by the proteasome*. J Biol Chem, 1995. **270**(37): p. 21645-51.
70. Bakkeren, D.L., et al., *Release of iron from endosomes is an early step in the transferrin cycle*. Int J Biochem, 1987. **19**(2): p. 179-86.
71. Ohgami, R.S., et al., *Identification of a ferrireductase required for efficient transferrin-dependent iron uptake in erythroid cells*. Nat Genet, 2005. **37**(11): p. 1264-9.
72. Tabuchi, M., et al., *Human NRAMP2/DMT1, which mediates iron transport across endosomal membranes, is localized to late endosomes and lysosomes in HEp-2 cells*. J Biol Chem, 2000. **275**(29): p. 22220-8.
73. De Domenico, I., D. McVey Ward, and J. Kaplan, *Regulation of iron acquisition and storage: consequences for iron-linked disorders*. Nat Rev Mol Cell Biol, 2008. **9**(1): p. 72-81.
74. Anderson, G.J. and C.D. Vulpe, *Mammalian iron transport*. Cell Mol Life Sci, 2009. **66**(20): p. 3241-61.
75. Theil, E.C., *Ferritin: structure, gene regulation, and cellular function in animals, plants, and microorganisms*. Annu Rev Biochem, 1987. **56**: p. 289-315.
76. Shi, H., et al., *A cytosolic iron chaperone that delivers iron to ferritin*. Science, 2008. **320**(5880): p. 1207-10.
77. Kaur, J. and J. Debnath, *Autophagy at the crossroads of catabolism and anabolism*. Nat Rev Mol Cell Biol, 2015. **16**(8): p. 461-72.
78. Mancias, J.D., et al., *Quantitative proteomics identifies NCOA4 as the cargo receptor mediating ferritinophagy*. Nature, 2014. **509**(7498): p. 105-9.
79. De Domenico, I., D.M. Ward, and J. Kaplan, *Specific iron chelators determine the route of ferritin degradation*. Blood, 2009. **114**(20): p. 4546-51.

80. Mancias, J.D., et al., *Ferritinophagy via NCOA4 is required for erythropoiesis and is regulated by iron dependent HERC2-mediated proteolysis*. *Elife*, 2015. **4**.
81. Dowdle, W.E., et al., *Selective VPS34 inhibitor blocks autophagy and uncovers a role for NCOA4 in ferritin degradation and iron homeostasis in vivo*. *Nat Cell Biol*, 2014. **16**(11): p. 1069-79.
82. Patel, B.N., et al., *Ceruloplasmin regulates iron levels in the CNS and prevents free radical injury*. *J Neurosci*, 2002. **22**(15): p. 6578-86.
83. Bosio, S., et al., *Anemia and iron overload due to compound heterozygosity for novel ceruloplasmin mutations*. *Blood*, 2002. **100**(6): p. 2246-8.
84. Chen, C. and B.H. Paw, *Cellular and mitochondrial iron homeostasis in vertebrates*. *Biochim Biophys Acta*, 2012. **1823**(9): p. 1459-67.
85. Shaw, G.C., et al., *Mitoferrin is essential for erythroid iron assimilation*. *Nature*, 2006. **440**(7080): p. 96-100.
86. Troadec, M.B., et al., *Targeted deletion of the mouse Mitoferrin1 gene: from anemia to protoporphyria*. *Blood*, 2011. **117**(20): p. 5494-502.
87. Paradkar, P.N., et al., *Regulation of mitochondrial iron import through differential turnover of mitoferrin 1 and mitoferrin 2*. *Mol Cell Biol*, 2009. **29**(4): p. 1007-16.
88. Chen, W., et al., *Abcb10 physically interacts with mitoferrin-1 (Slc25a37) to enhance its stability and function in the erythroid mitochondria*. *Proc Natl Acad Sci U S A*, 2009. **106**(38): p. 16263-8.
89. Sheftel, A.D., et al., *Direct interorganellar transfer of iron from endosome to mitochondrion*. *Blood*, 2007. **110**(1): p. 125-32.
90. Lim, J.E., et al., *A mutation in Sec15l1 causes anemia in hemoglobin deficit (hbd) mice*. *Nat Genet*, 2005. **37**(11): p. 1270-3.

91. Zhang, A.S., A.D. Sheftel, and P. Ponka, *The anemia of "haemoglobin-deficit" (hbd/hbd) mice is caused by a defect in transferrin cycling*. Exp Hematol, 2006. **34**(5): p. 593-8.
92. Levi, S., et al., *A human mitochondrial ferritin encoded by an intronless gene*. J Biol Chem, 2001. **276**(27): p. 24437-40.
93. Corsi, B., et al., *Human mitochondrial ferritin expressed in HeLa cells incorporates iron and affects cellular iron metabolism*. J Biol Chem, 2002. **277**(25): p. 22430-7.
94. Cavadini, P., et al., *RNA silencing of the mitochondrial ABCB7 transporter in HeLa cells causes an iron-deficient phenotype with mitochondrial iron overload*. Blood, 2007. **109**(8): p. 3552-9.
95. Ichikawa, Y., et al., *Disruption of ATP-binding cassette B8 in mice leads to cardiomyopathy through a decrease in mitochondrial iron export*. Proc Natl Acad Sci U S A, 2012. **109**(11): p. 4152-7.
96. Lill, R. and U. Muhlenhoff, *Maturation of iron-sulfur proteins in eukaryotes: mechanisms, connected processes, and diseases*. Annu Rev Biochem, 2008. **77**: p. 669-700.
97. Sato, K., et al., *Loss of ABCB7 gene: pathogenesis of mitochondrial iron accumulation in erythroblasts in refractory anemia with ringed sideroblast with isodicentric (X)(q13)*. Int J Hematol, 2011. **93**(3): p. 311-318.
98. Sipos, K., et al., *Maturation of cytosolic iron-sulfur proteins requires glutathione*. J Biol Chem, 2002. **277**(30): p. 26944-9.
99. Srinivasan, V., A.J. Pierik, and R. Lill, *Crystal structures of nucleotide-free and glutathione-bound mitochondrial ABC transporter Atm1*. Science, 2014. **343**(6175): p. 1137-40.
100. Bayeva, M., et al., *ATP-binding cassette B10 regulates early steps of heme synthesis*. Circ Res, 2013. **113**(3): p. 279-87.

101. Gille, G. and H. Reichmann, *Iron-dependent functions of mitochondria--relation to neurodegeneration*. J Neural Transm (Vienna), 2011. **118**(3): p. 349-59.
102. Ross, K.L. and R.S. Eisenstein, *Iron deficiency decreases mitochondrial aconitase abundance and citrate concentration without affecting tricarboxylic acid cycle capacity in rat liver*. J Nutr, 2002. **132**(4): p. 643-51.
103. Hirst, J., *Mitochondrial complex I*. Annu Rev Biochem, 2013. **82**: p. 551-75.
104. Yoshikawa, S., et al., *Structural studies on bovine heart cytochrome c oxidase*. Biochim Biophys Acta, 2012. **1817**(4): p. 579-89.
105. Sheftel, A., O. Stehling, and R. Lill, *Iron-sulfur proteins in health and disease*. Trends Endocrinol Metab, 2010. **21**(5): p. 302-14.
106. Chandramouli, K., et al., *Formation and properties of [4Fe-4S] clusters on the IscU scaffold protein*. Biochemistry, 2007. **46**(23): p. 6804-11.
107. Gerber, J., U. Muhlenhoff, and R. Lill, *An interaction between frataxin and Isu1/Nfs1 that is crucial for Fe/S cluster synthesis on Isu1*. EMBO Rep, 2003. **4**(9): p. 906-11.
108. Mochel, F. and R.G. Haller, *Myopathy with Deficiency of ISCU*, in *GeneReviews((R))*, M.P. Adam, et al., Editors. 1993: Seattle (WA).
109. Olsson, A., et al., *Myopathy with lactic acidosis is linked to chromosome 12q23.3-24.11 and caused by an intron mutation in the ISCU gene resulting in a splicing defect*. Hum Mol Genet, 2008. **17**(11): p. 1666-72.
110. Puccio, H., et al., *Mouse models for Friedreich ataxia exhibit cardiomyopathy, sensory nerve defect and Fe-S enzyme deficiency followed by intramitochondrial iron deposits*. Nat Genet, 2001. **27**(2): p. 181-6.
111. Patel, P.I. and G. Isaya, *Friedreich ataxia: from GAA triplet-repeat expansion to frataxin deficiency*. Am J Hum Genet, 2001. **69**(1): p. 15-24.

112. Netz, D.J., et al., *Maturation of cytosolic and nuclear iron-sulfur proteins*. Trends Cell Biol, 2014. **24**(5): p. 303-12.
113. Hunter, G.A. and G.C. Ferreira, *Molecular enzymology of 5-aminolevulinate synthase, the gatekeeper of heme biosynthesis*. Biochim Biophys Acta, 2011. **1814**(11): p. 1467-73.
114. Abu-Farha, M., J. Niles, and W.G. Willmore, *Erythroid-specific 5-aminolevulinate synthase protein is stabilized by low oxygen and proteasomal inhibition*. Biochem Cell Biol, 2005. **83**(5): p. 620-30.
115. Sadlon, T.J., et al., *Regulation of erythroid 5-aminolevulinate synthase expression during erythropoiesis*. Int J Biochem Cell Biol, 1999. **31**(10): p. 1153-67.
116. Sawicki, K.T., et al., *Increased Heme Levels in the Heart Lead to Exacerbated Ischemic Injury*. J Am Heart Assoc, 2015. **4**(8): p. e002272.
117. Schultz, I.J., et al., *Iron and porphyrin trafficking in heme biogenesis*. J Biol Chem, 2010. **285**(35): p. 26753-9.
118. Chiabrando, D., et al., *The mitochondrial heme exporter FLVCR1b mediates erythroid differentiation*. J Clin Invest, 2012. **122**(12): p. 4569-79.
119. Higdon, A.N., et al., *Hemin causes mitochondrial dysfunction in endothelial cells through promoting lipid peroxidation: the protective role of autophagy*. Am J Physiol Heart Circ Physiol, 2012. **302**(7): p. H1394-409.
120. Landaw, S.A., E.W. Callahan, Jr., and R. Schmid, *Catabolism of heme in vivo: comparison of the simultaneous production of bilirubin and carbon monoxide*. J Clin Invest, 1970. **49**(5): p. 914-25.
121. Cantarow, A., C.W. Wirts, and et al., *Excretion of bilirubin and bromsulfalein in bile*. Am J Physiol, 1948. **154**(2): p. 211-9.

122. Maines, M.D., *Heme oxygenase: function, multiplicity, regulatory mechanisms, and clinical applications*. FASEB J, 1988. **2**(10): p. 2557-68.
123. Han, F., et al., *Hypoxemia induces expression of heme oxygenase-1 and heme oxygenase-2 proteins in the mouse myocardium*. J Biochem, 2010. **147**(1): p. 143-51.
124. Anning, P.B., et al., *Iron overload upregulates haem oxygenase 1 in the lung more rapidly than in other tissues*. FEBS Lett, 1999. **447**(1): p. 111-4.
125. Guernsey, D.L., et al., *Mutations in mitochondrial carrier family gene SLC25A38 cause nonsyndromic autosomal recessive congenital sideroblastic anemia*. Nat Genet, 2009. **41**(6): p. 651-3.
126. Horton, J.R., et al., *Characterization of a Linked Jumonji Domain of the KDM5/JARID1 Family of Histone H3 Lysine 4 Demethylases*. J Biol Chem, 2016. **291**(6): p. 2631-46.
127. Takeuchi, T., et al., *Gene trap capture of a novel mouse gene, jumonji, required for neural tube formation*. Genes Dev, 1995. **9**(10): p. 1211-22.
128. Sengoku, T. and S. Yokoyama, *Structural basis for histone H3 Lys 27 demethylation by UTX/KDM6A*. Genes Dev, 2011. **25**(21): p. 2266-77.
129. Yamane, K., et al., *JHDM2A, a JmjC-containing H3K9 demethylase, facilitates transcription activation by androgen receptor*. Cell, 2006. **125**(3): p. 483-95.
130. Accari, S.L. and P.R. Fisher, *Emerging Roles of JmjC Domain-Containing Proteins*. Int Rev Cell Mol Biol, 2015. **319**: p. 165-220.
131. Clifton, I.J., et al., *Structural studies on 2-oxoglutarate oxygenases and related double-stranded beta-helix fold proteins*. J Inorg Biochem, 2006. **100**(4): p. 644-69.
132. Chen, H., et al., *Nickel ions increase histone H3 lysine 9 dimethylation and induce transgene silencing*. Mol Cell Biol, 2006. **26**(10): p. 3728-37.
133. Chang, B., et al., *JMJD6 is a histone arginine demethylase*. Science, 2007. **318**(5849): p. 444-7.

134. Cloos, P.A., et al., *The putative oncogene GASC1 demethylates tri- and dimethylated lysine 9 on histone H3*. Nature, 2006. **442**(7100): p. 307-11.
135. Bayeva, M., et al., *When less is more: novel mechanisms of iron conservation*. Trends Endocrinol Metab, 2013. **24**(11): p. 569-77.
136. Hentze, M.W., et al., *Identification of the iron-responsive element for the translational regulation of human ferritin mRNA*. Science, 1987. **238**(4833): p. 1570-3.
137. Walden, W.E., et al., *Structure of dual function iron regulatory protein 1 complexed with ferritin IRE-RNA*. Science, 2006. **314**(5807): p. 1903-8.
138. Schalinske, K.L., et al., *The iron-sulfur cluster of iron regulatory protein 1 modulates the accessibility of RNA binding and phosphorylation sites*. Biochemistry, 1997. **36**(13): p. 3950-8.
139. Iwai, K., et al., *Iron-dependent oxidation, ubiquitination, and degradation of iron regulatory protein 2: implications for degradation of oxidized proteins*. Proc Natl Acad Sci U S A, 1998. **95**(9): p. 4924-8.
140. Vashisht, A.A., et al., *Control of iron homeostasis by an iron-regulated ubiquitin ligase*. Science, 2009. **326**(5953): p. 718-21.
141. Marro, S., et al., *Heme controls ferroportin1 (FPN1) transcription involving Bach1, Nrf2 and a MARE/ARE sequence motif at position -7007 of the FPN1 promoter*. Haematologica, 2010. **95**(8): p. 1261-8.
142. Huang, Y., et al., *The complexity of the Nrf2 pathway: beyond the antioxidant response*. J Nutr Biochem, 2015. **26**(12): p. 1401-13.
143. Han, A.P., et al., *Heme-regulated eIF2alpha kinase (HRI) is required for translational regulation and survival of erythroid precursors in iron deficiency*. EMBO J, 2001. **20**(23): p. 6909-18.

144. Chen, J.J., *Translational control by heme-regulated eIF2alpha kinase during erythropoiesis*. *Curr Opin Hematol*, 2014. **21**(3): p. 172-8.
145. Bayeva, M., et al., *mTOR regulates cellular iron homeostasis through tristetraprolin*. *Cell Metab*, 2012. **16**(5): p. 645-57.
146. Shakoury-Elizeh, M., et al., *Transcriptional remodeling in response to iron deprivation in Saccharomyces cerevisiae*. *Mol Biol Cell*, 2004. **15**(3): p. 1233-43.
147. Puig, S., E. Askeland, and D.J. Thiele, *Coordinated remodeling of cellular metabolism during iron deficiency through targeted mRNA degradation*. *Cell*, 2005. **120**(1): p. 99-110.
148. Brooks, S.A. and P.J. Blackshear, *Tristetraprolin (TTP): interactions with mRNA and proteins, and current thoughts on mechanisms of action*. *Biochim Biophys Acta*, 2013. **1829**(6-7): p. 666-79.
149. Caput, D., et al., *Identification of a common nucleotide sequence in the 3'-untranslated region of mRNA molecules specifying inflammatory mediators*. *Proc Natl Acad Sci U S A*, 1986. **83**(6): p. 1670-4.
150. Lai, W.S., et al., *Evidence that tristetraprolin binds to AU-rich elements and promotes the deadenylation and destabilization of tumor necrosis factor alpha mRNA*. *Mol Cell Biol*, 1999. **19**(6): p. 4311-23.
151. Brewer, B.Y., et al., *RNA sequence elements required for high affinity binding by the zinc finger domain of tristetraprolin: conformational changes coupled to the bipartite nature of Au-rich MRNA-destabilizing motifs*. *J Biol Chem*, 2004. **279**(27): p. 27870-7.
152. Fabian, M.R., et al., *Structural basis for the recruitment of the human CCR4-NOT deadenylase complex by tristetraprolin*. *Nat Struct Mol Biol*, 2013. **20**(6): p. 735-9.
153. Carballo, E., W.S. Lai, and P.J. Blackshear, *Feedback inhibition of macrophage tumor necrosis factor-alpha production by tristetraprolin*. *Science*, 1998. **281**(5379): p. 1001-5.

154. Taylor, G.A., et al., *A pathogenetic role for TNF alpha in the syndrome of cachexia, arthritis, and autoimmunity resulting from tristetraprolin (TTP) deficiency*. *Immunity*, 1996. **4**(5): p. 445-54.
155. Marderosian, M., et al., *Tristetraprolin regulates Cyclin D1 and c-Myc mRNA stability in response to rapamycin in an Akt-dependent manner via p38 MAPK signaling*. *Oncogene*, 2006. **25**(47): p. 6277-90.
156. Cao, H., L.J. Deterding, and P.J. Blakeshear, *Identification of a major phosphopeptide in human tristetraprolin by phosphopeptide mapping and mass spectrometry*. *PLoS One*, 2014. **9**(7): p. e100977.
157. Taylor, G.A., et al., *Phosphorylation of tristetraprolin, a potential zinc finger transcription factor, by mitogen stimulation in intact cells and by mitogen-activated protein kinase in vitro*. *J Biol Chem*, 1995. **270**(22): p. 13341-7.
158. Lai, W.S., D.J. Stumpo, and P.J. Blakeshear, *Rapid insulin-stimulated accumulation of an mRNA encoding a proline-rich protein*. *J Biol Chem*, 1990. **265**(27): p. 16556-63.
159. Mahtani, K.R., et al., *Mitogen-activated protein kinase p38 controls the expression and posttranslational modification of tristetraprolin, a regulator of tumor necrosis factor alpha mRNA stability*. *Mol Cell Biol*, 2001. **21**(19): p. 6461-9.
160. Lai, W.S., et al., *Promoter analysis of Zfp-36, the mitogen-inducible gene encoding the zinc finger protein tristetraprolin*. *J Biol Chem*, 1995. **270**(42): p. 25266-72.
161. Lai, W.S., M.J. Thompson, and P.J. Blakeshear, *Characteristics of the intron involvement in the mitogen-induced expression of Zfp-36*. *J Biol Chem*, 1998. **273**(1): p. 506-17.
162. Gaba, A., et al., *Cutting edge: IL-10-mediated tristetraprolin induction is part of a feedback loop that controls macrophage STAT3 activation and cytokine production*. *J Immunol*, 2012. **189**(5): p. 2089-93.

163. Laplante, M. and D.M. Sabatini, *mTOR signaling in growth control and disease*. Cell, 2012. **149**(2): p. 274-93.
164. Jewell, J.L., R.C. Russell, and K.L. Guan, *Amino acid signalling upstream of mTOR*. Nat Rev Mol Cell Biol, 2013. **14**(3): p. 133-9.
165. Sarbassov, D.D., et al., *Phosphorylation and regulation of Akt/PKB by the rictor-mTOR complex*. Science, 2005. **307**(5712): p. 1098-101.
166. Zou, Z., et al., *mTORC2 promotes cell survival through c-Myc-dependent up-regulation of E2F1*. J Cell Biol, 2015. **211**(1): p. 105-22.
167. Soliman, G.A., et al., *mTOR Ser-2481 autophosphorylation monitors mTORC-specific catalytic activity and clarifies rapamycin mechanism of action*. J Biol Chem, 2010. **285**(11): p. 7866-79.
168. Acosta-Jaquez, H.A., et al., *Site-specific mTOR phosphorylation promotes mTORC1-mediated signaling and cell growth*. Mol Cell Biol, 2009. **29**(15): p. 4308-24.
169. Chiang, G.G. and R.T. Abraham, *Phosphorylation of mammalian target of rapamycin (mTOR) at Ser-2448 is mediated by p70S6 kinase*. J Biol Chem, 2005. **280**(27): p. 25485-90.
170. McMahon, L.P., et al., *The rapamycin-binding domain governs substrate selectivity by the mammalian target of rapamycin*. Mol Cell Biol, 2002. **22**(21): p. 7428-38.
171. Meyuhas, O., *Ribosomal Protein S6 Phosphorylation: Four Decades of Research*. Int Rev Cell Mol Biol, 2015. **320**: p. 41-73.
172. Schalm, S.S., et al., *TOS motif-mediated raptor binding regulates 4E-BP1 multisite phosphorylation and function*. Curr Biol, 2003. **13**(10): p. 797-806.
173. Modrak-Wojcik, A., et al., *Eukaryotic translation initiation is controlled by cooperativity effects within ternary complexes of 4E-BP1, eIF4E, and the mRNA 5' cap*. FEBS Lett, 2013. **587**(24): p. 3928-34.

174. Morita, M., et al., *mTOR coordinates protein synthesis, mitochondrial activity and proliferation*. Cell Cycle, 2015. **14**(4): p. 473-80.
175. Duvel, K., et al., *Activation of a metabolic gene regulatory network downstream of mTOR complex 1*. Mol Cell, 2010. **39**(2): p. 171-83.
176. Laplante, M. and D.M. Sabatini, *Regulation of mTORC1 and its impact on gene expression at a glance*. J Cell Sci, 2013. **126**(Pt 8): p. 1713-9.
177. Sancak, Y., et al., *Ragulator-Rag complex targets mTORC1 to the lysosomal surface and is necessary for its activation by amino acids*. Cell, 2010. **141**(2): p. 290-303.
178. Campbell, W.A. and N.L. Thompson, *Overexpression of LAT1/CD98 light chain is sufficient to increase system L-amino acid transport activity in mouse hepatocytes but not fibroblasts*. J Biol Chem, 2001. **276**(20): p. 16877-84.
179. Sekine, Y., et al., *Amino acid transporter LAT3 is required for podocyte development and function*. J Am Soc Nephrol, 2009. **20**(7): p. 1586-96.
180. Bar-Peled, L., et al., *A Tumor suppressor complex with GAP activity for the Rag GTPases that signal amino acid sufficiency to mTORC1*. Science, 2013. **340**(6136): p. 1100-6.
181. Kim, J.S., et al., *Sestrin2 inhibits mTORC1 through modulation of GATOR complexes*. Sci Rep, 2015. **5**: p. 9502.
182. Tsun, Z.Y., et al., *The folliculin tumor suppressor is a GAP for the RagC/D GTPases that signal amino acid levels to mTORC1*. Mol Cell, 2013. **52**(4): p. 495-505.
183. Bar-Peled, L., et al., *Ragulator is a GEF for the rag GTPases that signal amino acid levels to mTORC1*. Cell, 2012. **150**(6): p. 1196-208.
184. Bar-Peled, L. and D.M. Sabatini, *Regulation of mTORC1 by amino acids*. Trends Cell Biol, 2014. **24**(7): p. 400-6.

185. Hughes, J., et al., *Knockout of the epilepsy gene Depdc5 in mice causes severe embryonic dysmorphology with hyperactivity of mTORC1 signalling*. *Sci Rep*, 2017. **7**(1): p. 12618.
186. Chantranupong, L., et al., *The CASTOR Proteins Are Arginine Sensors for the mTORC1 Pathway*. *Cell*, 2016. **165**(1): p. 153-164.
187. Rebsamen, M., et al., *SLC38A9 is a component of the lysosomal amino acid sensing machinery that controls mTORC1*. *Nature*, 2015. **519**(7544): p. 477-81.
188. Wang, S., et al., *Metabolism. Lysosomal amino acid transporter SLC38A9 signals arginine sufficiency to mTORC1*. *Science*, 2015. **347**(6218): p. 188-94.
189. Wyant, G.A., et al., *mTORC1 Activator SLC38A9 Is Required to Efflux Essential Amino Acids from Lysosomes and Use Protein as a Nutrient*. *Cell*, 2017. **171**(3): p. 642-654 e12.
190. Han, J.M., et al., *Leucyl-tRNA synthetase is an intracellular leucine sensor for the mTORC1-signaling pathway*. *Cell*, 2012. **149**(2): p. 410-24.
191. Wek, S.A., S. Zhu, and R.C. Wek, *The histidyl-tRNA synthetase-related sequence in the eIF-2 alpha protein kinase GCN2 interacts with tRNA and is required for activation in response to starvation for different amino acids*. *Mol Cell Biol*, 1995. **15**(8): p. 4497-506.
192. B'Chir, W., et al., *The eIF2alpha/ATF4 pathway is essential for stress-induced autophagy gene expression*. *Nucleic Acids Res*, 2013. **41**(16): p. 7683-99.
193. Ye, J., et al., *GCN2 sustains mTORC1 suppression upon amino acid deprivation by inducing Sestrin2*. *Genes Dev*, 2015. **29**(22): p. 2331-6.
194. Usuki, F., M. Fujimura, and A. Yamashita, *Endoplasmic reticulum stress preconditioning modifies intracellular mercury content by upregulating membrane transporters*. *Sci Rep*, 2017. **7**(1): p. 12390.

195. Tee, A.R., et al., *Tuberous sclerosis complex-1 and -2 gene products function together to inhibit mammalian target of rapamycin (mTOR)-mediated downstream signaling*. Proc Natl Acad Sci U S A, 2002. **99**(21): p. 13571-6.
196. Howell, J.J. and B.D. Manning, *mTOR couples cellular nutrient sensing to organismal metabolic homeostasis*. Trends Endocrinol Metab, 2011. **22**(3): p. 94-102.
197. Ben-Sahra, I. and B.D. Manning, *mTORC1 signaling and the metabolic control of cell growth*. Curr Opin Cell Biol, 2017. **45**: p. 72-82.
198. Inoki, K., et al., *TSC2 is phosphorylated and inhibited by Akt and suppresses mTOR signalling*. Nat Cell Biol, 2002. **4**(9): p. 648-57.
199. McGee, S.L., et al., *Normal hypertrophy accompanied by phosphorylation and activation of AMP-activated protein kinase alpha1 following overload in LKB1 knockout mice*. J Physiol, 2008. **586**(6): p. 1731-41.
200. Gwinn, D.M., et al., *AMPK phosphorylation of raptor mediates a metabolic checkpoint*. Mol Cell, 2008. **30**(2): p. 214-26.
201. DeYoung, M.P., et al., *Hypoxia regulates TSC1/2-mTOR signaling and tumor suppression through REDD1-mediated 14-3-3 shuttling*. Genes Dev, 2008. **22**(2): p. 239-51.
202. Hoxhaj, G., et al., *The mTORC1 Signaling Network Senses Changes in Cellular Purine Nucleotide Levels*. Cell Rep, 2017. **21**(5): p. 1331-1346.
203. Ben-Sahra, I., et al., *mTORC1 induces purine synthesis through control of the mitochondrial tetrahydrofolate cycle*. Science, 2016. **351**(6274): p. 728-733.
204. Ohsumi, Y., *Historical landmarks of autophagy research*. Cell Res, 2014. **24**(1): p. 9-23.
205. Lamb, C.A., T. Yoshimori, and S.A. Tooze, *The autophagosome: origins unknown, biogenesis complex*. Nat Rev Mol Cell Biol, 2013. **14**(12): p. 759-74.

206. Kim, J., et al., *AMPK and mTOR regulate autophagy through direct phosphorylation of Ulk1*. Nat Cell Biol, 2011. **13**(2): p. 132-41.
207. Maejima, Y., M. Isobe, and J. Sadoshima, *Regulation of autophagy by Beclin 1 in the heart*. J Mol Cell Cardiol, 2016. **95**: p. 19-25.
208. Maejima, Y., et al., *Mst1 inhibits autophagy by promoting the interaction between Beclin1 and Bcl-2*. Nat Med, 2013. **19**(11): p. 1478-88.
209. Russell, R.C., et al., *ULK1 induces autophagy by phosphorylating Beclin-1 and activating VPS34 lipid kinase*. Nat Cell Biol, 2013. **15**(7): p. 741-50.
210. Otomo, C., et al., *Structure of the human ATG12~ATG5 conjugate required for LC3 lipidation in autophagy*. Nat Struct Mol Biol, 2013. **20**(1): p. 59-66.
211. Yang, Q., et al., *Regulation of neuronal survival factor MEF2D by chaperone-mediated autophagy*. Science, 2009. **323**(5910): p. 124-7.
212. Nishida, Y., et al., *Discovery of Atg5/Atg7-independent alternative macroautophagy*. Nature, 2009. **461**(7264): p. 654-8.
213. Hirota, Y., et al., *Mitophagy is primarily due to alternative autophagy and requires the MAPK1 and MAPK14 signaling pathways*. Autophagy, 2015. **11**(2): p. 332-43.
214. Nasrallah, C.M. and T.L. Horvath, *Mitochondrial dynamics in the central regulation of metabolism*. Nat Rev Endocrinol, 2014. **10**(11): p. 650-8.
215. Liesa, M. and O.S. Shirihai, *Mitochondrial dynamics in the regulation of nutrient utilization and energy expenditure*. Cell Metab, 2013. **17**(4): p. 491-506.
216. Chen, H., et al., *Mitofusins Mfn1 and Mfn2 coordinately regulate mitochondrial fusion and are essential for embryonic development*. J Cell Biol, 2003. **160**(2): p. 189-200.
217. Chen, Y. and G.W. Dorn, 2nd, *PINK1-phosphorylated mitofusin 2 is a Parkin receptor for culling damaged mitochondria*. Science, 2013. **340**(6131): p. 471-5.

218. Song, Z., et al., *OPA1 processing controls mitochondrial fusion and is regulated by mRNA splicing, membrane potential, and Yme1L*. J Cell Biol, 2007. **178**(5): p. 749-55.
219. Mishra, P., et al., *Proteolytic cleavage of Opa1 stimulates mitochondrial inner membrane fusion and couples fusion to oxidative phosphorylation*. Cell Metab, 2014. **19**(4): p. 630-41.
220. Head, B., et al., *Inducible proteolytic inactivation of OPA1 mediated by the OMA1 protease in mammalian cells*. J Cell Biol, 2009. **187**(7): p. 959-66.
221. Smirnova, E., et al., *A human dynamin-related protein controls the distribution of mitochondria*. J Cell Biol, 1998. **143**(2): p. 351-8.
222. Lackner, L.L., J.S. Horner, and J. Nunnari, *Mechanistic analysis of a dynamin effector*. Science, 2009. **325**(5942): p. 874-7.
223. Ni, H.M., J.A. Williams, and W.X. Ding, *Mitochondrial dynamics and mitochondrial quality control*. Redox Biol, 2015. **4**: p. 6-13.
224. Liu, L., et al., *Receptor-mediated mitophagy in yeast and mammalian systems*. Cell Res, 2014. **24**(7): p. 787-95.
225. Youle, R.J. and A.M. van der Bliek, *Mitochondrial fission, fusion, and stress*. Science, 2012. **337**(6098): p. 1062-5.
226. Toyama, E.Q., et al., *Metabolism. AMP-activated protein kinase mediates mitochondrial fission in response to energy stress*. Science, 2016. **351**(6270): p. 275-281.
227. Wong, Y.C., D. Ysselstein, and D. Krainc, *Mitochondria-lysosome contacts regulate mitochondrial fission via RAB7 GTP hydrolysis*. Nature, 2018. **554**(7692): p. 382-386.
228. Kumar, R., et al., *Mitochondrial dynamics following global cerebral ischemia*. Mol Cell Neurosci, 2016. **76**: p. 68-75.
229. Neary, M.T., et al., *Hypoxia signaling controls postnatal changes in cardiac mitochondrial morphology and function*. J Mol Cell Cardiol, 2014. **74**: p. 340-52.

230. Kruidenier, L., et al., *A selective jumonji H3K27 demethylase inhibitor modulates the proinflammatory macrophage response*. *Nature*, 2012. **488**(7411): p. 404-8.
231. Wang, L., et al., *A small molecule modulates Jumonji histone demethylase activity and selectively inhibits cancer growth*. *Nat Commun*, 2013. **4**: p. 2035.
232. Kuma, A., M. Komatsu, and N. Mizushima, *Autophagy-monitoring and autophagy-deficient mice*. *Autophagy*, 2017. **13**(10): p. 1619-1628.
233. Glick, D., et al., *BNip3 regulates mitochondrial function and lipid metabolism in the liver*. *Mol Cell Biol*, 2012. **32**(13): p. 2570-84.
234. Stumvoll, M., et al., *Human kidney and liver gluconeogenesis: evidence for organ substrate selectivity*. *Am J Physiol*, 1998. **274**(5 Pt 1): p. E817-26.
235. Shinkai, Y. and M. Tachibana, *H3K9 methyltransferase G9a and the related molecule GLP*. *Genes Dev*, 2011. **25**(8): p. 781-8.
236. Knutson, S.K., et al., *A selective inhibitor of EZH2 blocks H3K27 methylation and kills mutant lymphoma cells*. *Nat Chem Biol*, 2012. **8**(11): p. 890-6.
237. McDonald, O.G., et al., *Epigenomic reprogramming during pancreatic cancer progression links anabolic glucose metabolism to distant metastasis*. *Nat Genet*, 2017. **49**(3): p. 367-376.
238. Chapman-Rothe, N., et al., *Chromatin H3K27me3/H3K4me3 histone marks define gene sets in high-grade serous ovarian cancer that distinguish malignant, tumour-sustaining and chemo-resistant ovarian tumour cells*. *Oncogene*, 2013. **32**(38): p. 4586-92.
239. Pathiraja, T.N., et al., *Epigenetic reprogramming of HOXC10 in endocrine-resistant breast cancer*. *Sci Transl Med*, 2014. **6**(229): p. 229ra41.
240. Dong, C., et al., *G9a interacts with Snail and is critical for Snail-mediated E-cadherin repression in human breast cancer*. *J Clin Invest*, 2012. **122**(4): p. 1469-86.

241. Kim, M.S., et al., *JIB-04, A Small Molecule Histone Demethylase Inhibitor, Selectively Targets Colorectal Cancer Stem Cells by Inhibiting the Wnt/beta-Catenin Signaling Pathway*. *Sci Rep*, 2018. **8**(1): p. 6611.
242. Hashizume, R., et al., *Pharmacologic inhibition of histone demethylation as a therapy for pediatric brainstem glioma*. *Nat Med*, 2014. **20**(12): p. 1394-6.
243. Chiarini, F., et al., *Current treatment strategies for inhibiting mTOR in cancer*. *Trends Pharmacol Sci*, 2015. **36**(2): p. 124-35.
244. Dienstmann, R., et al., *Picking the point of inhibition: a comparative review of PI3K/AKT/mTOR pathway inhibitors*. *Mol Cancer Ther*, 2014. **13**(5): p. 1021-31.
245. White, E., *The role for autophagy in cancer*. *J Clin Invest*, 2015. **125**(1): p. 42-6.
246. Ledermann, J., et al., *Olaparib maintenance therapy in patients with platinum-sensitive relapsed serous ovarian cancer: a preplanned retrospective analysis of outcomes by BRCA status in a randomised phase 2 trial*. *Lancet Oncol*, 2014. **15**(8): p. 852-61.
247. Tutt, A., et al., *Oral poly(ADP-ribose) polymerase inhibitor olaparib in patients with BRCA1 or BRCA2 mutations and advanced breast cancer: a proof-of-concept trial*. *Lancet*, 2010. **376**(9737): p. 235-44.
248. Wong, P.M., et al., *The ULK1 complex: sensing nutrient signals for autophagy activation*. *Autophagy*, 2013. **9**(2): p. 124-37.
249. Landes, T., et al., *The BH3-only Bnip3 binds to the dynamin Opa1 to promote mitochondrial fragmentation and apoptosis by distinct mechanisms*. *EMBO Rep*, 2010. **11**(6): p. 459-65.
250. Burte, F., et al., *Disturbed mitochondrial dynamics and neurodegenerative disorders*. *Nat Rev Neurol*, 2015. **11**(1): p. 11-24.

251. Mortensen, M., et al., *Loss of autophagy in erythroid cells leads to defective removal of mitochondria and severe anemia in vivo*. Proc Natl Acad Sci U S A, 2010. **107**(2): p. 832-7.
252. Inokuchi-Shimizu, S., et al., *TAK1-mediated autophagy and fatty acid oxidation prevent hepatosteatosis and tumorigenesis*. J Clin Invest, 2014. **124**(8): p. 3566-78.
253. Saito, T. and J. Sadoshima, *Molecular mechanisms of mitochondrial autophagy/mitophagy in the heart*. Circ Res, 2015. **116**(8): p. 1477-90.
254. Penhoat, A., et al., *Intestinal gluconeogenesis is crucial to maintain a physiological fasting glycemia in the absence of hepatic glucose production in mice*. Metabolism, 2014. **63**(1): p. 104-11.
255. Zhang, H., et al., *Loss of Tsc1/Tsc2 activates mTOR and disrupts PI3K-Akt signaling through downregulation of PDGFR*. J Clin Invest, 2003. **112**(8): p. 1223-33.

*Curriculum Vitale*  
06/2018

**Current Address**

Medical Scientist Training Program  
Northwestern University  
303 East Chicago Avenue  
Chicago, Illinois 60611

Tel: (631) 885-2804  
Fax: (312) 908-5253

CITIZENSHIP: USA

E-mail: [jason.shapiro@northwestern.edu](mailto:jason.shapiro@northwestern.edu)

**Education**

2017-present	Jikei University SOM	Post-Doctoral Fellow/ Lecturer
May 2014	Feinberg School of Medicine	USMLE – Step 1      Score: <b>243</b>
2012-2020	Northwestern University	MD-PhD      Graduate Year 4
2010-2011	Johns Hopkins University	M.S.    GPA: 3.91    Molecular and Cellular Biology
2007-2010	Johns Hopkins University	B.S.    GPA: 3.55    Molecular and Cellular Biology

**Research**

Nov. 2014 - Aug. 2017	Graduate Student, Department of Medicine-Cardiology, Northwestern University School of Medicine, Chicago IL. Advisor: Hossein Ardehali MD. PhD.
May-Oct 2014	Graduate Rotation, Department of Medicine-Hematology/Oncology, Robert H. Lurie Research Center, Chicago IL. Advisor: Chonghui Cheng MD. PhD.
June-Aug 2012	Graduate Rotation, Department of Pediatrics, Children’s Memorial Research Center, Chicago IL. Advisor: Christopher Payne Ph.D.
2010-2011	Graduate Researcher, Department of Neurology. Johns Hopkins University School of Medicine, Baltimore, MD. Advisor: Hongjun Song Ph.D.
2009-2010	Undergraduate Researcher, Department of Neurology. Johns Hopkins University School of Medicine, Baltimore, MD. Advisor: Hongjun Song Ph.D.
2006, Summer	Research Assistant, Department of Neurology. Stony Brook University School of Medicine, Stony Brook, NY, Advisor: Mirjana Savatic-Maletic M.D. Ph.D.

**Publications:**

- 1.) **Shapiro JS.**, Chang H.-C. and Ardehali H. “Iron and Sex Cross Paths in the Heart.” *J Am Heart Assoc.* 2017, 6(1):pii e005459. PMID 28115313
- 2.) Yang X, Park S-H, Chang H.-C., **Shapiro JS.**, Vasilopoulos A., Sawicki KT, Chen C, Shang M, Burrige P, Epting CL, Wilsbacher L, Jenkitkasemwong S, Knutson M, Gius D, and Ardehali H. “SIRT2 regulates cellular iron through deacetylating and destabilizing NRF2” Manuscript accepted to *Journal of Clinical Investigation*

- 3.) Rines AK, Chang H.-C., Wu R, Sato T, Khechaduri A, Kouzu H, **Shapiro JS**, Shang M, Burke MA, Jiang X, Chen C, Rawlings TA, Lopaschuk GD, Schumacker PT, Abel ED, and Ardehali H. Snf1-related Kinase Improves Cardiac Metabolic Efficiency by Decreasing Mitochondrial Uncoupling. *Nat. Comm.* 2017, 8:14095. PMID: 28117339
- 4.) Chang H.-C., **Shapiro JS.**, and Ardehali H. "Getting to the "Heart" of Cardiac Disease by Decreasing Mitochondrial Iron." *Circ. Res.* 2016, 119(11):1164-1166. PMID: 28051781
- 5.) Chang HC, Wu R, Shang M, Sato T, Chen C, **Shapiro JS**, Liu T, Thakur A, Sawicki KT, Prasad SV, Ardehali H. Reduction in mitochondrial iron alleviates cardiac damage during injury. *EMBO Mol Med.* 2016 Feb 19; 8(3): 247-67. PMID: 26896449
- 6.) Bonaguidi MA, Wheeler MA\*, **Shapiro JS\***, Stadel R, Sun GJ, Ming GL and Song HJ. In vivo clonal analysis reveals self-renew and multipotent adult neural stem cell characteristics. *Cell.* 2011 Jun 24; 145(7): 1142-55 PMID: 21664664

\*: These authors contributed equally.

### Awards, Scholarships, Presentations and Honors

2015-2017	NIH Grant for MD/PhD Students: <b>NRSA F30 DK109608-02</b> (Provides complete funding/tuition for PhD years and Medical School years 3 /4 as well as a personal stipend and annual research budget)
2016	Poster Presentation at AHA 2016
2010	Poster Presentation at SFN 2010
2007-2011	Woodrow Wilson Fellowship
2006	Siemens Competition Semi-Finalist

### Professional Societies

2016-present	American Heart Association
2012-present	American Physician-Scientist Association
2012-present	American Medical Students Association
2009-2011	Society for Neuroscience (SFN)

### Clinical Experience

Sept. 2012-June 2015	Education Centered Medical Home: Bi-monthly participation in patient care (internal medicine).
June-July 2011	Stony Brook University EMT-B Certification Course with 16 hours of on-ambulance clinical training. New York State Registered EMT as of 8/16/11.

### Teaching

Spring 2018 – Fall 2018	Lecturer	Scientific Literature
Fall 2017 – Spring 2018	Lecturer	Basic Tumor Biology
Spring 2011	Teaching Assistant	General Biology Lab II
Fall 2010	Teaching Assistant	General Biology Lab I

Languages

English

Japanese

References**Hossein Ardehali, MD, PhD** (Graduate Thesis Advisor)

Professor of Medicine-Cardiology and Pharmacology

Feinberg Cardiovascular Research Institute

Tarry Building Room 12-725

300 E Superior

Chicago IL 60611 USA

(312) 503-2342

[h-ardehali@northwestern.edu](mailto:h-ardehali@northwestern.edu)**Dane Chetkovich, MD, PhD** (Former Director MSTP)

Professor of Neurology

Ward Building Room 10-201

303 E Chicago Avenue

Chicago IL 60611 USA

(312) 503-4362

[d-chetkovich@northwestern.edu](mailto:d-chetkovich@northwestern.edu)**Teresa Woodruff, PhD** (Collaborator and Mentor)

Director, Women's Health Research Institute

Thomas J. Watkins Memorial Professor, Obstetrics and Gynecology

Robert H. Lurie Medical Research Center

303 E Superior

Chicago IL 60611 USA

(312) 503-2503

[tkw@northwestern.edu](mailto:tkw@northwestern.edu)**Michael Bonaguidi, PhD** (Undergraduate/Masters Research Advisor)

Assistant Professor, Department of Medicine

Keck School of Medicine

University of Southern California

1425 San Pablo

Health Sciences Campus

Los Angeles California 90033

E-mail: [mbonagui@usc.edu](mailto:mbonagui@usc.edu), [mbonagu1@jhmi.edu](mailto:mbonagu1@jhmi.edu)